UNCLASSIFIED

AD 274 140

Reproduced by the

ARMED SERVICES TECHNICAL INFORMATION AGENCY
ARLINGTON HALL STATION
ARLINGTON 12, VIRGINIA

UNCLASSIFIED

NOTICE: When government or other drawings, specifications or other data are used for any purpose other than in connection with a definitely related government procurement operation, the U. S. Government thereby incurs no responsibility, nor any obligation whatsoever; and the fact that the Government may have formulated, furnished, or in any way supplied the said drawings, specifications, or other data is not to be regarded by implication or otherwise as in any manner licensing the holder or any other person or corporation, or conveying any rights or permission to manufacture, use or sell any patented invention that may in any way be related thereto.

62 3-1

274140

CATALOGED BY ASTIA
AS AD No.

274 140

WADC-TR-59-602
PART II

INVESTIGATION OF MATERIALS CAPABILITIES OF MATERIAL SYSTEMS IN SOLID ROCKET MOTORS

PART II. ANALYSIS OF HEAT TRANSFER FACTORS

TECHNICAL REPORT No. WADC-TR-59-602, PART II

ASTIA
APR 17 1962
TISIA

FEBRUARY 1962

DIRECTORATE OF MATERIALS AND PROCESSES
AERONAUTICAL SYSTEMS DIVISION
AIR FORCE SYSTEMS COMMAND
WRIGHT-PATTERSON AIR FORCE BASE, OHIO

PROJECT No. 7350, TASK No. 73500

(Prepared under Contract No. AF 33(616)-7365
by Aerojet-General Corporation, Sacramento, California;
E. M. Sadownick, Author)

NOTICES

When Government drawings, specifications, or other data are used for any purpose other than in connection with a definitely related Government procurement operation, the United States Government thereby incurs no responsibility nor any obligation whatsoever; and the fact that the Government may have formulated, furnished, or in any way supplied the said drawings, specifications, or other data, is not to be regarded by implication or otherwise as in any manner licensing the holder or any other person or corporation, or conveying any rights or permission to manufacture, use, or sell any patented invention that may in any way be related thereto.

Qualified requesters may obtain copies of this report from the Armed Services Technical Information Agency, (ASTIA), Arlington Hall Station, Arlington 12, Virginia.

This report has been released to the Office of Technical Services, U. S. Department of Commerce, Washington 25, D. C., for sale to the general public.

Copies of ASD Technical Reports and Technical Notes should not be returned to the Aeronautical Systems Division unless return is required by security considerations, contractual obligations, or notice on a specific document.

800 - April 1962 - 27-1116 & 1117

FOREWORD

This report was prepared by the Aerophysics Department of Aerojet-General Corporation, Sacramento, California, under Contract No. AF 33(616)-7365. The contract was initiated under Project No. 7350, "Refractory Inorganic Non-Metallic Materials," Task No. 73500, "Ceramic and Cermet Materials Development." The work was administered under the direction of the Directorate of Materials and Processes, Deputy for Technology, Aeronautical Systems Division, with Lt. T. E. Lippart acting as project engineer.

The work was conducted between 15 June 1960 and 15 May 1961, supervised by G. Kraus through March 1961 and by S. E. Colucci from April 1961 to May 1961.

The author is grateful to C. M. Gracey for extensive assistance with heat transfer calculations and test data analyses, and to Dr. W. W. Clauson, who was one of the originators of the program and who always made himself available for advice and consultation. The author wishes also to acknowledge the contributions of S. S. Jackson, who saw to the procurement and proper assembly of the test hardware and gave whatever other assistance was required in drawing curves and making calculations; of J. D. Sohl, who acted as test engineer; of W. E. Billings, who made the many repetitious preliminary calculations for the two-dimensional heat transfer problems; of J. M. Chapp and L. O. Fagan, who edited this summary report and most of the monthly progress reports; and of all other Aerojet-General personnel, too numerous to mention here, who assisted in various ways in the completion of this project.

ABSTRACT

Temperature histories of various nozzle materials systems were analyzed parametrically, and a series of hot-flow tests were conducted in support of the analytical study. The analysis showed that chamber pressure and gas temperature affect duration capability significantly, but throat diameter does not. Thermophysical properties of the flame barrier and heat sink also affect duration, but, by comparison, the effect of variations of thermophysical properties of the insulator and load-bearing member is relatively small. High product of density and heat capacity, and moderately high thermal conductivity, are desirable for the flame barrier and heat sink. The heat transfer analysis indicated that significant increases in nozzle duration capability are possible when properly oriented anisotropic material is used. Tests of six nozzles with varying tungsten flame barrier thicknesses showed fairly good agreement between calculated temperatures and measured data when no aluminum oxide was deposited on the walls. When deposition occurred, the measured temperatures were lower than those calculated; but the temperatures could be brought close to agreement by considering the thermal blocking effect of the deposit.

PUBLICATION REVIEW

This report has been reviewed and is approved.

FOR THE COMMANDER:

W. G. RAMKE
Chief, Ceramics and Graphite Branch
Metals and Ceramics Laboratory
Directorate of Materials and Processes

TABLE OF CONTENTS

LIST OF TABLES

LIST OF FIGURES

LIST OF FIGURES (cont.)

LIST OF FIGURES (cont.)

LIST OF SYMBOLS

a	inner radius
b	outer radius
B	Biot modulus
c_p	specific heat
D_T	throat diameter
F	Fourier modulus
h	heat transfer coefficient
k	thermal conductivity
P_c	chamber pressure
R	radius ratio
T_g	gas temperature
T_o	initial material temperature
ρ	density
θ	time

I. INTRODUCTION

The trend in chemical rocket propulsion is toward the development of propellant with higher combustion temperatures. As propellant gas temperatures reach and exceed the melting points of most known materials, the problem of what nozzle materials to use becomes more difficult to solve. As a prelude to the development of nozzle-materials systems for use in future high-performance solid rocket motors, this theoretical and experimental investigation was undertaken. The effects of nozzle design and materials variables on system duration capability were described to indicate the most promising areas for subsequent materials research and development.

Many complicated factors enter into a proper understanding of nozzle materials behavior, but the role played by heat transfer is basic to all. The investigation was accomplished primarily through an analytical parametric study of the temperature histories of various nozzle systems. A series of nozzle test firings was made in support of the analytical work. Other areas of interest, such as thermal stress and erosion characteristics, were not considered here.

As materials for use at high temperatures are developed, the question arises of how accurately one needs to know the thermophysical properties to design a nozzle materials system. Consequently, the effects of errors or uncertainties in thermophysical properties were also studied, and their relative importance was determined.

Manuscript released May 1961 for publication as a WADC Technical Report.

II. ANALYTICAL STUDIES

A. PROCEDURE

The current study was conducted with both three-material and four-material model systems. The three-materials system consists of a high-temperature flame barrier, an insulator, and a load-bearing member. The four-materials system consists of a high-temperature flame barrier, a high-temperature heat sink, an insulator, and a load-bearing member.

The design variables investigated were the following:

1. Chamber pressure
2. Gas temperature
3. Throat diameter
4. Radius of curvature of the throat
5. Material thickness

The material variables investigated were the following:

1. Thermal conductivity
2. Product of density and heat capacity
3. Maximum allowable material temperature

Table 1 is a list of some materials that have been used, are currently being developed for use, or are suggested by this study for use in nozzles. They are grouped by distinguishing characteristics and their function in a three- or four-materials system. The range of thermophysical properties of these materials is compiled in Table 2.

In determining the effects of the design and materials variables, the following procedure was used. Material thicknesses were arbitrarily chosen and put into a digital computer (either the IBM 704 or IBM 7090 were used) along with

other design data and material properties. This was basically a parametric study; constant material properties were chosen that were representative of values for actual materials. The analysis assumed one-dimensional heat transfer to a hollow cylinder; in some cases, however, two-dimensional, axisymmetric heat-transfer calculations were made. The values used for the convective coefficients of heat transfer to the nozzle wall were typical of aluminized polyurethane propellants, assuming no particle deposition (see Appendix I). The computer outputs, which were temperature histories, were then evaluated to determine the effects of the variables of interest. The computer program and the outputs are discussed more fully in Appendix II.

A single three-materials system and a basic set of design conditions were chosen as references. The reference system was tungsten-asbestos phenolic-steel. The basic design conditions were 1000 psi chamber pressure, 7000°F gas temperature, 4-in. throat diameter, and a throat radius of curvature-to-throat radius ratio of infinity (the case for a hollow cylinder). Representative material properties used for the reference system are listed in Table III.

Design conditions and material properties were varied in turn. The four-materials system was studied by introducing heat sinks with various properties and evaluating the effect on temperature distribution and duration.

In most cases, conditions were investigated only at the throat. However, the methods used can be extended to other parts of the nozzle by selecting the appropriate combination of chamber pressure and throat diameter.

B. THREE-MATERIALS SYSTEMS

1. Effect of Design Variables on Duration Capability

a. Optimum Duration

Nozzle material thicknesses may be represented by nozzle weights per unit length. The minimum weight of a particular nozzle materials system, for a specific set of design conditions, is obtained when the material thicknesses are minimum and the maximum allowable temperature of any of the materials is not exceeded. For a particular chamber pressure, gas temperature, throat diameter, and materials system, there is a minimum nozzle weight for each duration.

Nozzle weight per unit length at the throat section is plotted as a function of duration in Figure 1 for the reference system, tungsten-asbestos phenolic-steel, and for design conditions of 1000 psi, 7000°F, and 4.0-in. throat diameter. The flame barrier and insulator thicknesses were minimized at each duration and the steel thickness was kept constant at 0.25 in. This thickness of steel does not absorb any significant amount of heat and could have been neglected in the heat transfer calculation. Small changes in insulator thickness will have a great effect on steel temperature, but a negligible effect upon weight. For example, the following sets of thicknesses result in weights per unit length and surface and interface temperatures at the end of 120 sec:

	Tungsten	Asbestos Phenolic	Steel	Tungsten	Asbestos Phenolic	Steel
Thickness, in.	3.350	0.250	0.250	3.350	0.200	0.250
Temperature, °F	6109	3010	376	6109	3020	1271
Wt/length, lb/in.		55.46			55.33	

A 0.050-in. change in insulation thickness results in a 900°F change in steel temperature, but a difference of only 0.13 lb/in. in throat weight per unit length. For this reason, it was considered sufficient to have the steel within a few hundred degrees of its allowable temperature when calculating minimum nozzle weight.

The initial weight increase shown on the curve of Figure 1 is nearly proportional to the duration increase. Then, the slope of the curve changes abruptly and small additional increases in duration are accompanied by very large increases in throat weight per unit length. At short duration, the maximum allowable temperature is reached only in the insulator and load-bearing members, but not in the flame barrier. At higher durations, on the steep portion of the curve, the flame barrier and load-bearing members reach their limiting temperatures, but the insulator does not.

At the point where the slope of the curve changes abruptly, and only at this point, the maximum allowable temperature is reached simultaneously in all three materials. If we consider that maximum use is made of a nozzle material when it is heated to the highest temperature it can withstand under the given conditions, then only at this point is maximum use made of each material in the system. For this reason, the point is called an optimum point, and the duration at which it occurs is called an optimum duration. For the three-materials system, the optimum duration is a practical indication of duration capability because, once reached, nozzle duration can be extended only a short time by increasing the material thickness. Soon a point will be reached at which no further increases in duration are possible, unless some of the design conditions are changed.

Figure 2 shows the effect of chamber pressure on the position and shape of curve shown in Figure 1 for throat weight per unit length vs duration. Decreasing the chamber pressure results in an increase in optimum duration. At chamber pressures of 600 psi and below, the optimum

duration is so great (beyond 350 sec) that it is not shown on the curve. Although such high durations are beyond any contemplated for the forseeable future, they are valid as a measure of the relative effect of chamber pressure.

Figures 3 and 4 show the effects of gas temperature and throat diameter, respectively, on minimum nozzle weight. An increase in gas temperature results in a decrease in optimum duration. An increase in throat diameter results first in a decrease then a small increase in optimum duration. This effect of increasing throat diameter is the result of the balancing of two effects: (1) the increased heat transfer to the wall due to the geometry change (increased ratio of inner-to-outer diameter), and (2) the decreased heat transfer to the wall due to a decrease in the convective heat transfer coefficient (resulting directly from the increased diameter). At higher diameters, the curve changes a slope a short distance above the indicated optimum point.

The relationship between the design conditions and optimum duration is shown more clearly in Figure 5. Here, optimum duration is plotted as a function of chamber pressure, gas temperature, and throat diameter. Each curve was obtained by cross-plotting the optimum points shown in Figure 2 through 4 as a function of the design variable. Small increases in chamber pressure or gas temperature result in very large decreases in optimum duration, but, by comparison, a change in throat diameter affects optimum duration very little.

Increases in optimum duration that result from decreases in chamber pressure or gas temperature always result in nozzle weight increases. This is because a decrease in pressure or temperature requires an increase in material thickness for the same allowable temperatures to be reached simultaneously in all three materials. It is therefore of interest to investigate the effect of these variables on systems of equal weight.

b. Duration Capability for Systems of Constant Weight

The manner in which chamber pressure and gas temperature affect duration for systems of equal throat weight per unit length is shown in Figure 6. Nozzle duration capability is plotted for the tungsten-asbestos phenolic-steel system as a function of the design variable, for constant throat weight per unit length. The curves show a significant decrease in duration capability with an increase in either chamber pressure or gas temperature. This decrease becomes more marked at higher durations. Also shown on these curves is the optimum duration. At or near the optimum line, the direction of curvature changes. Above the optimum point, weight increases very rapidly for small increases in duration. A similar curve could be drawn for throat diameter, showning a generally similar trend.

c. Maximum Duration Capability

While the optimum duration is a practical indication of duration capability of a particular system at specified conditions, operation above the optimum may sometimes be necessary. Above the optimum, nozzle duration can be extended a short time by increasing the flame barrier thickness. Eventually, a point would be reached when any further increases in flame barrier thickness would not result in an increase in the time necessary for the surface temperature to reach a predetermined value (the maximum allowable material temperature). Finding this maximum duration is equivalent to the problem of heat transfer to an infinitely thick hollow cylinder, which was solved by Carslaw and Jaeger[1]. The solution is plotted in Figure 7.

---

1. H. S. Carslaw and J. C. Jaeger, Conduction of Heat in Solids, 2nd Edition, p. 338.

Application of this solution to the reference case shows that the maximum duration for the tungsten-asbestos phenolic-steel system lies between 210 and 280 sec (the curve cannot be read any more accurately in this region). The optimum duration for this case is 120 sec.

d. Effect of Radius of Curvature at Throat

The effect of the radius of curvature at the throat was determined by comparing temperature histories of nozzles with different ratios of throat radius of curvature-to-throat radius. The heat transfer calculations in this case were two-dimensional asisymmetric. Results for the tungsten-asbestos phenolic-steel system are shown in Figure 8. The curves in Figure 8 show temperature-time distributions in the throat sections of nozzles with radius ratios of 0.5, 2, and infinity; the case for infinity corresponds to a hollow cylinder. The nozzle configurations are shown in Figure 9. Each nozzle has a 15-degree exit-cone half-angle and a 29-degree approach-section angle. The difference in surface temperature which results from using two different radius ratios (0.5 and 2.0) is approximately 1%, and the difference in duration which results is approximately 8%. A similar curve was calculated for a nozzle with a bell-shaped exit section but is not shown. It would lie between the cases for radius ratios of 0.5 and 2.

The curves shown in Figure 8 also provide a comparison between one- and two-dimensional heat transfer calculations. The surface temperature calculated assuming one-dimensional heat transfer is 3.2% lower than the closest two-dimensional case, and the duration is nearly 40% greater (based on the two-dimensional case). This result is not universal for all one- vs two-dimensional heat transfer calculations, however. The size and shape of the nozzles being compared are important factors. For example, in the two test nozzles for which both one- and two-dimensional heat transfer calculations were made, the temperature calculations assuming one-dimensional heat transfer was slightly higher.

2. Effect of Material Variables

a. Thermophysical Properties

The material variables of primary interest are the thermophysical properties -- thermal conductivity, the product of density and specific heat ($\rho\ c_p$), and the maximum allowable material temperature.

The effects of the thermophysical properties on optimum duration are shown graphically in Figure 10. Optimum duration is plotted as a function of thermal conductivity for two products of density and specific heat for the insulator and the flame barrier.

The products of density and specific heat shown are approximately equivalent to those for tungsten (41.3 Btu/cu ft-°F), titanium carbide (76.5 Btu/cu ft-°F), asbestos phenolic (41.9 Btu/cu ft-°F), and porous silicon carbide (12.5 Btu/cu ft-°F). The other figures shown on the graph are throat weight per unit length.

The curves in Figure 10 show that, for the insulator, a change in either thermal conductivity or the product of density and heat capacity has a negligible effect on optimum duration, while an increase in thermal conductivity of the flame barrier results in a very great increase in optimum duration. Also, an increase in the product of density and specific heat in the flame barrier results in a significant increase in optimum duration. Increases in optimum duration, resulting from increases in thermal conductivity are accompanied by increases in nozzle weight.

Although it may seem unusual to be able to increase duration capability by using a "poorer" insulator, the reason is quite clear. As insulator conductivity increases, heat is transferred from the flame barrier more rapidly; the time required for the flame barrier to reach its limiting temperature is therefore increased.

All of the weight calculations shown in Figure 10 were made for one insulator density and one flame barrier density. The weight decrease shown for different products of density and heat capacity, therefore, represents the influence of heat capacity only. Although the change in weight is small, and it is reasonable to expect that the material system capable of absorbing more heat will weigh less to do the same job, an increase in specific heat is the only means by which ultimate capability (as indicated by optimum duration) can be increased with a corresponding decrease in nozzle weight.

The weights shown in Figure 10a were calculated by assuming a density of 110 lb/cu ft for the insulating material. Usually insulators with a low value of the product of density and heat capacity have lower densities, while those with a higher value (of about 50 to 60 Btu/cu ft °F) tend towards higher densities (Table 2). The weights shown in Figure 10 could be reduced by 1.5 lb/in. by substituting a low-density insulation and increased as much as 6 lb/in. by substituting a high-density insulation. The flame barrier density is 1170 lb/cu ft. Flame barrier densities vary much more widely and have a much greater effect on nozzle weight than do insulator densities.

To dissociate the effects of the thermophysical properties on duration and weight, duration was plotted as a function of conductivity for systems of equal weight. The resulting curves are shown in Figure 11.

At low thermal conductivity levels, increases in flame barrier conductivity are indicated by the curves in Figure 11 to result in increases in duration capability. At moderate and high conductivities, further increases in conductivity have a negligible effect on duration. Duration drops off sharply after the limiting temperature of the insulator is reached, because the flame barrier is then operating below its allowable maximum.

As the nozzle weight (flame barrier thickness) is increased, the value of flame barrier conductivity above which there can be no further increases in duration is also increased.

b. Maximum Allowable Material Temperature

The proper choice of maximum allowable, or limiting, material temperature is based on knowledge of the behavior of the material at conditions under which it will be used. Choice is also dependent upon the function of the material in the system. The temperature limitation of the flame barrier is thus below the melting temperature and is influenced by the melting or softening point and by design conditions such as chamber pressure and material thickness. The limitation of the heat sink and insulator is the temperature above which these components can no longer transmit pressure forces to the load-bearing member. Since these materials are in the interior of the system, the possibility of decomposition must also be considered. The load-bearing member is limited by the relationship between temperature and yield strength.

In this study, the choice of maximum allowable flame barrier and heat sink temperatures was somewhat arbitrary, being based on limited knowledge of material behavior at very high temperatures. Some value close to and below the melting point was chosen. For the plastic insulators, asbestos phenolic for example, 3000°F was chosen as the limiting temperature.

Although the phenolic resin begins to decompose at approximately 600°F, this insulation material has been successfully tested by Aerojet-General at temperatures above 3000°F when the nozzle design included passages for the escaping gas. The limiting temperature of the load-bearing member was taken as the temperature at which the slope of the yield strength curve changes sharply.

It was not the object of this study to provide sufficient information about material behavior so that a proper choice of limiting temperature may be made. What was determined, however, was the effect of a change in the choice of maximum allowable material temperature on duration and weight, once such a choice has been made.

In Figure 12, throat weight per unit length is plotted as a function of duration for the reference system and design conditions. With the allowable temperature of the insulator kept constant at 3000°F, the allowable temperature of the flame barrier was decreased to 5800°F. With the allowable temperature of the flame barrier kept constant at 6100°F, the insulator allowable temperature was varied to 1500°F and 4000°F.

Increasing the limiting temperature of the flame barrier increases the duration or decreases the weight for the same duration, at durations above the optimum. At or below the optimum duration, an increase in the limiting temperature of the flame barrier has no effect on weight or duration because the limiting temperature is not reached in the flame barrier. The maximum duration of the system with a 5800°F allowable flame barrier temperature is approximately 95 sec, as compared to more than 200 sec for the system with a 6100°F limitation.

Increases in allowable insulator temperatures also result in duration increases and weight decreases, but only at durations below the optimum. At or above the optimum, the limiting insulator temperature is not reached, so any increases in the allowable temperature have no effect. Increases in insulator allowable temperature actually result in decreases in optimum duration, because the portion of the curve above the optimum is extended downward to the new allowable temperature. The effect of an increase in insulator allowable temperature becomes smaller at higher allowable temperatures.

Maximum allowable material temperature is an important material property only in its relationship to the gas temperature. For example, if the allowable temperature of the material were high in comparison to the gas temperature, the duration would be longer, or the nozzle would weigh less, than if the allowable material temperature were low. The relationship between the maximum allowable flame barrier temperature and the gas temperature may be expressed as a dimensionless temperature ratio,

$$\phi, \text{ where } \phi = \frac{T_{gas} - T_{allow}}{T_{gas} - T_o} .$$

Raising the allowable flame-barrier temperature has very nearly the same effect on weight and duration as lowering the gas temperature. For example, a gas temperature of 8000°F and an allowable temperature of 7000°F corresponds virtually to a gas temperature of 7000°F and an allowable temperature of 6126°F. The two cases will be almost exactly the same if the allowable insulator temperature is also changed, so that the dimensionless temperature ratios based on insulator allowable temperatures are equal in both cases. Otherwise, there will be a difference of several hundred degrees between the attained and allowable insulator temperatures. This assumes that very small changes in insulator thickness are required to maintain the load-bearing member at its allowable temperature, with a resultant negligible weight change.

The effect of dimensionless temperature ratio on optimum duration is plotted in Figure 13 for a simulated tungsten flame barrier. The flame barrier properties were identical with those used for tungsten, except that the maximum allowable temperature was varied from 4700 to 7000°F. Although the high value is considerably higher than the melting point of tungsten, its use is justified because the object here is to investigate the trend of the curve rather than the performance of any specific materials.

The curves in Figure 13 are for allowable insulator temperatures of 1500, 3000, and 4000°F at a chamber pressure of 1000 psia. The curves take the same shape as the curve of optimum duration vs gas temperature. As the maximum allowable flame-barrier temperature approaches the gas temperature, the optimum duration increases very rapidly. The increases in optimum duration are, as usual, accompanied by weight increases, but the weight increases become smaller as ϕ approaches zero.

C. FOUR-MATERIALS SYSTEMS

1. Use of a Heat Sink

A heat sink in a nozzle materials system will:

a. absorb heat entering the system and keep it from reaching the insulator,

b. keep the flame barrier cooler than if it were backed by an insulator alone, and

c. reduce the weight of the system when it replaces part of the higher-density flame barrier. A heat sink should be used when:

(1) the flame barrier cannot absorb enough of the heat entering the system to protect the insulator,

(2) the gas temperature is much greater than the flame barrier allowable temperature, and

(3) the density of the flame barrier is high in comparison with the density of the heat sink which could replace a portion of it.

The effect of the design variables is essentially the same for the four-materials system as for the three-materials system. That is, chamber pressure and gas temperature have a very pronounced effect on duration capability, and the effect of throat diameter is much less significant, except for very small diameters. This is seen more clearly if the four-materials system is considered as a three-materials system in which either (a) the heat sink and flame barrier are considered as a single flame barrier material or (b) the heat sink is considered as the insulator. The first case would apply when the flame barrier of the four-materials system is very thin and experiences a small temperature drop. The second case applies when the flame barrier is nearly as thick as the heat sink or experiences a large temperature drop.

2. Effect of Material Thickness

The flame barrier thickness in the four-materials system should generally be just sufficient to keep the heat sink from reaching its maximum allowable temperature or to prevent its erosion. The effect of varying the flame-barrier and heat-sink thicknesses was investigated for the tungsten-graphite-asbestos phenolic-steel system. The properties used for graphite were similar to those of ATJ* graphite and are shown in Table 4 with properties used for other heat sinks investigated.

*National Carbon Co. designation

Figure 14 shows the effect upon duration of increasing heat-sink thickness for several constant flame-barrier thicknesses. Increasing the thickness of the heat sink results in a duration increase and a reduction in the heat sink-to-insulator interface temperature. The curve in Figure 14 also shows the duration increase which results when the temperature at the heat sink-to-insulator interface is kept constant and the flame-barrier surface temperature is permitted to increase to 6100°F. As the flame barrier is thickened, the duration capability is also increased. However, the nozzle weight increases more rapidly with increasing flame-barrier thickness than with increasing heat-sink thickness, because the specific heat of graphite is more than ten times as great as the specific heat of tungsten. Since the product of density and specific heat is approximately equal for both tungsten and graphite, the total thickness of the flame barrier and heat sink remains essentially equal at any duration.

3. Effect of Material Properties

The effect of heat-sink material properties on duration capability was studied by comparing the performance of the four heat sinks shown in Table 4. In addition, a second value was used for the thermal conductivity of graphite. The results are shown in Figure 15.

A comparison of the curves for graphite shows the effect of doubling the thermal conductivity. For small heat-sink thicknesses, the effect of conductivity is negligible. At thicknesses of 1.5 in. or greater, the nozzle system with the more highly conductive heat sink has a greater duration capability; this effect increases with increased heat-sink thickness.

The curves for the beryllium oxide and boron carbide heat sinks again show the effect of thermal conductivity for heat sinks with nearly equal products of density and specific heat. Here the advantage of using the higher-conductivity material starts to become significant at 1.2 to 1.5 in.

A comparison of the curves for the low-conductivity graphite and beryllium oxide shows the effect of nearly doubling the product of density and specific heat while keeping the thermal conductivity constant. Both curves appear to flatten out at approximately the same heat-sink thickness, but the curve for the material with the higher product of density and specific heat shows a maximum of 46% greater duration capability based on the lower duration.

The curves for boron carbide and high conductivity graphite also show the effect of the product of density and specific heat. The conductivity of boron carbide is 22% lower than that used for the high-conductivity graphite and the product of density and specific heat is 87% higher. Durations with the boron carbide heat sink are as much as 50% higher for the same thickness.

Again, the strong effect of the product of density and specific heat is seen in a comparison of the curves for boron carbide and pyrolytic graphite, with the graphite oriented so that the high conductivity is in the radial direction. The product of density and specific heat of the boron carbide is 16% higher, but the thermal conductivity is 80% lower; yet the nozzle system with the boron carbide heat sink shows durations almost as high, and higher, than the one with pyrolytic graphite, for thickness up to 3 in. This result corroborates the finding for the three-materials system: increases in flame barrier thermal conductivity have an insignificant effect upon duration when the conductivity is already very high (see Figure 10).

D. EFFECT OF UNCERTAINTIES IN PHYSICAL PROPERTIES

As materials for use at high temperatures are developed, the question arises of how accurately one needs to know the thermophysical properties to design a nozzle materials system.

The effect of thermal conductivity, density, and heat capacity on temperature distribution is a function of the heat transfer to, and geometry of, the system. These may be expressed in terms of three dimensionless moduli:

1. the Fourier modulus, $F = \dfrac{k\,\theta}{\rho c_p b^2}$
2. the Biot modulus, $B = \dfrac{hb}{k}$, and
3. the radius ratio $R = \dfrac{a}{b}$

The density and heat capacity affect temperature distribution only through the Fourier modulus, whereas the thermal conductivity affects temperature distribution through both the Fourier and Biot moduli. The effect of errors in density and specific heat on temperature distribution was found for a material insulated on the outside; temperature tables for internally heated hollow cylinders[1] were used along with the following equation[2]:

$$\frac{F + \Delta F}{F} = \frac{1}{1 + \dfrac{\Delta \rho}{\rho} + \dfrac{\Delta c_p}{c_p}}$$

1. G. Fluke, Temperature Tables for Internally-Heated Hollow Cylinders, Aerojet-General Corporation, Technical Memorandum 121-SRP, October 1959 (Aerojet-General internal publication).

2. $F = \dfrac{k\theta}{\rho c_p b^2}$, $F + \Delta F = \dfrac{k\theta}{(\rho + \Delta\rho)(c_p + \Delta c_p)\, b^2} = \dfrac{k\theta}{(\rho c_p + \Delta\rho\, c_p + \rho\,\Delta c_p + \Delta\rho\,\Delta c_p) b^2}$

$$= \frac{k\theta}{\rho c_p b^2 \left(1 + \dfrac{\Delta\rho}{\rho} + \dfrac{\Delta c_p}{c_p}\right)}, \quad \frac{1}{1 + \dfrac{\Delta\rho}{\rho} + \dfrac{\Delta c_p}{c_p}} = \frac{F + \Delta F}{F}$$

The effect of large errors in thermal conductivity cannot be found by this method because a linear combination of errors in the Fourier and Biot moduli yields an accurate result for only very small errors in conductivity. The effect of conductivity errors was found by comparing the results of several computer runs in which only the thermal conductivity was changed.

Fourier numbers of interest in solid-rocket nozzle heat-transfer range from about 0.005, for nonconductive materials with large diameters or at small times of a few seconds, to about 2, for conductive materials with small diameters and long durations of approximately 100 sec. Biot numbers range from about 0.8 for low chamber pressures, small diameters, and high conductivities, to about 150 for high chamber pressures, large diameters, and low conductivities.

Figure 16 shows the effect of errors in density and heat capacity on exposed and insulated surface temperatures for $B = 10$, $R = 0.8$, and $F = 0.05$ and 0.10. This combination of conditions would apply to an 8-in. thick tungsten, hot-flow tested at a pressure of 750 psi at 30 and 60 sec. The gas temperature for this case is 7000°F, but other calculations show that gas temperature has a negligible effect upon the percentage error.

Figure 16 shows that errors in either density or specific heat of 20% or less result in surface temperature errors of less than 5%. The effect of errors in density or specific heat decreases with increasing Fourier number: at the higher Fourier number a 40% error results in less than a 5% error in surface temperature. Also, positive errors in density or specific heat (values greater than the actual) result in negative errors in temperature (values less than the actual) and vice versa.

The effect of thermophysical property errors on temperature is much greater at the insulated than at the exposed surface. The curves of Figure 16 also show that the insulated surface temperature error which arises as a result of errors in density or heat capacity is 2 to 2.5 times greater than at the exposed surface. For the same conditions, the effect of errors in thermal conductivity on surface temperature is negligible. A positive error of 50% or a negative error of 25% in conductivity results in a surface temperature error of less than 1%. Insulated-surface temperature errors which arise from thermal-conductivity errors, shown in Figure 17, are many times greater.

Errors in duration that arise from density or heat capacity errors will have the same magnitude and direction as the errors in density or heat capacity. This is a direct result of the fact that time appears only in the denominator.

For the conditions discussed, positive and negative conductivity errors of 20% will result in duration errors of -8% and 12%, respectively.

An examination of many curves of thermophysical properties as a function of temperature shows that, on the average, the variation in thermal conductivity between room temperature and several thousand degrees is approximately 2 to 2.5 times as great as the variation in heat capacity and 40 to 50 times as great as the variation in density. Although the exact magnitude of the error will depend on the specific heat transfer conditions involved, generally errors resulting from uncertainties in thermal conductivity and heat capacity at elevated temperatures are of the same order of importance, whereas errors resulting from uncertainties in density are important only for the most precise calculations.

The use of constant, as opposed to variable, thermal properties was also investigated for the basic system. In most heat transfer calculations, constant thermal properties are used because of the added complexities of handling variable properties. Sometimes, large errors can result if the constant properties are not chosen properly. In this case, as shown in Figure 18, only a small difference resulted when constant properties were used. The difference increases in going towards the outside of the nozzle.

E. EFFECT OF ANISOTROPY

The recent development of pyrolytic graphite, a material that has considerably different thermal conductivities along different axes, has created interest in the use of anisotropic materials for nozzles. Since the initial announcement of the development of pyrolytic graphite approximately 2 years ago, work has been conducted on the development of a group of other high-temperature anistropic materials, pyrolitic carbides(1). Under the current program, an effort was made to show the possible advantages of using either a material which is inherently anisotropic or a design in which anisotropy is figuratively inferred.

Most present-day nozzle designs that incorporate pyrolytic graphite make use only of its high-temperature limitation and its insulative qualities. For example, it may be used as a very-high-temperature insulator or as an insulating flame barrier to block heat transfer to the wall. Its use as a flame barrier at the throat, however, is in question because the hot surface heats up quickly to within a few hundred degrees of the gas temperature while the surface furthest from the gas remains cool; a serious thermal shock problem is the result.

---

(1). Being developed by Raytheon Company Research Division, Waltham, Massachusetts.

For this study, a conceptual nozzle design was made that uses the high thermal conductivity of pyrolytic graphite parallel to the grain. This design is shown in Figure 19. The nozzle throat is tungsten and the rest of the nozzle is made of graphite and pyrolytic graphite, with an asbestos phenolic insulator and a steel load-bearing member. The pyrolytic graphite is oriented so that the highest conductivity is in the direction parallel to its longest axis. The pyrolytic graphite acts as an insulating flame barrier along the surface of the nozzle in the upstream and downstream sections and, in the interior, conducts heat away from the tungsten throat to cooler portions of the nozzle. The pyrolytic graphite on both sides of the tungsten conducts heat away from the hot surface and prevents heat from entering the tungsten throat area from the side. (Considerable modifications would probably have to be made before such a nozzle could be built.)

Temperature distribution in the nozzle is shown at 93 sec, when the tungsten surface temperature reaches 6100°F (Figure 20a). For comparison, the temperature distribution in a similar nozzle, with all the pyrolytic graphite replaced by ordinary graphite, is shown in Figure 20b. The temperatures reached in the nozzle with pyrolytic graphite are 470 to 600°F lower than those in the nozzle without pyrolytic graphite. The tungsten throat of the nozzle shown in Figure 20b reached 6100°F at its surface within 53 sec. A portion of the pyrolytic graphite section that shows temperatures of 6800°F would have eroded by 93 sec, but this should not seriously affect the condition at the throat. The high temperatures at the graphite-asbestos phenolic interface indicate that either an insulator with a higher maximum allowable temperature (for example, pyrolytic graphite) or thicker graphite should be used.

III. TEST PROGRAM

A. TEST OBJECTIVES

The objectives of the test program were to determine the effects of flame barrier and insulation thickness upon duration capability, to establish the proximity of actual to calculated temperature distributions, and to investigate the effect of aluminum oxide deposition on materials system capability.

B. NOZZLE DESIGN

Six nozzles of 0.70-in. throat diameter were tested. The three-material model was used for the nozzle, and the flame barrier and insulator throat thicknesses were varied. The nozzle consisted of a tungsten flame barrier, a zirconium oxide insulator, and a chrome-molybdenum (4130) steel load-bearing member. Flame barrier thicknesses at the throat varied from 0.150 to 1.00 in., and insulator thicknesses varied from 0.155 to 0.55 in. The insulator thickness was at least large enough to maintain the steel at its maximum allowable temperature of 700°F. Steel thicknesses were 0.11 in., except for the nozzle with the thinnest throat, where design considerations necessitated a 0.23-in. thickness. Also because of design considerations, the steel member was omitted from the nozzle with the thickest throat. Figure 21a is a sketch of the basic materials system tested. The nozzles with the two thinnest throats were of slightly different design. These are shown in Figures 21b and 21c.

The entrance section consisted of a thin graphite cone, cemented inside a precast zirconium oxide shell. Use of a large heat sink in the entrance section was deliberately avoided.

The tungsten throat insert was machined from a forging of 95+ percent theoretical density and a purity of 99.75%, certified by the vendor.[1] The tungsten was flame sprayed on the outside with zirconium oxide (Rokide Z) of 72- percent theoretical density. A steel sleeve was cemented to the outside of the oxide coating. Flat-bottomed thermocouple holes were then drilled to various depths. The entire nozzle throat assembly was made by the same vendor.

C. TEST CONDITIONS AND EQUIPMENT

1. Test Conditions

The propellant consisted of a polyurethane rubber matrix containing ammonium perchlorate oxidizer and 16% aluminum. Nominal chamber pressure was 350 psi. The calculated combustion temperature was 5750°F at 1000 psi and the actual temperature was estimated to be 5600°F at 350 psi. Nominal firing durations for the motor were all higher than calculated expected durations for the nozzle, assuming no aluminum oxide deposition, and ranged from 50 to 110 sec.

2. Test Rocket Motor

The test rocket motor contained an end-burning grain and had a nominal diameter of 8 in. Nominal length was about 25 in. and firing durations were increased by using a longer chamber. The chamber was made of steel pipe and was water-cooled during the test.

(1) Straza Industries, El Cajon, California

The steel aft closure shown in Figure 22 was designed to accomodate thermocouples. The nozzle assembly was cemented to the aft closure, which was bolted to the motor. Figure 23 is a photograph of a typical aft closure assembly before firing. The thermocouple connection plugs are shown wrapped with insulation material.

3. Instrumentation

Pressure was measured with a Taber pressure transducer by means of a pressure tap in the aft end of the chamber. This was connected to a continuous recorder. Two readings were taken and averaged.

Each nozzle was instrumented with six thermocouples, all located at the throat at various depths. Four types were used: tungsten/tungsten-26% rhenium, tungsten/rhenium, platinum/platinum-13% rhodium, and chromel/alumel.

The use of tungsten-type thermocouples represented an attempt to measure temperatures above 3200°F near the hot surface of the flame barrier. Neither of the two tungsten/tungsten-rhenium thermocouples[1] produced any usable results. The tungsten/rhenium thermocouples[1] were insulated with beryllium oxide and were assumed to be reliable up to 4000°F; one of the 10 used was chosen at random and calibrated between 2000 and 4000°F. The calibration data agreed very well with the accepted calibration curve for tungsten–rhenium. During the tests, some of these thermocouples showed signs of erratic behavior at about 3000°F.

(1) Continental Sensing, Inc., Melrose Park, Ill.

Four thermocouples of the first three types were used to measure temperatures in the tungsten. One platinum/platinum-13% rhodium thermocouple measured the temperature in each insulator and the temperatures in each steel section were measured with one chromel/alumel thermocouple. Two thermocouples were placed in the insulator of the nozzle in which the steel load-bearing member was omitted. The thermocouples, except for the tungsten/tungsten-rhenium, were secured with Swagelok fittings[1]. Table 5 shows the locations of the thermocouple holes. The radial distances from the nozzle axis were obtained from prefiring measurements of the depths of the holes, the throat radii, and the outside diameter. These were checked against direct measurements of two holes in each nozzle after the nozzle was hot-flow-tested and sectioned. The measurements agreed within 0.005 in.

D. PROCEDURES

Each nozzle assembly was inspected after receipt. The throat diameter was measured to the nearest 0.001 in. and the average of four readings was taken. The depths of the thermocouple holes were measured to the nearest 0.001 in. Photographs of the nozzle and aft closure were taken immediately before and after firing. During firing, the nozzle was photographed with high-speed motion picture and closed-circuit television cameras. After disassembly, each insert was photographed, and the throat contour was traced on transparent paper with an optical comparator at a magnification of 10X. The throat area was then measured from the trace (shadowgraph) with a planimeter. The diameter after firing was calculated by assuming a true circle. The nozzles were cut in half along the long axes and photographed again; each cut was made through two of the thermocouple holes, and the distance to the inside nozzle surface was measured directly.

(1) Swagelok Tube Fittings, Cleveland, Ohio.

Temperature distributions were calculated for each nozzle, assuming one-dimensional heat transfer and a heat transfer coefficient based on constant nominal pressure. Two-dimensional, axisymmetric heat transfer calculations were also made for the nozzles with 0.45 and 1.00-in. tungsten throat thicknesses. The calculated temperature distributions were then compared with the thermocouple readings for the nozzles in which no aluminum oxide deposition occurred. Where deposition occurred, the measured temperature data were used to obtain an experimental heat transfer coefficient. The difference in resistance to heat transfer represented by the experimental and theoretical heat transfer coefficients was assumed to be a measure of the resistance offered by the deposited oxide layer. This was compared to the measured deposit thickness and an average thermal conductivity was obtained for the deposit.

E. TEST RESULTS

Photographs taken immediately after testing of each of the six nozzles are shown in Figure 24. (The nozzle shown in Figure 24c is an exception to this statement, as the photograph taken immediately after firing was not usable; the one shown was taken after disassembly of the aft closure.) The nozzles are arranged in order of decreasing tungsten throat thickness. Considerable deposition occurred where the nozzle throats were thick. The thinnest nozzles were burned through during the firing. The test results are summarized in Table 6. Pressure vs time, temperature vs time, and shadowgraphs for each nozzle are shown in Figures 25 through 40. Shadowgraphs were not taken of the two nozzles that burned through during firing. Ignition delays of approximately 10 sec occurred in tests No. 3 and 4 and are shown graphically in Figures 27, 28, 32, and 33.

The amount of aluminum oxide deposition, as determined from the shadowgraphs, is shown as a function of tungsten throat thickness in Figure 41.

F. CORRELATION OF TEST DATA

1. Discussion of Nozzle Burnthrough

The nozzle designs were such that the thinnest sections were upstream of the throat. A hoop-stress calculation[1] shows that 0.08-in.-thick tungsten is required at an area ratio of 3.2, upstream of the throat, for a chamber pressure of 350 psi. The tungsten inserts in the two nozzles that failed during firing were 0.10 and 0.13 in. thick, respectively. These values are represented by safety factors of 1.3 and 1.6. It is postulated that the failure of these two nozzles occurred in the entrance section when the insulation was heated beyond its softening point and could no longer transmit load to the steel. The tungsten, forced to carry the full load, yielded and failed.

Calculations show that the insulator at the throat should reach its assumed limiting temperature of 4600°F at 6 and 14 sec for the 0.15-in.-thick and the 0.30-in.-thick tungsten, respectively. The time for the insulation in the entrance section to reach the same temperature was not calculated, but should be approximately the same, or a little greater, because of the balance between decrease in heat transfer coefficient and decrease in tungsten flame barrier thickness. The pressure and temperature curves indicate that burnthrough started at approximately 1.5 and 3.5 sec after ignition for the nozzles with 0.15-in.-thick and 0.30-in.-thick tungsten, respectively. The starting of burnthrough so soon after ignition could be attributed either to an assumption of too high a value for the limiting insulator temperature or to a slight crack in the tungsten that went undetected because it occurred after assembly. In this

---

(1) $t = \frac{Pd}{2\sigma\cos\phi}$ = wall thickness, in.

where: $P = 0.976\ (350)$ psi
$d = t + 0.70$ in.
$\sigma = 2000$ psi allowable stress for tungsten at 4800°F
$\phi = 32°$ entrance angle

instance, thermal shock was discounted as a reason for failure because the thickest nozzles, which remained intact, should have suffered the most severe shock.

The next larger insert (0.45-in. tungsten throat thickness) was 0.13 in. thick at its thinnest section. Although the throat remained intact, a portion of the entrance section was burned through to the steel shell (Figure 42).

2. Comparison of Calculated Temperatures with Test Data

For the two thinnest nozzles, calculated temperatures and the test data agree fairly well, but, because of deposition, the results for the other nozzles show consistently lower temperatures than calculated.

In tests No. 4 and 5, the two thinnest nozzles, the thermocouples in the tungsten at the section where burnthrough occurred show lower temperatures than those on the opposite side and show the greatest temperature rise after burnthrough started, as indicated by the pressure curves. These thermocouples were probably not operating after about 3.5 sec and are not represented on the comparison curves. In addition, TN 3 on test No. 4 was inoperative and is not shown.

In test No. 4, where 0.030-in.-thick tungsten was used, agreement was excellent for thermocouples TN 1 and TN 2 (Figure 43). The calculated temperatures began at the end of the ignition delay of 9.7 sec. After 30 sec, the pressure was very low, with a corresponding reduction in heat transfer coefficient. This probably accounts for the leveling off of the temperature shown by TN 3.

In test No. 5, where 0.15-in.-thick tungsten was used, agreement was fairly good for TN 1 and TN 2 (Figure 44). The measured

insulator temperature (TN 3) was far below the calculated value; the discrepancy is probably a result of improper installation of the thermocouple. The insulator material is such that particles come off when it is scraped. The scraping action of the thermocouple when installed could easily rub off enough particles to cause a large displacement of thermocouple location. A difference of 0.03 in. in location could result in temperature error of 25%.

A two-dimensional heat transfer calculation made for the nozzles of tests No. 1 and 2 and shown in Figures 45 and 46 account for only a very small portion of the difference between measured and calculated temperatures. The remainder of the difference was ascribed to aluminum oxide deposition. An attempt was made to determine an average heat transfer coefficient for the entire firing time by comparing the measured data with temperature distributions calculated by assuming various heat transfer coefficients as shown in Figure 47. The result was an "experimental heat transfer coefficient" (h_{exp}). Assuming a steady-state condition exists between the film and the wall, the difference between reciprocals of the experimental heat transfer coefficient and the heat transfer coefficient calculated from the average chamber pressures should be equal to the average thermal resistance of the aluminum oxide film. The film resistance is compared with the average film thickness, and a film conductivity (k_f) is calculated. The average film thickness is taken as half the thickness measured after firing. The calculation is summarized in Table 7. Values of k_f found by this method average 5.4 Btu/hr-ft-°F. The best available data for solid aluminum oxide[1] show conductivities of about 5.8 Btu/hr-ft-°F for the dense material, when the data are extrapolated to the melting point; this is an excellent agreement. No data are available for the conductivity of molten aluminum oxide. This calculation demonstrates that temperature data and deposition thickness can be correlated.

---

(1) A. Goldsmith and T. E. Waterman, Thermophysical Properties of Solid Materials, WADC TR 58-475, October 1958, p. VII-M-1.

IV. CONCLUSIONS

A. ANALYSIS

1. For a nozzle materials system, an optimum balance between duration and material thickness may be found. This optimum is a practical measure of duration capability; above it, nozzle weight increases rapidly for small increases in duration.

2. Optimum duration decreases rapidly with small increases in chamber pressure or gas temperature, but increases in throat diameter for diameters above 4 in. affect optimum duration only slightly.

3. In constant-weight systems, increases in chamber pressure or gas temperature result in decreases in duration; the effect is greater at higher durations.

4. Flame-barrier and heat-sink thermophysical properties significantly affect duration capability, while insulator and load-bearing member properties do not. Flame barriers should generally have moderately high thermal conductivities, high products of density and specific heat, and low densities. A high product of density and specific heat is more important than high conductivity in selecting heat-sink materials.

5. Four-material systems can be designed lighter in weight than three-material systems because heat sinks usually have lower densities than flame barriers.

6. Increases in maximum allowable material temperature result in duration increases or weight decreases; the increase or decrease is above the optimum point for the flame barrier and below the optimum for the insulator.

7. Thermal conductivity and heat capacity errors that result from uncertainties in thermophysical properties at elevated temperatures are of the same relative order of importance, but errors resulting from uncertainties in density are important for only the most precise calculations. Positive thermal conductivity errors and negative density or heat-capacity errors will result in conservative estimates of duration capability.

8. Use of a properly oriented anisotropic material could result in increased duration capability.

B. TEST PROGRAM

1. The test data show that it is possible to predict nozzle temperatures fairly accurately only when no deposition occurs on the nozzle wall during firing.

2. When deposition occurs, the measured temperature is lower than the calculated value but may be brought very close to agreement by consideration of the deposit thermal blocking effect in the calculation.

3. The amount of deposition that occurs during a firing increases as the heat-sink thickness increases, resulting in longer durations than could be achieved with the lower surface temperatures due to increased thickness alone.

4. Insulator temperatures are difficult to measure accurately because of the difficulties involved in obtaining a good seat at the bottom of the thermocouple hole and in measuring thermocouple locations accurately.

V. RECOMMENDATIONS

A. MATERIALS RESEARCH AND DEVELOPMENT

The following areas are most promising for future materials research and development, as applied to solid rocket nozzles.

1. Use of the following criteria, listed in order of importance, to determine the potential of future nozzle materials from the heat transfer point of view.

a. flame barriers

(1) high allowable temperature
(2) high product of density and specific heat
(3) moderately high conductivity
(4) moderately low density

b. heat-sink materials

(1) high product of density and specific heat
(2) moderately high conductivity
(3) low density
(4) moderately high allowable temperature

c. insulator

(1) high allowable temperature

d. load-bearing member

(1) low density

2. Development of boron carbide for use as a nozzle heat-sink material.

3. Development of techniques to manufacture high-temperature anisotropic materials so that either the conducting or insulating properties may be used in any direction desired.

B. NOZZLE BEHAVIOR INVESTIGATIONS

In addition to the above areas for materials research and development, the following areas hold promise for future analytical and experimental investigations to obtain significant knowledge of nozzle behavior:

1. Effects of induced thermal stresses, thermal shock resistance of materials, and effects of erosion characteristics on duration capability should be investigated.

2. The effects of aluminum oxide deposition should be studied, especially the mechanism of deposition, the properties of the deposit, and the use of the deposit as an auxiliary flame barrier to block heat transfer to the wall.

3. Attention should be given to the use of anisotropic features in nozzle design. The use of anisotropic materials is merely a first step in this direction. The possibilities of conducting heat more efficiently to the cooler sections of the nozzle, perhaps with finned flame barriers, should be investigated.

4. A more detailed study of weight vs duration, especially as the entire missile system is affected, would be helpful to nozzle design.

VI. BIBLIOGRAPHY

1. Carslaw, H. S. and J. C. Jaeger. Conduction of Heat in Solids. 2nd ed. London, The Oxford Press, 1959.

2. Colucci, S. E. "Experimental Determination of Solid Rocket Nozzle Heat Transfer Coefficient," Proceedings of the Fifth AFBMD-STL Aerospace Symposium. Vol. II. New York, Academic Press, 1960.

3. Emmons, W. F. and R. D. Allen. 90Ta-10W Alloy: Summary of Thermal Properties to Melting Point and Tensile Properties from 2500° to 4500°F. Materials Report M-2089. Sacramento, Calif., Aerojet-General Corp., 1960.

4. Fluke, G. Temperature Tables for Internally Heated Hollow Cylinders. Aerojet-General Technical Memoradnum 121-SRP. Sacramento, Calif. Aerojet-General Corp., 1959.

5. Goldsmith, A. E. and T. E. Waterman. Thermophysical Properties of Solid Materials. WADC TR-58-476. Wright Air Development Center, Wright-Patterson Air Force Base, Ohio, October 1958.

6. Goldsmith, A. E. and T. E. Waterman. Thermophysical Properties of Solid Materials. WADC TR-58-476, Revised. Wright Air Development Center, Wright-Patterson Air Force Base, Ohio, August 1960.

7. Grover, S. S. Analysis of Nozzle Heat Transfer Coefficient. Aerojet-General Technical Memorandum 113-SRP. Sacramento, Calif., Aerojet-General Corp., 30 April 1959.

8. Landau, M. H. Aerojet-General Corporation memorandum 5510:0265M. Sacramento, Calif., Aerojet-General Corporation, 5 November 1958.

9. McAdams, W. H. Heat Transmission. 3rd ed. New York, McGraw-Hill, 1951.

10. Neel, D. S., C. D. Pears, and S. Oglesby, Jr. The Thermal Properties of Thirteen Solid Materials to 5000°F or Their Destruction Temperatures. WADD TR-60-924. Wright Air Development Center, Wright-Patterson Air Force Base, Ohio, November.

11. Porter, H. Rocket Refractories. NAVORD 4893 (AD-95 482). 26 August 1955.

12. Reactor Handbook. Vol. 3, Section 1. AEC, March 1955.

13. Solid Engine Design Handbook. Aerojet-General Corporation, August 1957

14. Thermal Properties of Certain Materials. AVCO RAD-TM-THERMO. 2 February 1957.

15. Tsang, S. and R. F. Kimpel. Investigation of Materials Capabilities of Materials Systems in Solid Rocket Motors. WADC TR-59-602, Part I. Wright Air Development Center, Wright-Patterson Air Force Base, Ohio, March 1960. (CONFIDENTIAL)

TABLE 1

LIKELY NOZZLE MATERIALS

Function	Material	Distinguishing Characteristics
Flame Barrier	1. Refractory Metals (W, Ta-W, Mo)	High conductivity High density
	2. Graphites	Moderate conductivity Low density
	3. Refractory Carbides (HfC, TaC, TiC, ZrC)	Low conductivity High melting points
	4. Pyrolytic Graphite, Pyrolytic Carbides	Anisotropy
Heat Sink	1. Graphites	High-Temperature Limitation
	2. Beryllium Oxide 3. Boron Carbide	High specific heat ($> 0.4 \frac{Btu}{lb - °F}$)
Insulator	1. Plastics (Refrasil or Asbestos Phenolic, Graphite Cloth with Phenolic Resin)	Low conductivity
	2. Ceramics (ZrO_2, Al_2O_3, Porous SiC)	Higher temperature limitation
Load-Bearing Member	1. Steels	
	2. Titanium Alloys 3. Super-Alloys (Udimet, Hastelloy) 4. W-Co Alloys	Strength at elevated temperatures

TABLE 2

RANGE OF THERMOPHYSICAL PROPERTY DATA FOR NOZZLE MATERIALS

Material	Type	k, $\frac{Btu}{hr-ft-°F}$	Temp. Range °F	C_p, $\frac{Btu}{lb-°F}$	Temp. Range °F	ρ, $\frac{lb}{ft^3}$	Melt Point, °F	References
Tungsten		110-58	70-3500	0.03-0.05	0-4500	1205	6170	1-4
Tantalum-tungsten	90Ta-10W	32.7-19.8	2600-5300	n.a.	- - -	1050	5500	8, Stauffer-Temescal Co.
Molybdenum		84-40	100-4100	0.063-0.125	100-4600	639	4750	6
Hafnium Carbide		5.3-9	585-1686	0.055-.072	500-5000	760	7030	5
Tantalum Carbide		16.6-31.8	533-4140	0.05-0.082	500-4500	899	7010	5
Titanium Carbide	95.6% dense	15-2.8	90-2.8	0.14-0.22	70-2000	306	5860	3,4
Zirconium Carbide		18.3-20	100-4300	0.091-0.170	500-4500	417	6386	5
Graphite	ATJ	50-8	470-5000	0.17-0.5	80-3200	108	6600**	5,National Carbon Co.
	ZT-5001	120-26.5	70-3500	0.2-0.5	70-3500	127	6600**	National Carbon Co.
	Pyrolytic (with grain)	235-194	70-750	0.13-0.30	70-750	140	6600**	Raytheon Co.
	(against grain)	2.06-0.176	70-1470	0.12-0.315	70-1470	140	6600**	Raytheon Co.
Beryllium Oxide	95% dense	46-9.4	400-2550	0.25-0.495	85-1600	179	4620	3
Boron Carbide		70.5-37.5	212-1292	0.427-0.581	80-2600	156	4440	3
Astrolite (Refrasil Phenolic)	1201	0.208-0.458	0-3000	0.2-0.275	0-3000	102	3000+	7
Asbestos Phenolic	461-179	0.167-0.258	100-400	0.197-0.34	100-400	108	3000+	John Manville Co.
Zirconium Oxide	Norton "H"	0.405-0.462	800-1600++	0.175	80-2550	200	4620	Norton Co.
Aluminum Oxide	51.3% dense	9.6-1.6	40-1620	0.10-0.184	68-3270	125	3700	4, 1
Silicon Carbide	30% dense	1.5-2	800-1900	0.16-0.318	70-2250	60	4000	1, Carborundum Co.
Steel	4130	24.7	70	0.107	70	489.6	700+	9
Inconel X		7.74-16.7	68-1200	0.110-0.145	68-1200	187	1000-1500	International Nickel Co.
Titanium Alloy	REM-CRU-C-130AM	6.3-11.3	60-1400	0.13-0.207	100-1500	284	900+	1

* at room temperature

** sublimates

\+ maximum allowable

\+\+ mean temperatures

References:

1. Thermal Properties of Certain Materials, AVCO RAD-TM-THERMO, 2 February 1957.
2. H. Porter, Rocket Refractories, NAVORD 4093 (AD-95 482), 26 August 1955.
3. Reactor Handbook, Vol. 3, Section 1, AEC, March 1955.
4. A. E. Goldsmith and T. E. Waterman, Thermophysical Properties of Solid Materials, WADC TR-58-476, October 1958.
5. D. S. Neel, C. D. Pears, and S. Oglesby, Jr., The Thermal Properties of Thirteen Solid Materials to 5000°F or Their Destruction Temperatures, WADD 60-924, November 1960 (Southern Research Center).
6. A. E. Goldsmith and T. E. Waterman, Thermophysical Properties of Solid Materials, WADC TR-58-476, Revised, August 1960.
7. H. L. Thompson Company letter to A. Q. Hardrath, Aerojet-General Corporation, 19 August 1959.
8. W. F. Ransons and R. D. Allen, 90Ta-10W Alloy: Summary of Thermal Properties to Melting Point and Tensile Properties from 2500° to 4500°F, Aerojet-General Corporation, Materials Report M-2009, 1960.
9. Solid Engine Design Handbook, Aerojet-General Corporation, August 1957.

TABLE 3

REPRESENTATIVE MATERIAL PROPERTIES OF REFERENCE-SYSTEM MATERIALS

Material	k, Btu/hr-ft-°F	ρc_p, Btu/cu ft-°F	Limiting Temp, °F
Tungsten	60.0	41.3	6100
Asbestos Phenolic	0.258	41.9	3000
Steel	23.7	52.4	700

TABLE 4

REPRESENTATIVE MATERIAL PROPERTIES OF HEAT SINKS

Material	k,Btu/hr-ft-°F	ρc_p, Btu/cu ft-°F	Limiting Temp, °F
ATJ Graphite	51.6 25.0*	41.8	6600
Pyrolytic Graphite**	194	67.2	6600
Boron Carbide	40	78.0	4400
Beryllium Oxide	25	72.3	4500

---

* second value of conductivity chosen for comparison with BeO.

** oriented so that highest conductivity is in the radial direction.

TABLE 5

LOCATION OF THERMOCOUPLES

Tungsten Throat Thickness, in.	Test No.	Thermo-couple No.	Thermo-couple Type *	Relative Angular Location	Radial Distance from Nozzle Axis, in.	Material in Which Located
1	1	TW1	WRE	0°	0.496	Tungsten
		2	PPR	60	0.792	Tungsten
		3	PPR	120	1.177	Tungsten
		4	PPR	180	1.321	Tungsten
		5	PPR	240	1.502	Zirconium Oxide
		6	CA	300	1.683	Steel
0.80	6	1	PPR	0	0.471	Tungsten
		2	PPR	60	0.779	Tungsten
		3	PPR	120	1.082	Tungsten
		4	CA	300	1.523	Zirconium Oxide
		5	PPR	240	1.306	Steel
		6	WRE	180	0.484	Tungsten
0.60	3	1	WRE	0	0.464	Tungsten
		2	WRE	60	0.665	Tungsten
		3	PPR	120	0.870	Tungsten
		4	PPR	240	1.070	Zirconium Oxide
		5	CA	300	1.261	Steel
		6	PPR	180	0.457	Tungsten
0.45	2	1	WRE	0	0.434	Tungsten
		2	WRE	60	0.579	Tungsten
		3	PPR	120	0.728	Tungsten
		4	PPR	240	0.893	Zirconium Oxide
		5	CA	300	1.057	Steel
		6	WWRE	180	---	Tungsten
0.30	4	1	WRE	0	0.434	Tungsten
		2	PPR	60	0.569	Tungsten
		3	PPR	240	0.710	Zirconium Oxide
		4	CA	300	0.855	Steel
		5	PPR	120	0.433	Tungsten
		6	WWRE	180	---	Tungsten
0.15	5	1	WRE	0	0.380	Tungsten
		2	PPR	60	0.480	Tungsten
		3	PPR	240	0.566	Zirconium Oxide
		4	CA	300	0.777	Steel
		5	PPR	120	0.380	Tungsten
		6	WRE	180	0.476	Tungsten

*WRE = tungsten/rhenium
WWRE = tungsten/tungsten-26% rhenium
PPR = platinum/platinum-13% rhodium
CA = chromel/alumel

TABLE 6

SUMMARY OF TEST RESULTS

Tungsten Throat Thickness, in.	Test No.	Pressure, psia Min	Max	Avg	Time, seconds At Max Pressure	Total Duration	Throat Dia, in. Before	After	Percent Change of Throat Area
1.00	1	321	860	503	103.4	105.0	0.698	0.489	-51.0
0.80	6	325	476	386	64.8	68.3	0.705	0.593	-35.9
0.60	3	304	670	428	59.8	67.6	0.696	0.542	-39.4
0.45	2	287	380	325	50.0	54.7	0.700	0.630	-18.97
0.30	4	64	326	112	2.8	99.1	0.700	-	-
0.15	5	60	364	130	1.5	98.3	0.700		

TABLE 7

CALCULATION OF OXIDE FILM CONDUCTIVITY FROM TEST DATA

Run No.	Average Chamber Pressure, psi	Heat Transfer Coefficient Btu/hr-ft^2-°F Average	Heat Transfer Coefficient Btu/hr-ft^2-°F Experimental	Average Deposit Thermal Resistance, in./Btu/hr-ft-°F	Measured Deposit Thickness in.	Average Deposit Thickness, in.	Calculated Average Deposit Thermal Conductivity Btu/hr-ft-°F
1.	503	1392	550	0.0131	0.105	0.052	4.0
2	325	980	835	0.0022	0.035	0.018	8.1
3	428	1220	738* 663+	0.0064* 0.0069+	0.077	0.038	6.0* 5.6+
6	386	1122	640* 745+	0.0081* 0.0045+	0.056	0.028	3.5* 6.2+
Average of 4 runs							5.4* 6.0+

*Extrapolated from first two values on basis of flame-barrier thickness
+Extrapolated on basis of deposit thickness

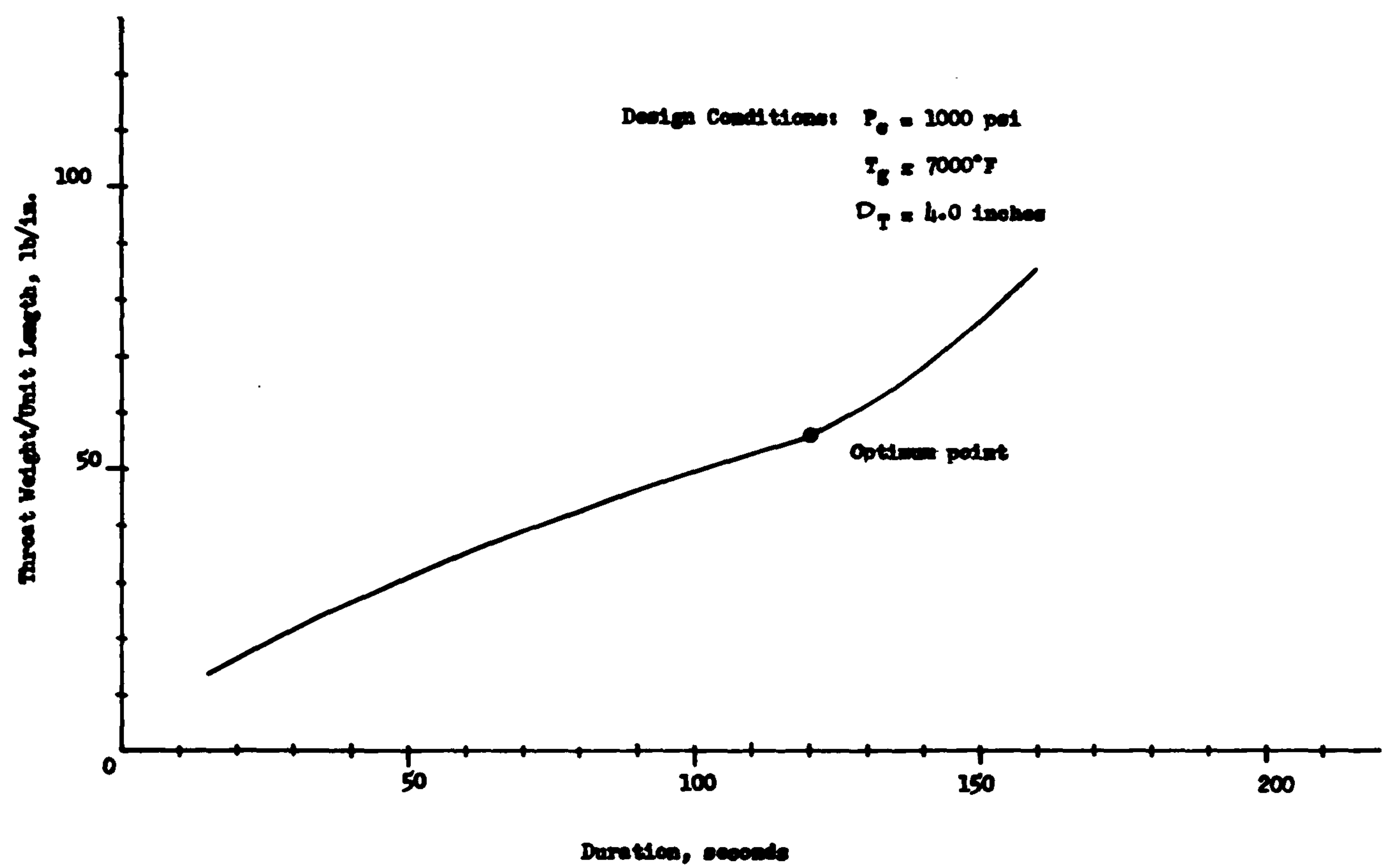

Figure 1: Minumum Nozzle Weight for Tungsten-Asbestos Phenolic-Steel

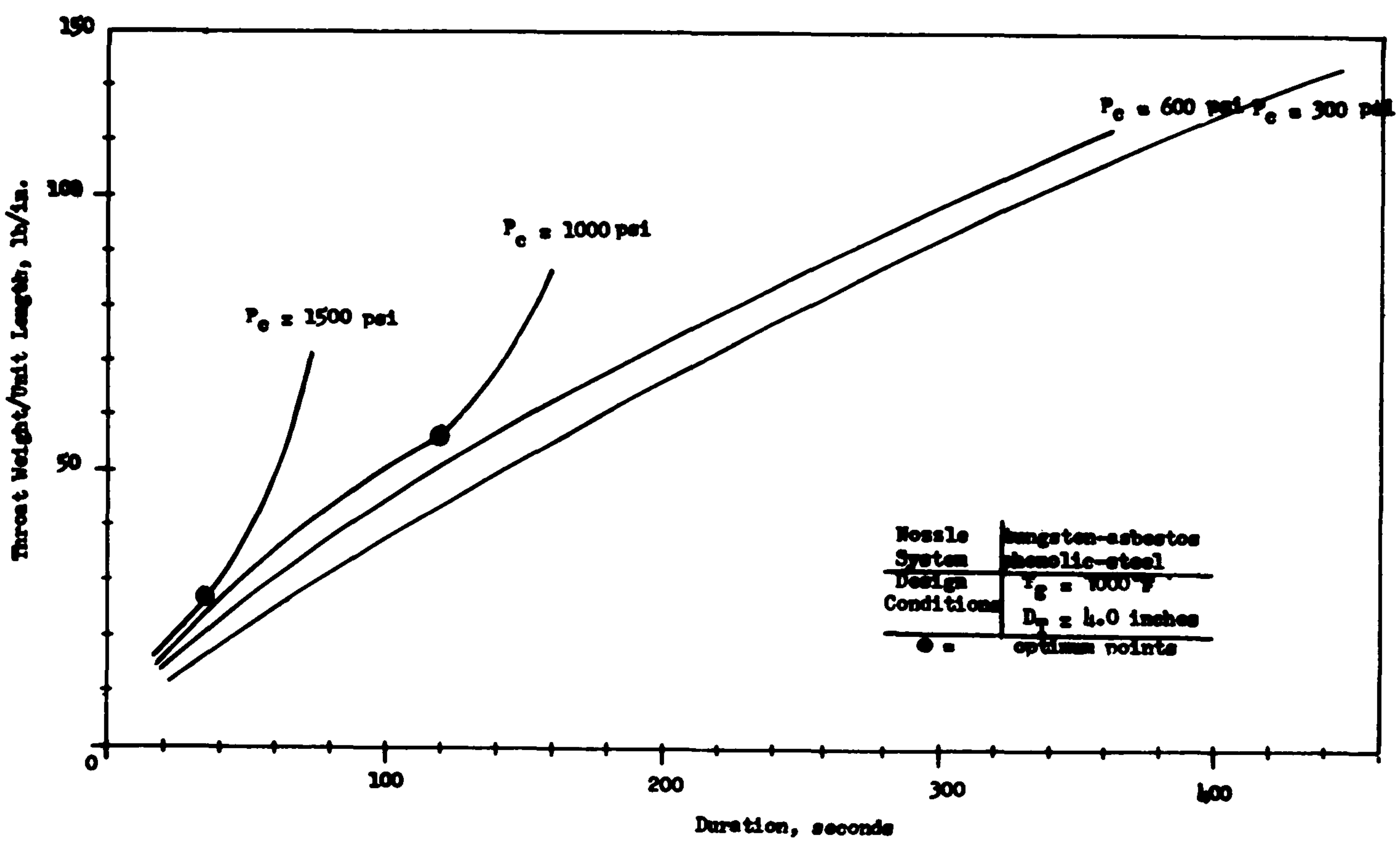

Figure 2: Minimum Nozzle Weight for Various Chamber Pressures

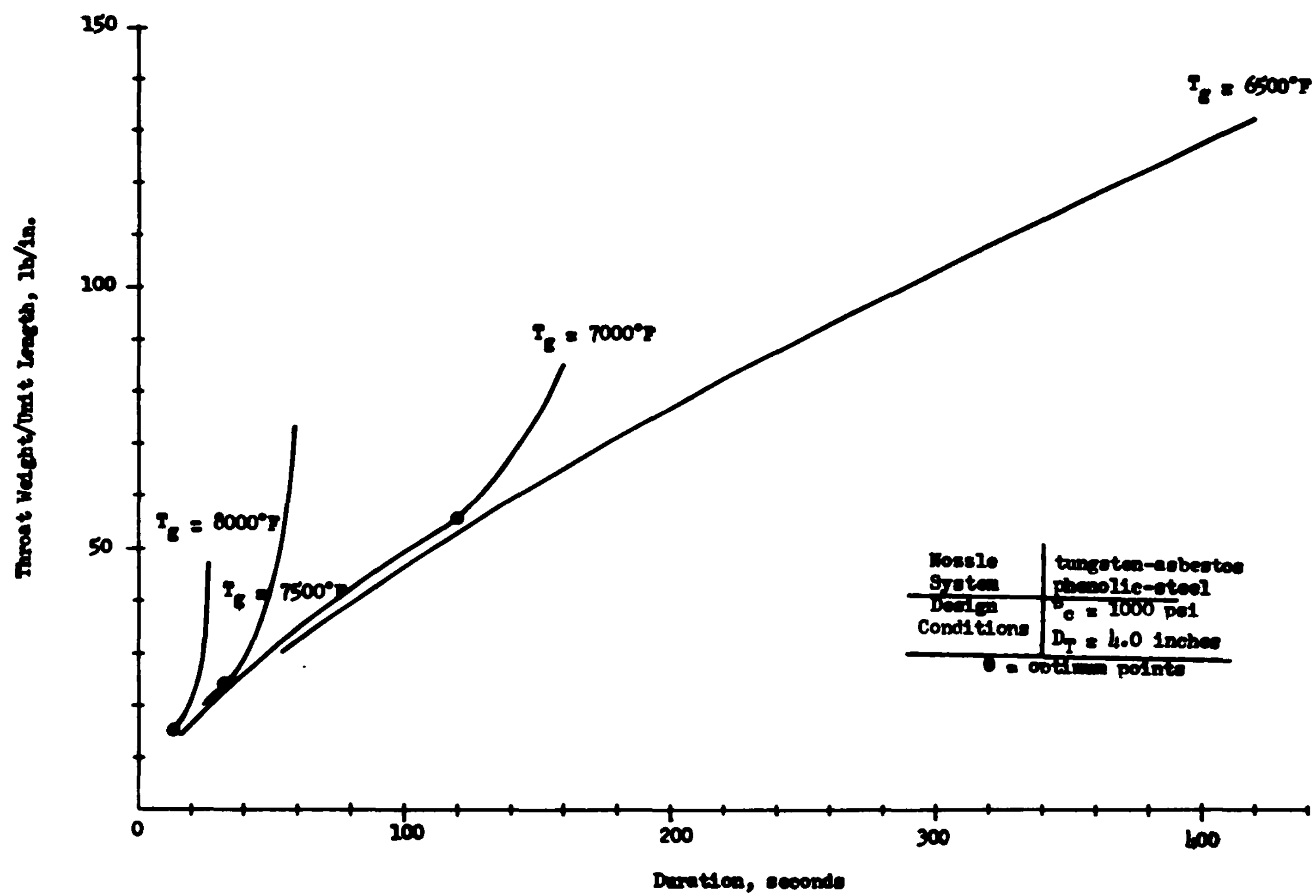

Figure 3: Minimum Nozzle Weight for Various Gas Temperatures

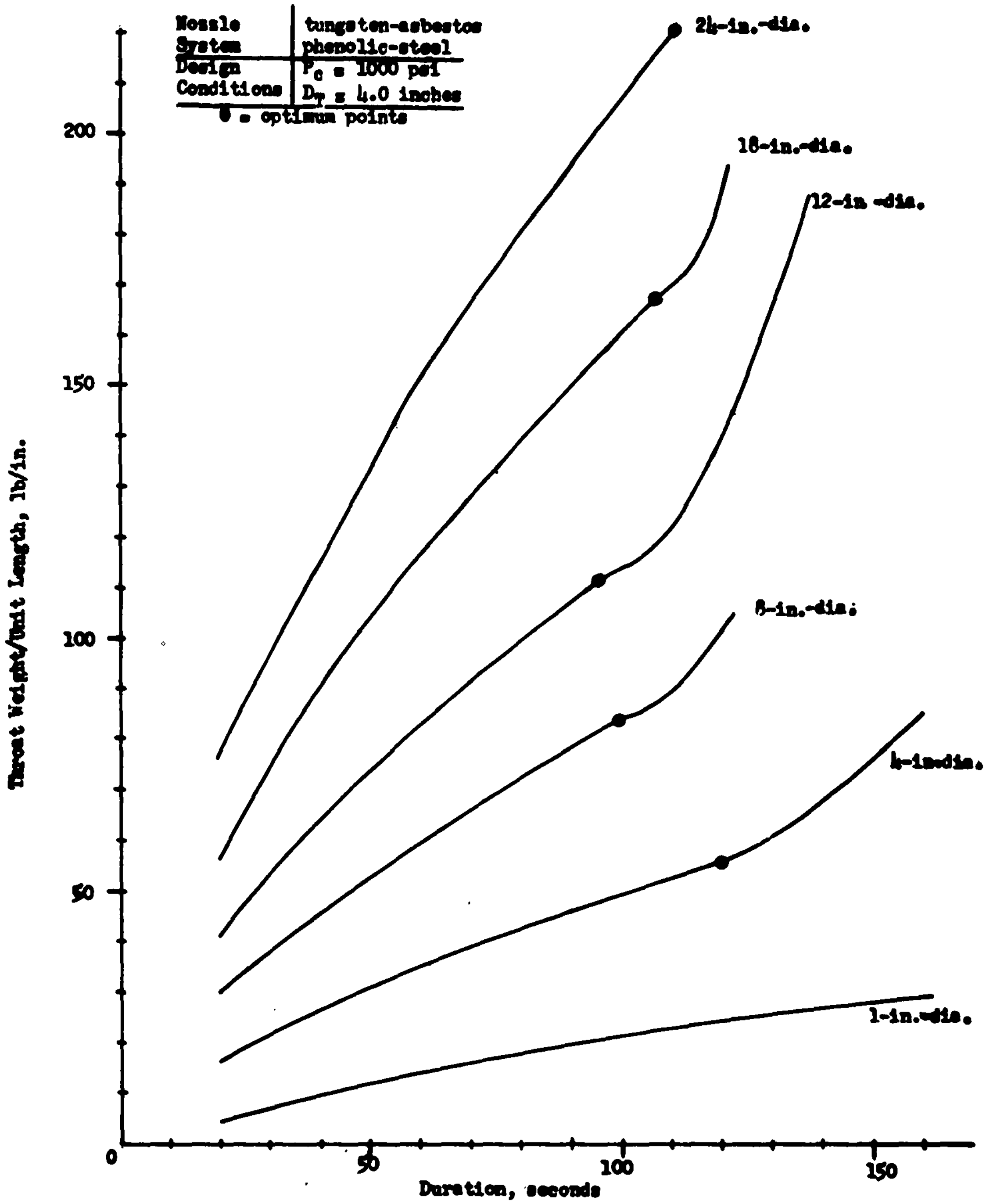

Figure 4: Minimum Nozzle Weight for Various Throat Diameters

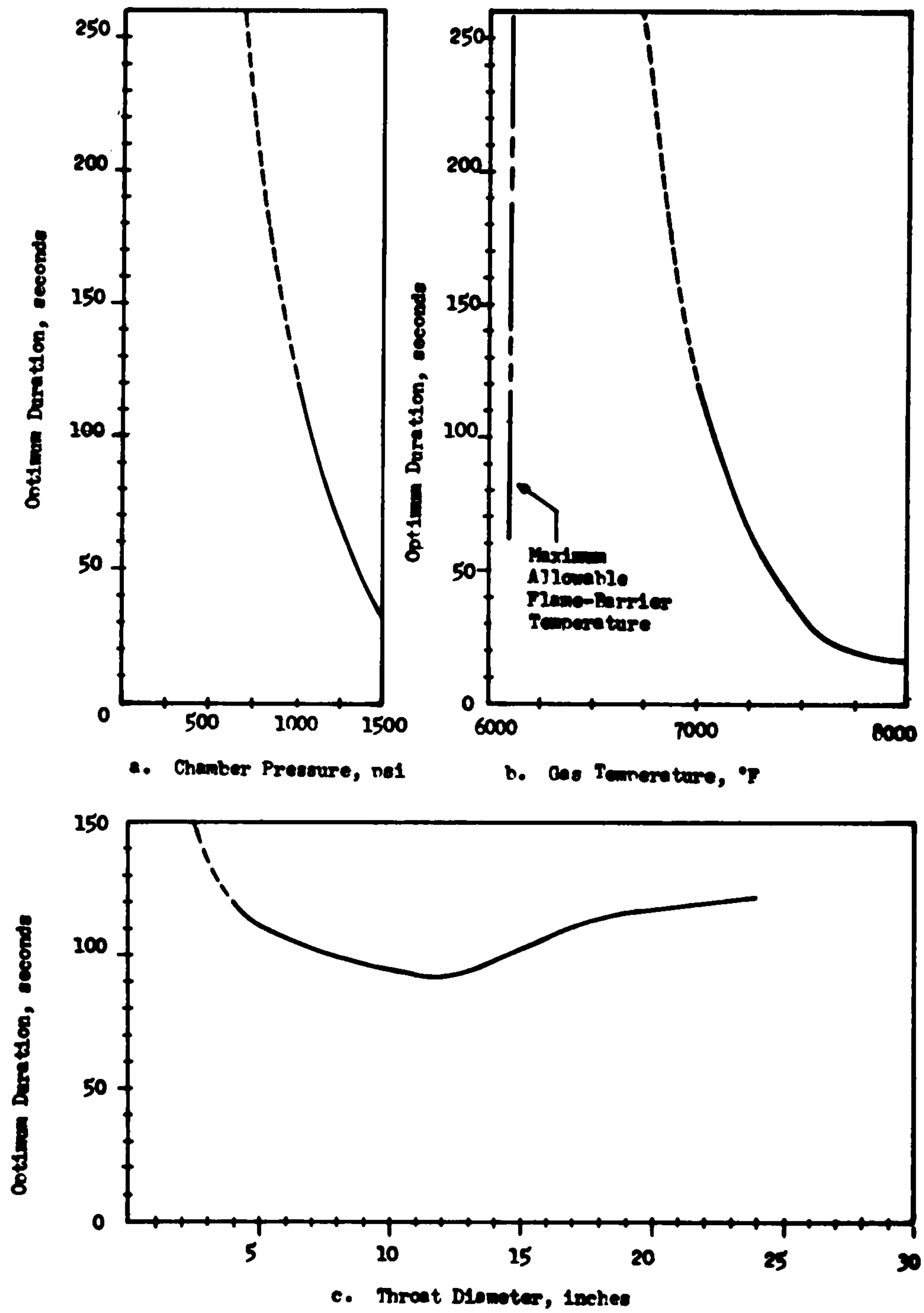

Figure 5: Optimum Nozzle Duration for Several Design Variables

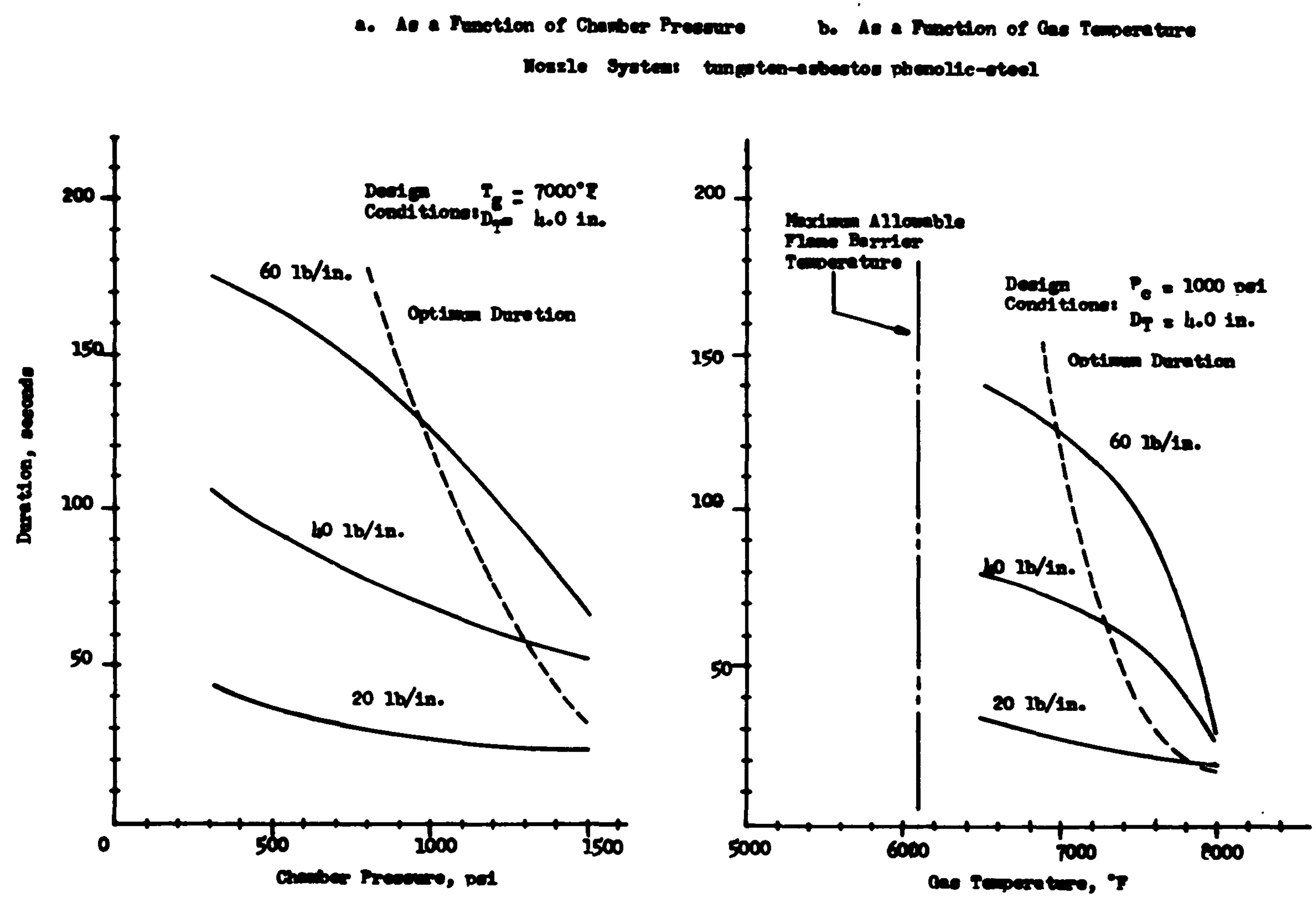

Figure 6: Nozzle Duration Capability for Constant Weight

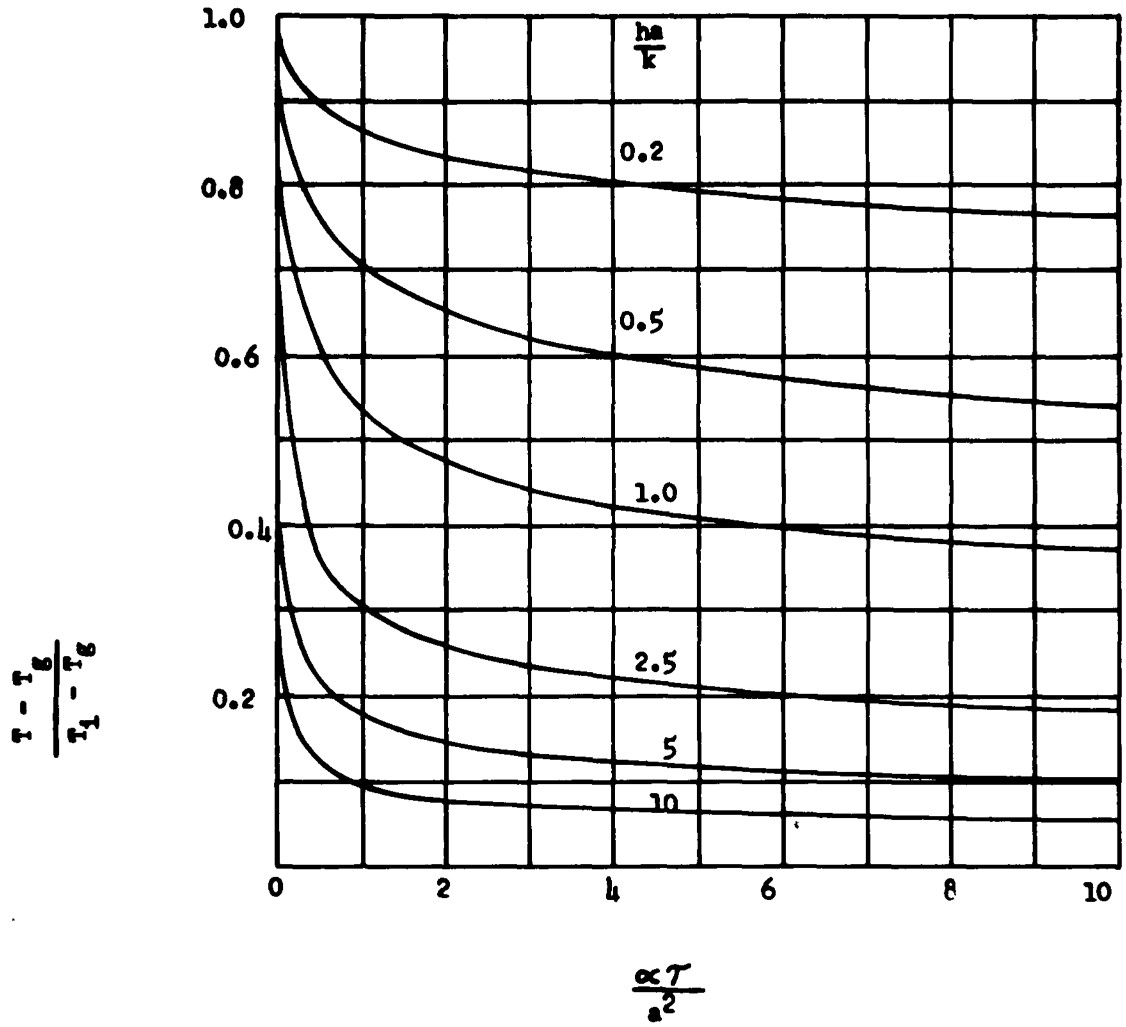

Figure 7: Temperature Distribution in Infinitely Thick Hollow Cylinder

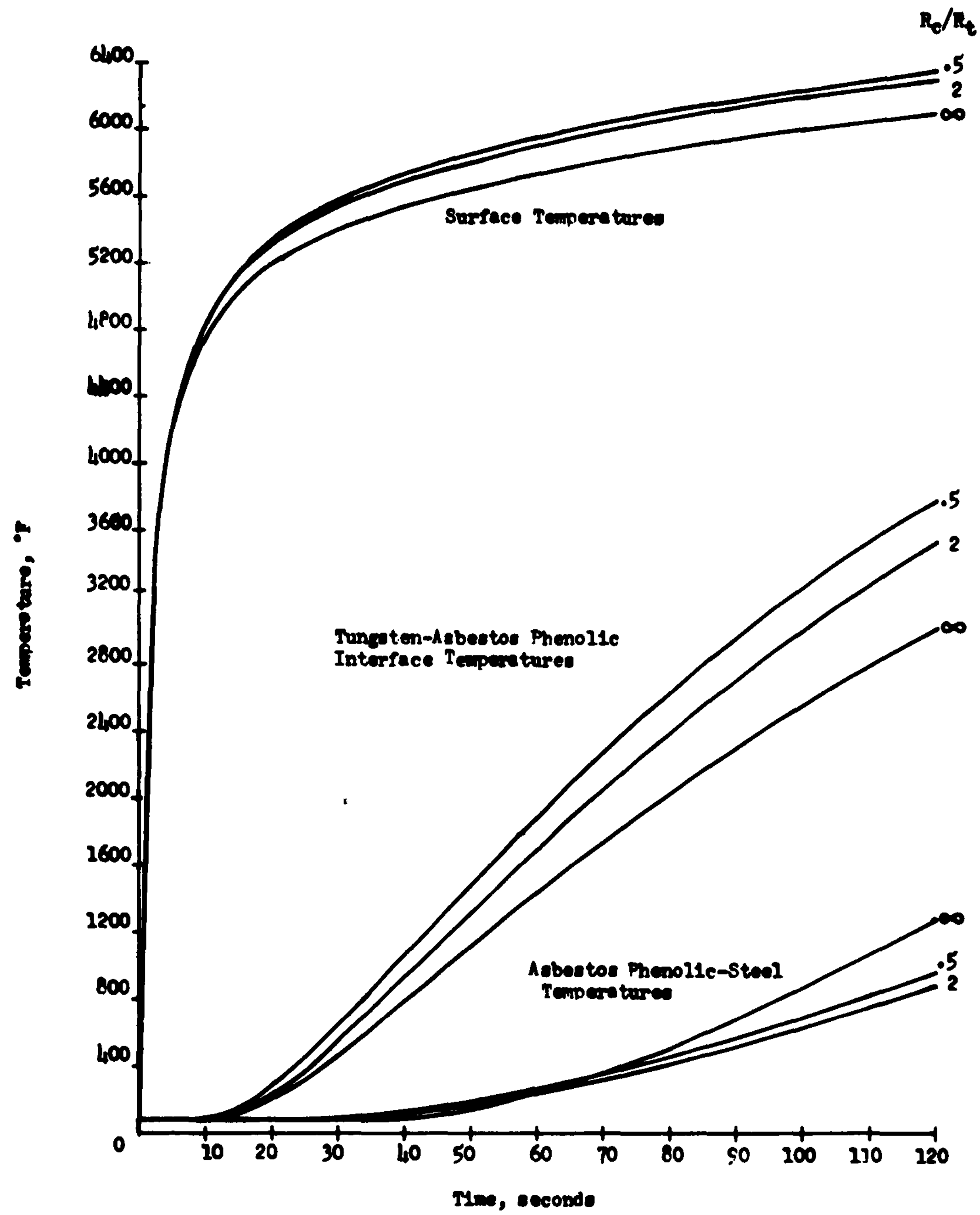

Figure 8: Effect of Radius of Curvature of Throat Upon Throat Temperature

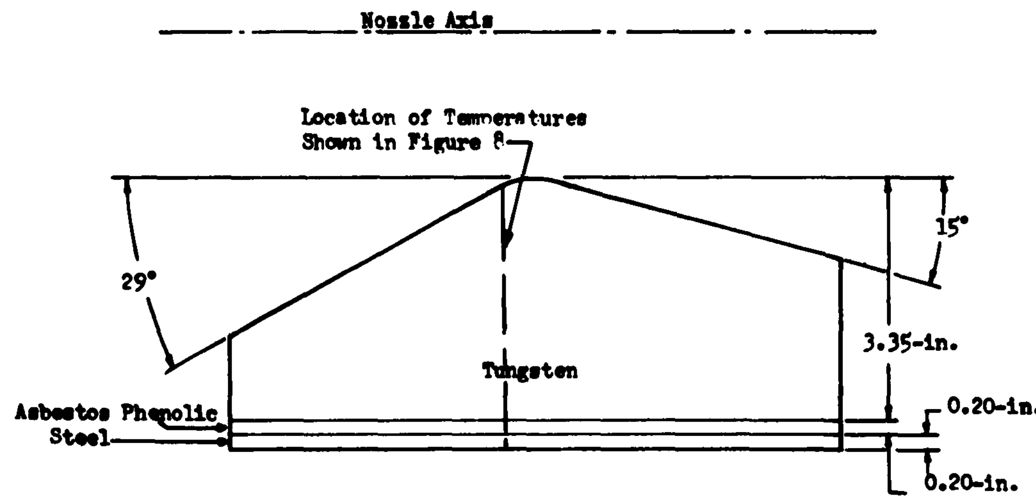

a. $\frac{\text{throat radius of curvature}}{\text{throat radius}} = 0.5$

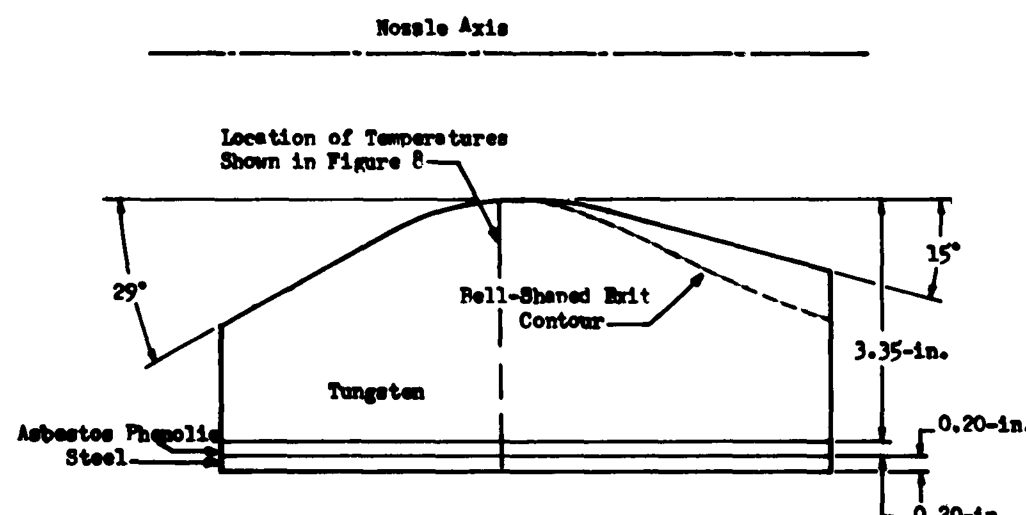

b. $\frac{\text{throat radius of curvature}}{\text{throat radius}} \approx 2.0$

Figure 9: Nozzle Models Used for Calculation of Effect of Throat Radius of Curvature

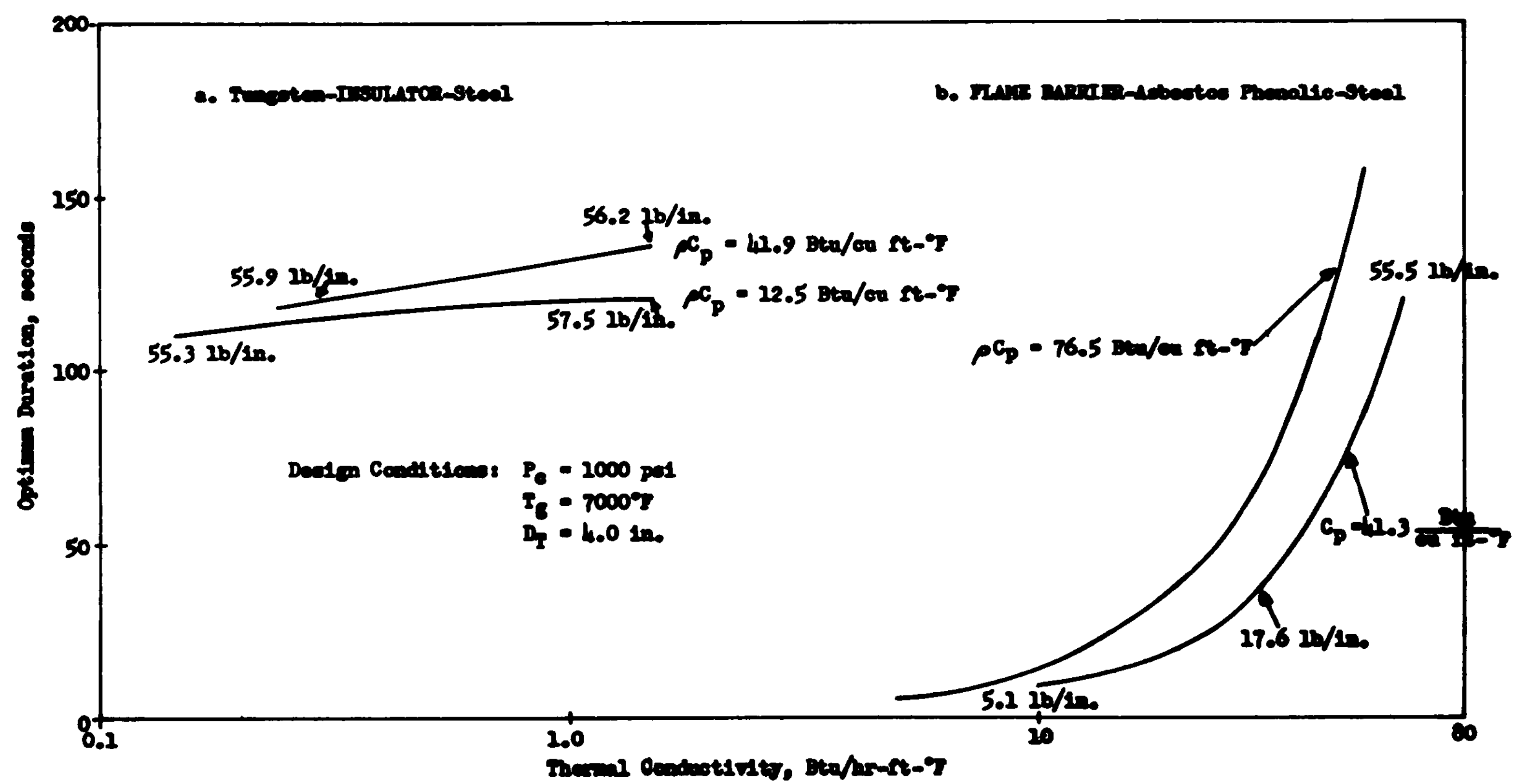

Figure 10: Effect of Thermophysical Properties Upon Optimum Duration

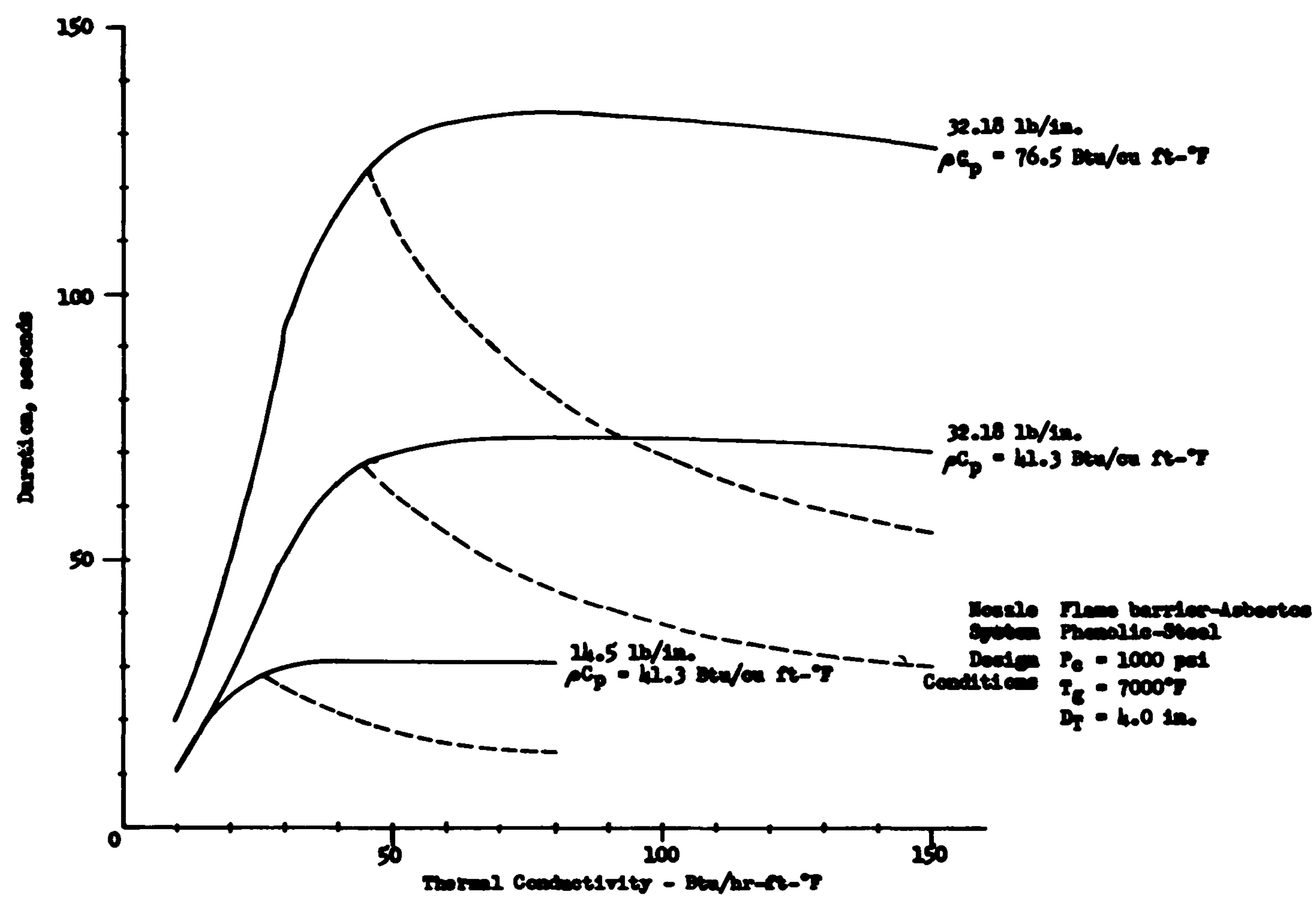

Figure 11: Effect of Thermophysical Properties Upon Duration for Constant Weight Systems

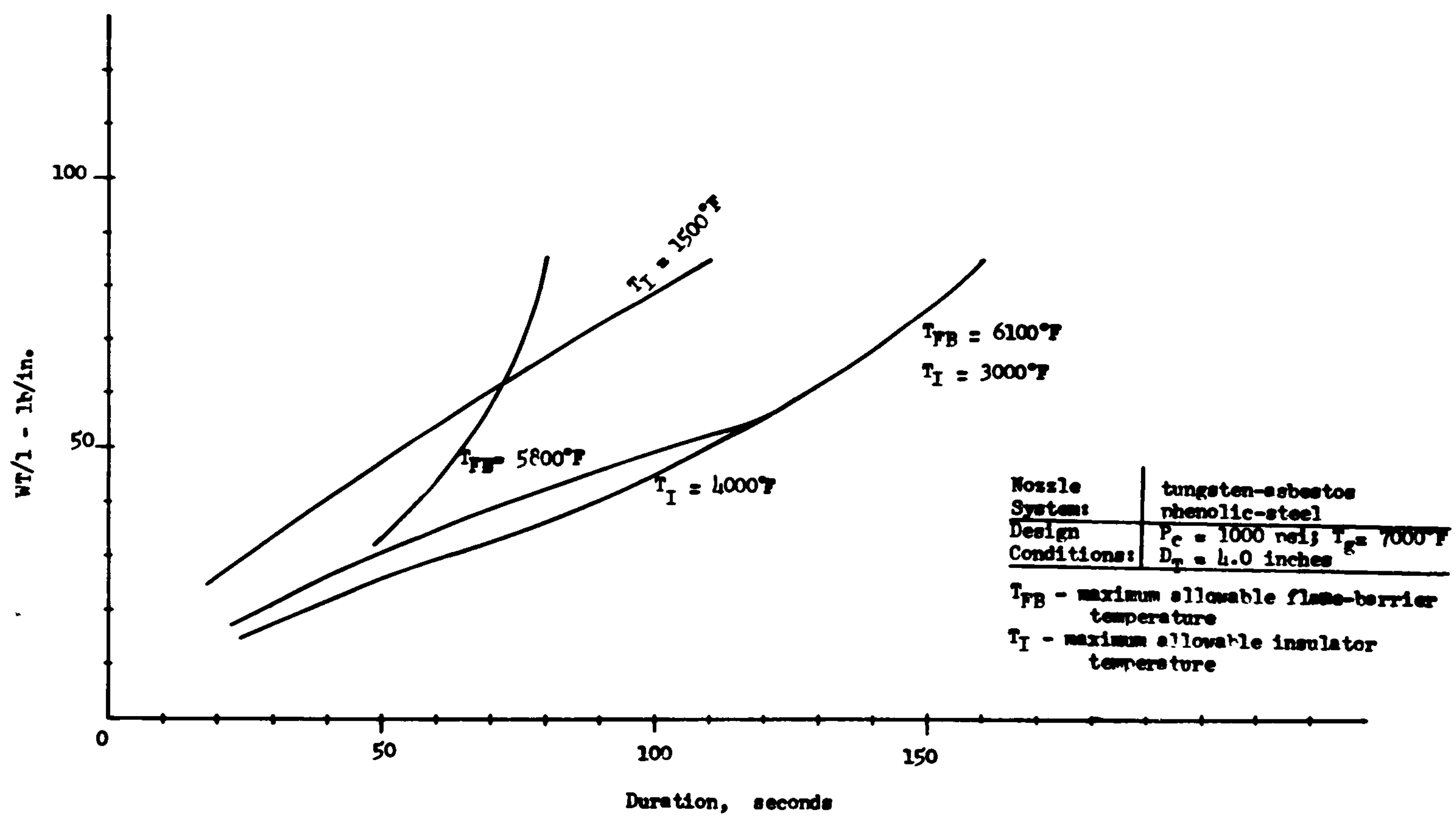

Figure 12: Effect of Maximum Allowable Material Temperature Upon Nozzle Weight and Duration

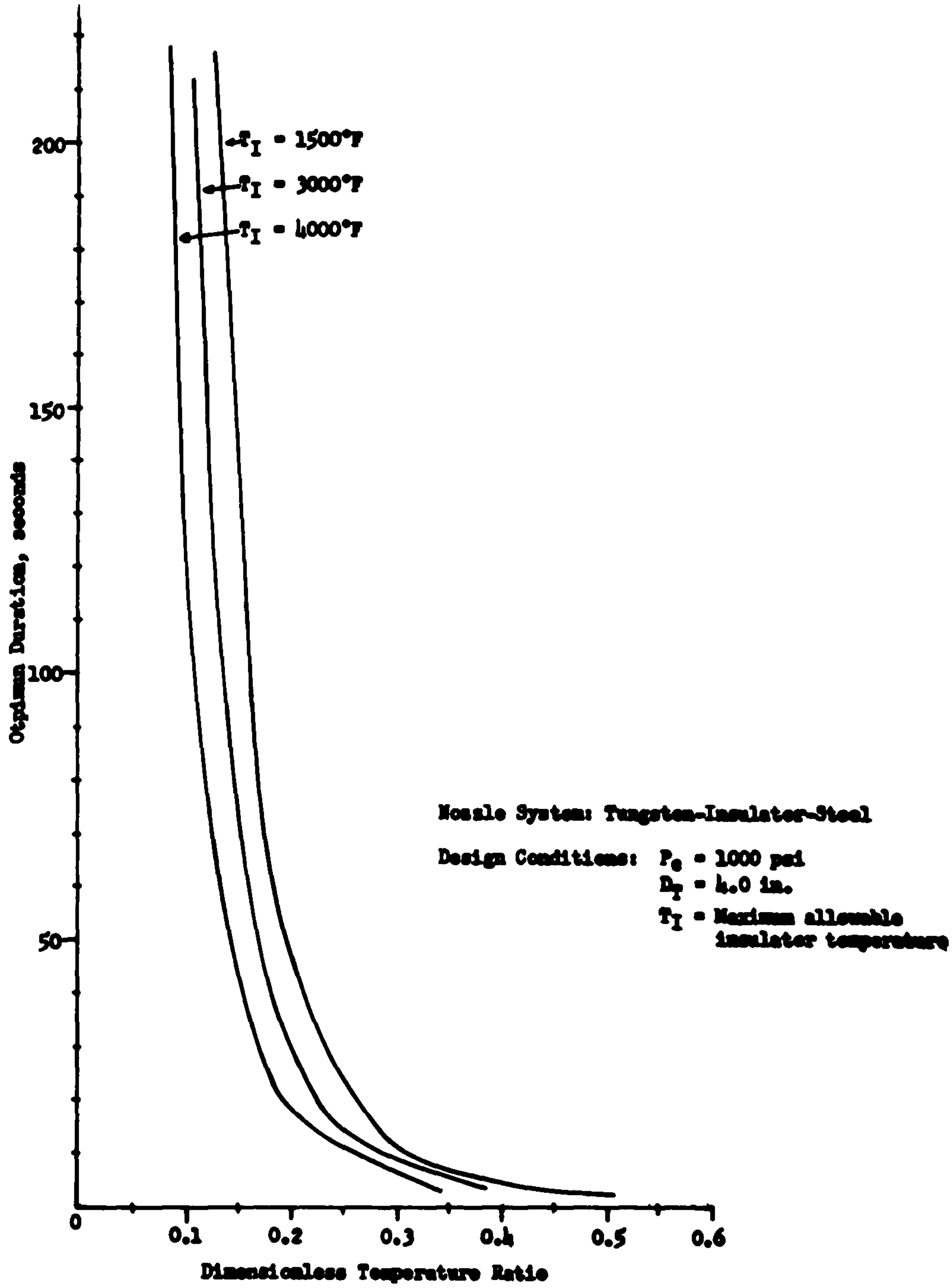

Figure 13: Effect of Dimensionless Temperature Ratio Upon Optimum Duration

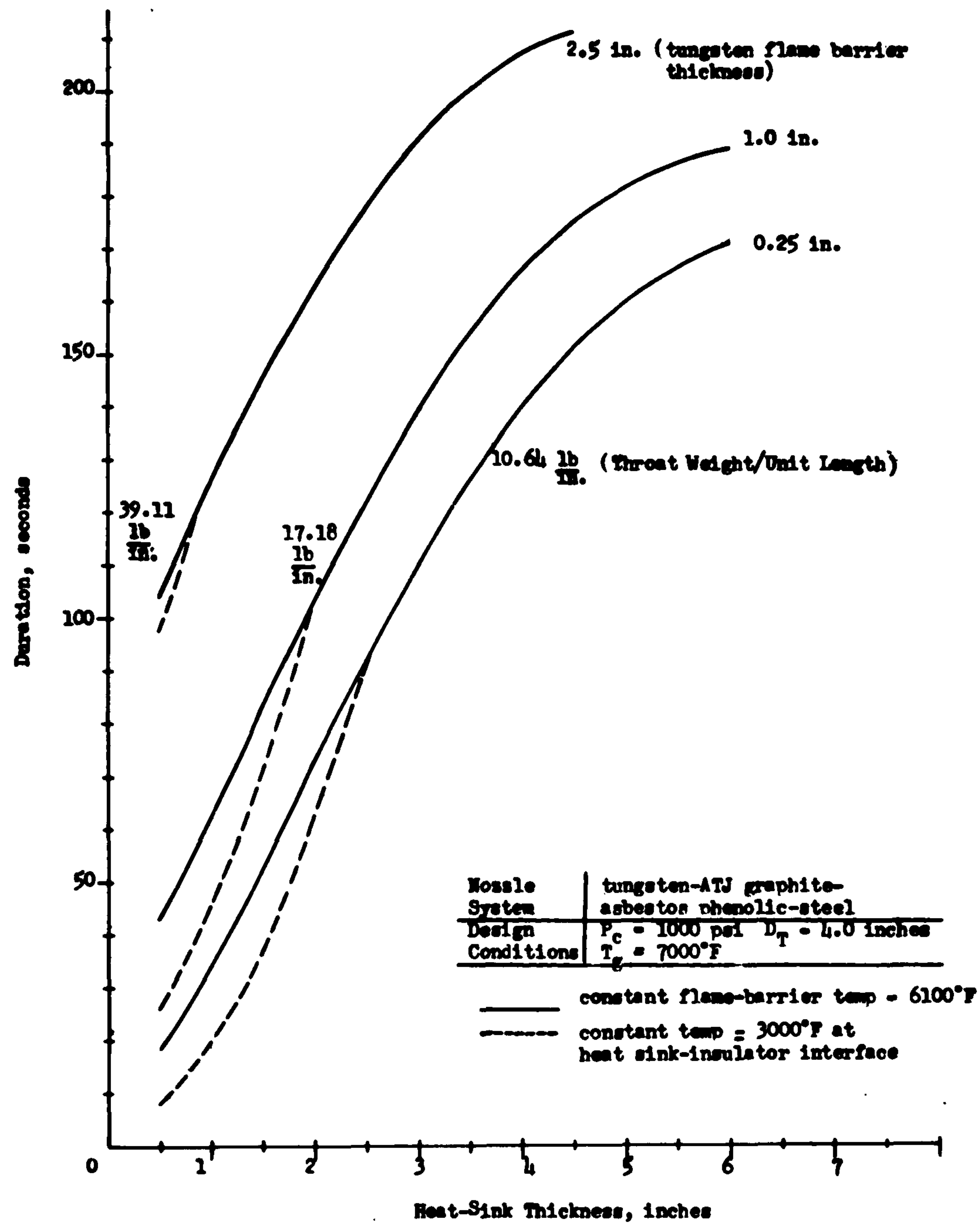

Figure 14: Effect of Heat-Sink Thickness Upon Duration

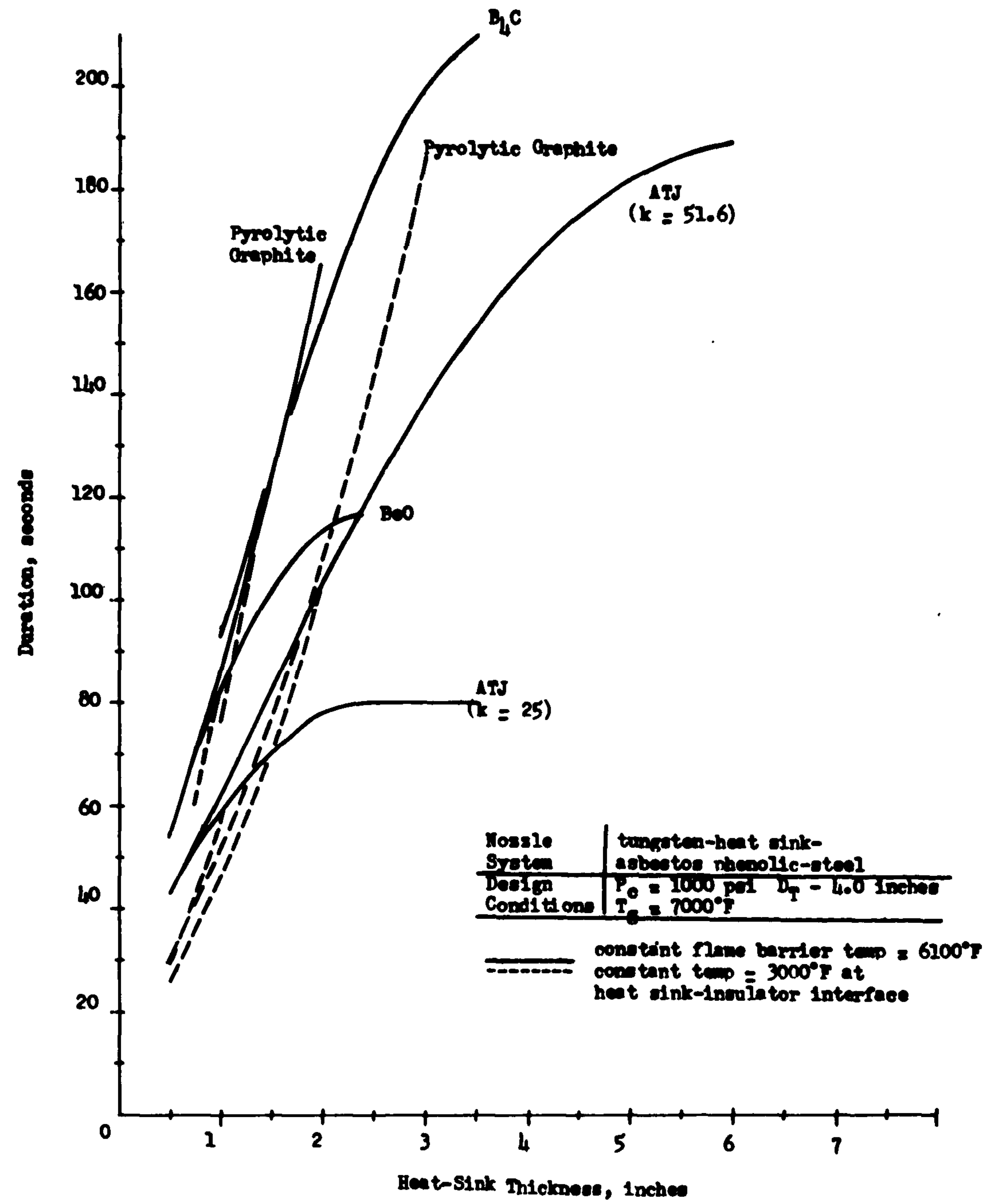

Figure 15: Effect of Heat-Sink Thermophysical Properties Upon Duration

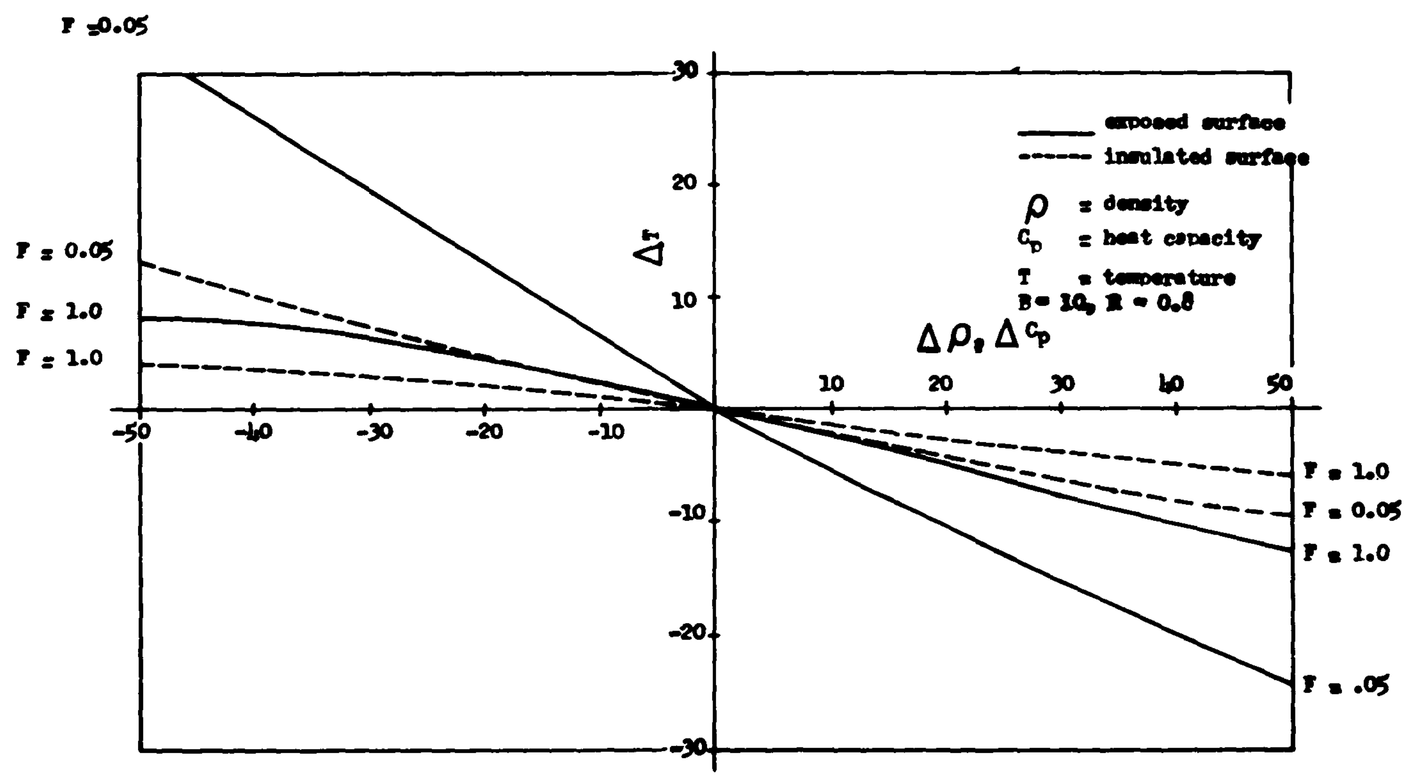

Figure 16: Effect of Density of Heat Capacity Errors Upon Exposed and Insulated Surface Temperatures

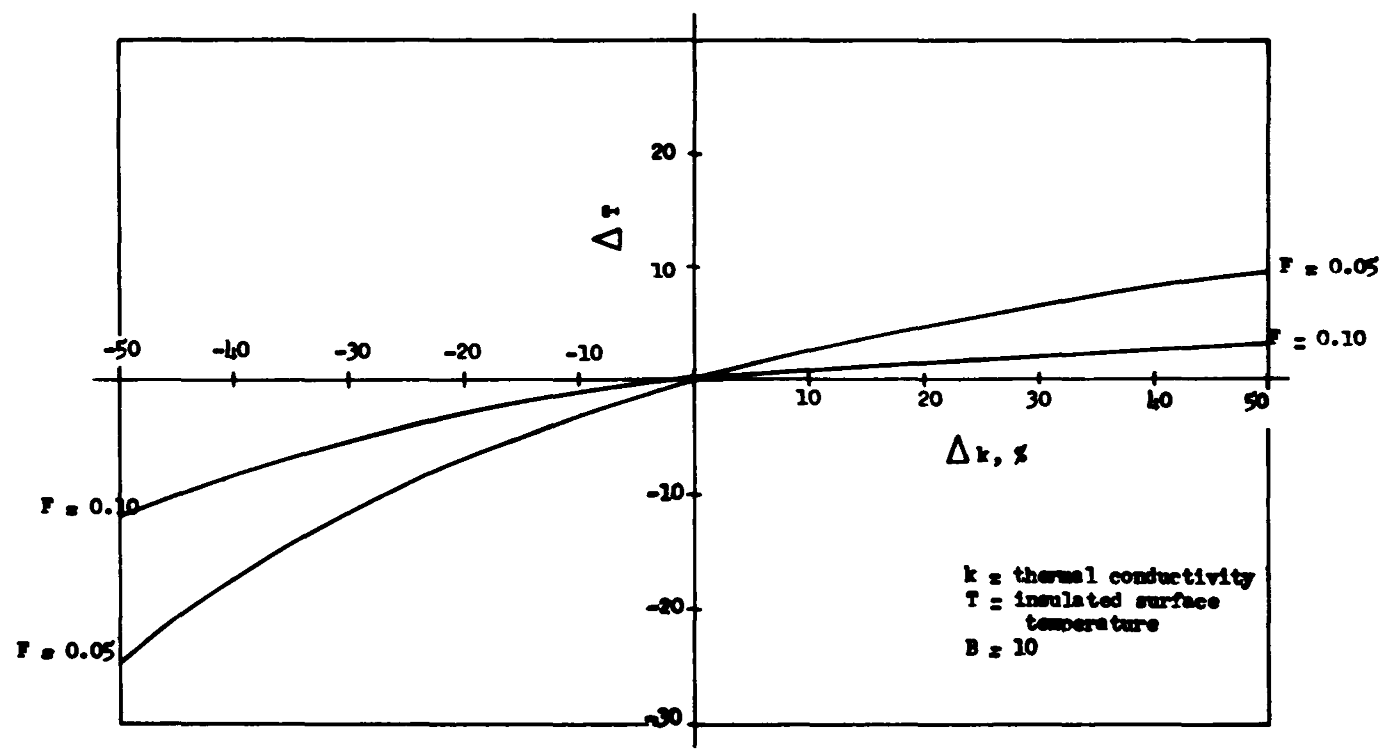

Figure 17: Effect of Thermal Conductivity Errors Upon Insulated Surface Temperature

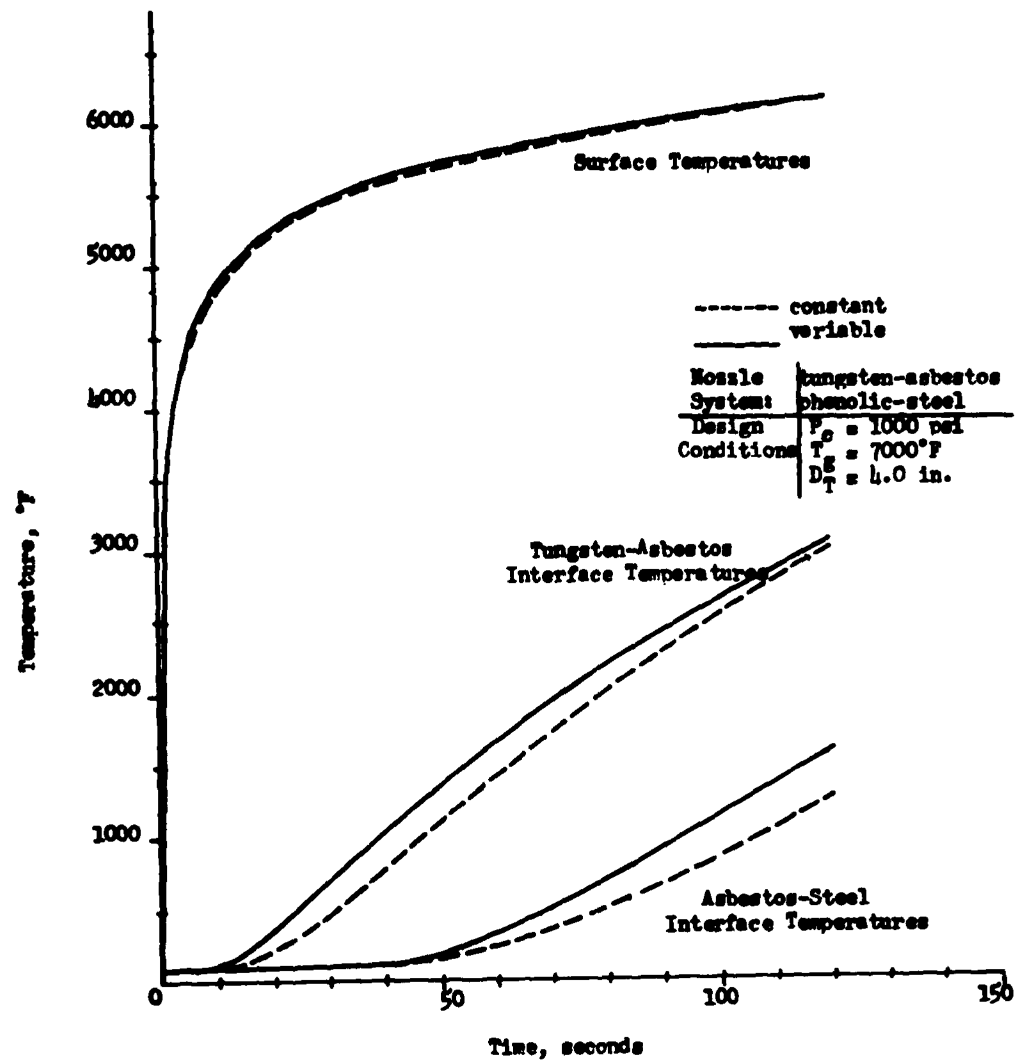

Figure 18: Comparison of Temperature Distributions Calculated by Using Constant and Variable Thermal Properties

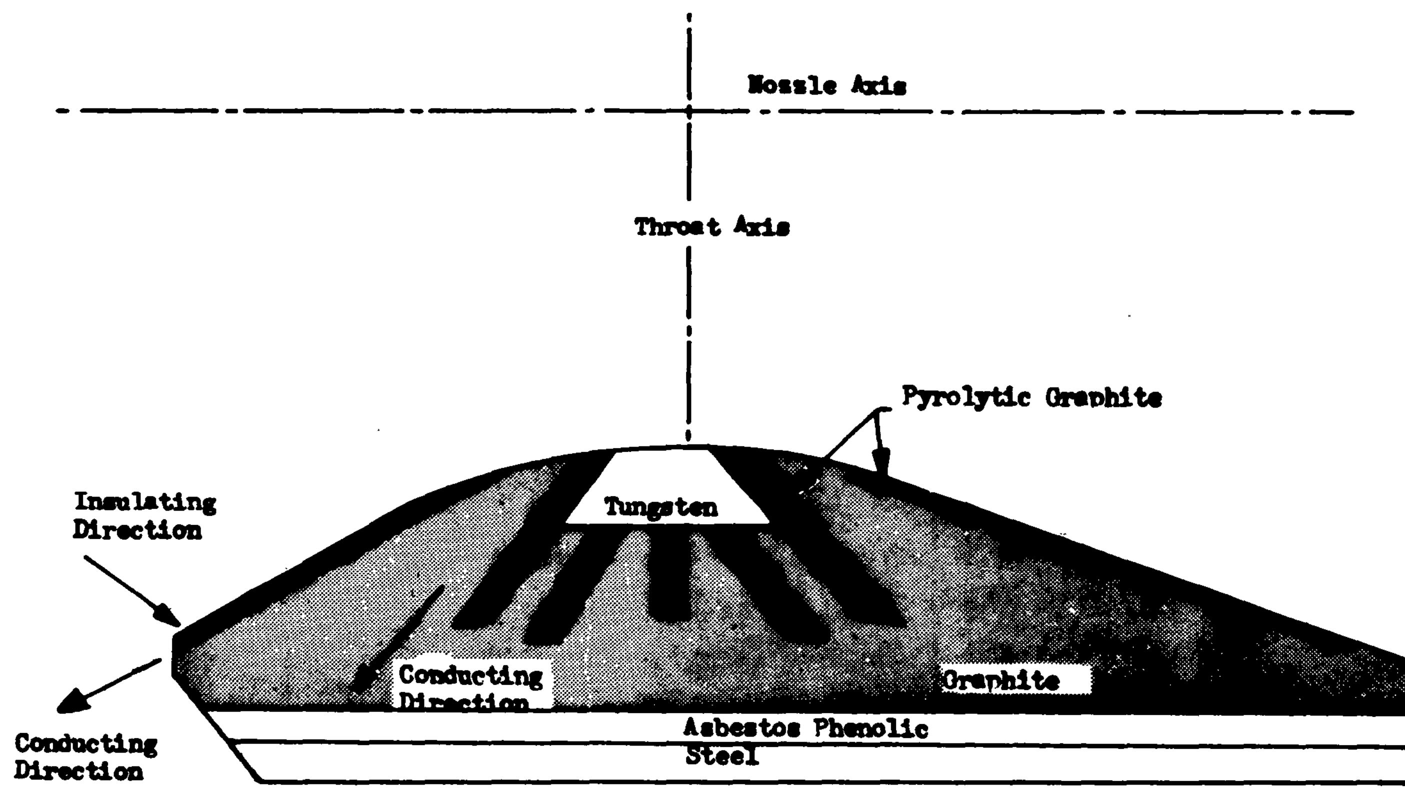

Figure 19: Conceptual Design of Nozzle Utilizing Pyrolytic Graphite

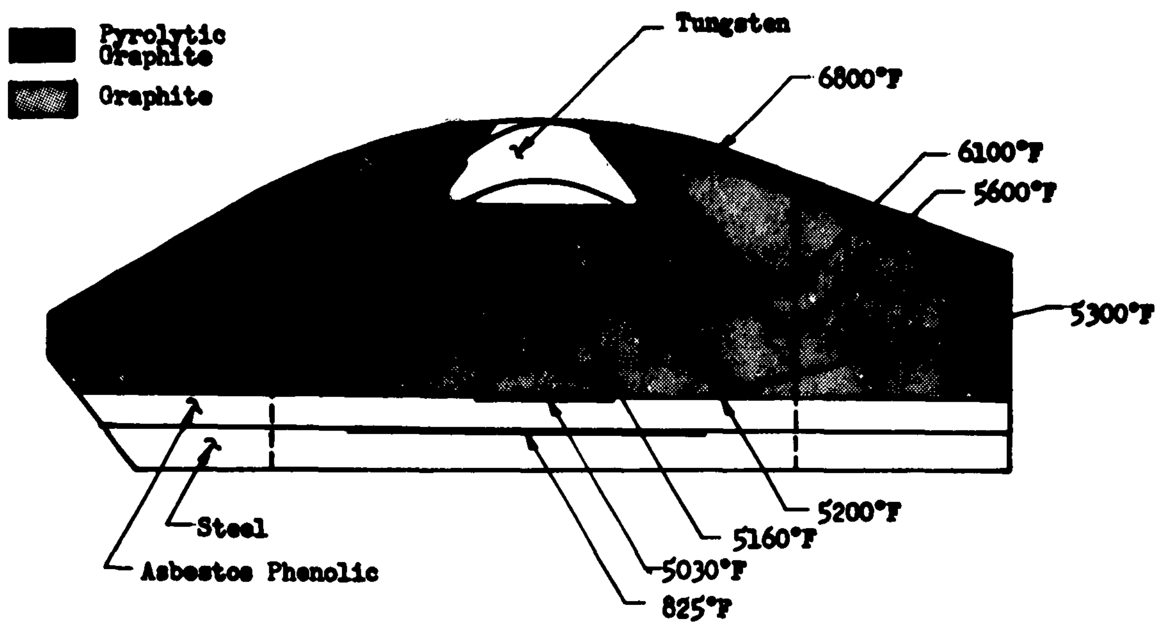

a. Nozzle with Pyrolytic Graphite

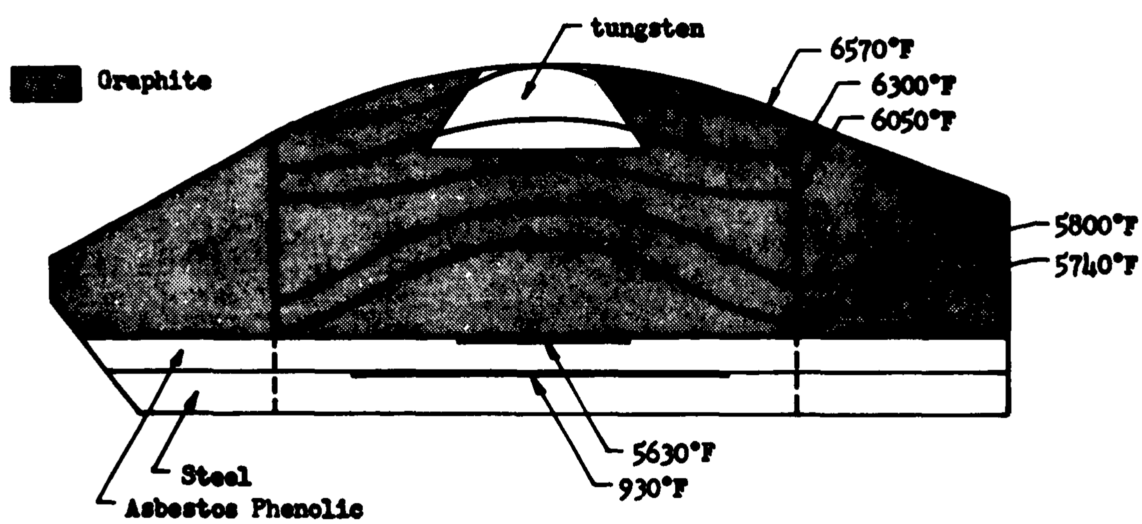

b. Nozzle without Pyrolytic Graphite

Figure 20: Comparison of Temperature Distributions at 93 Seconds in Nozzles With and Without Pyrolytic Graphite

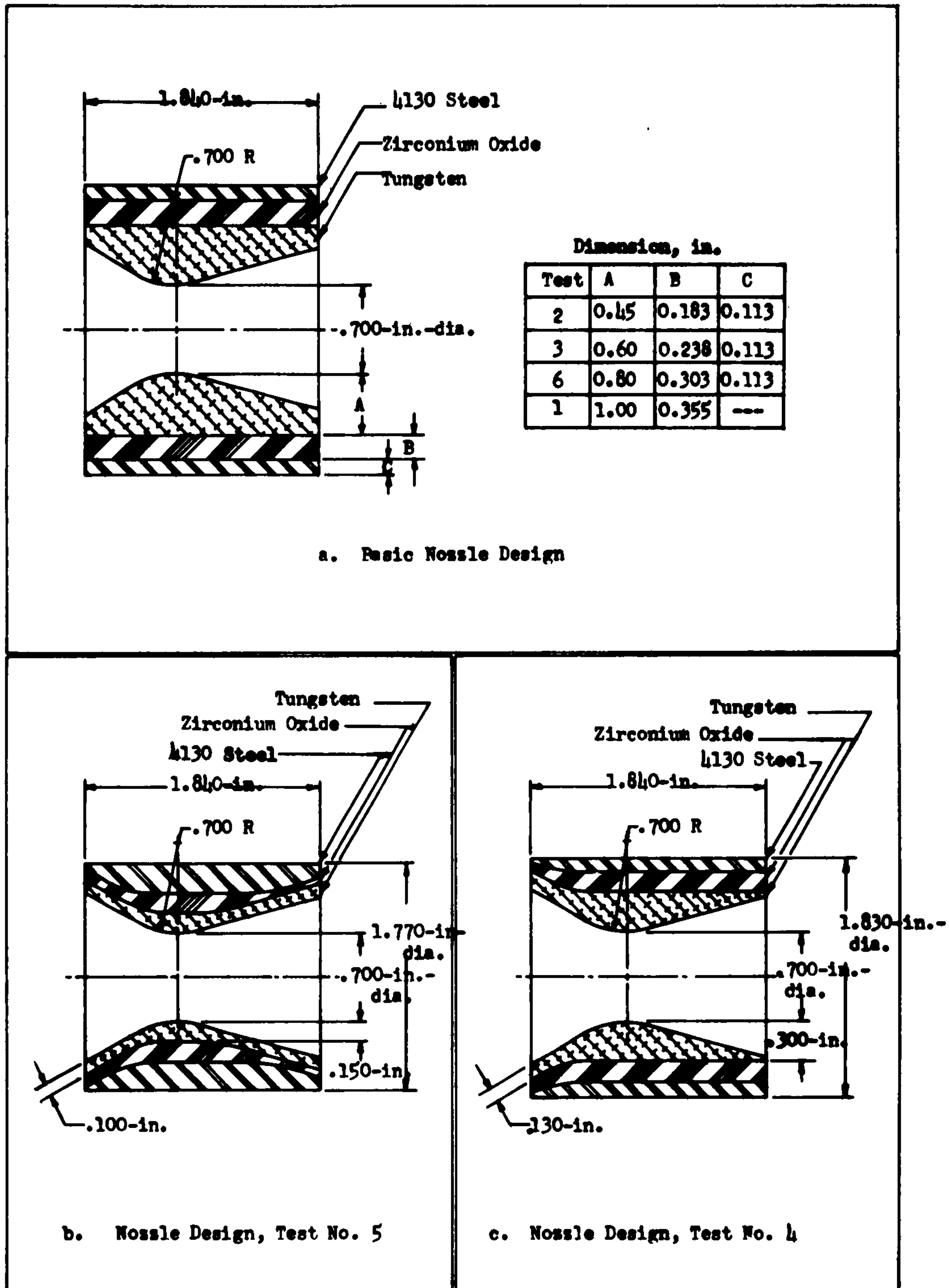

Dimension, in.

Test	A	B	C
2	0.45	0.183	0.113
3	0.60	0.238	0.113
6	0.80	0.303	0.113
1	1.00	0.355	---

Figure 21: Test Nozzle Designs

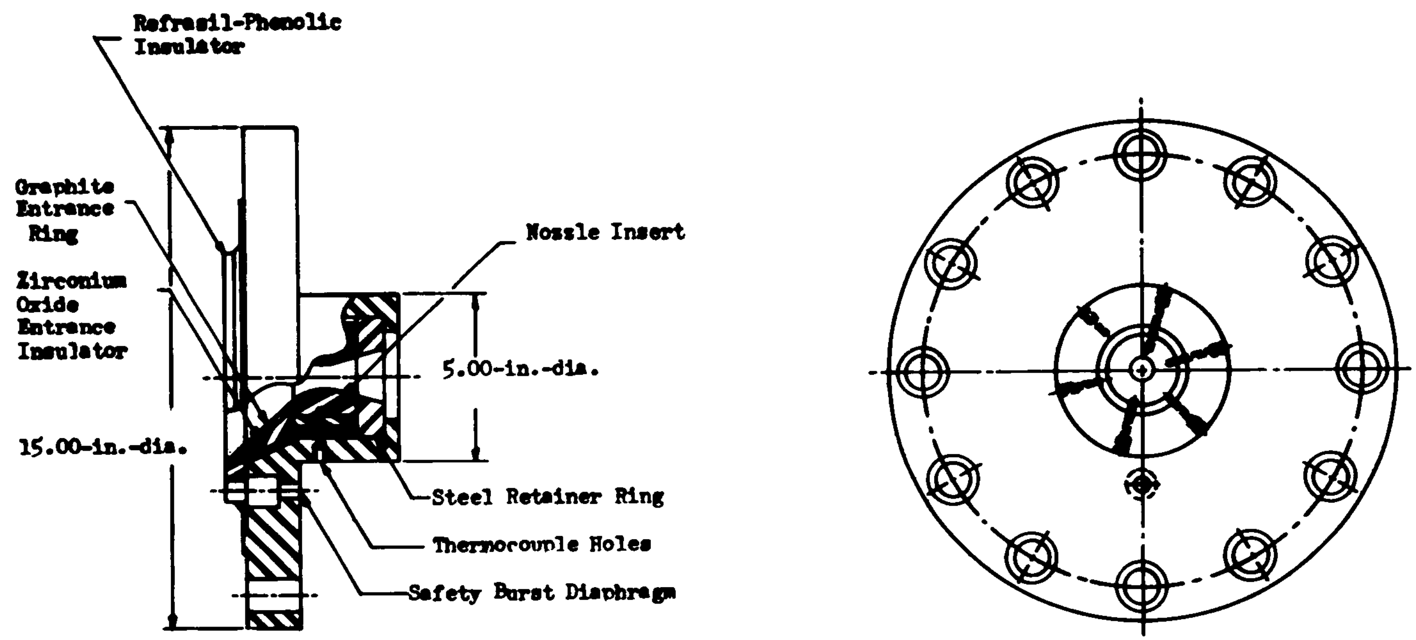

Figure 22: Aft Closure Assembly

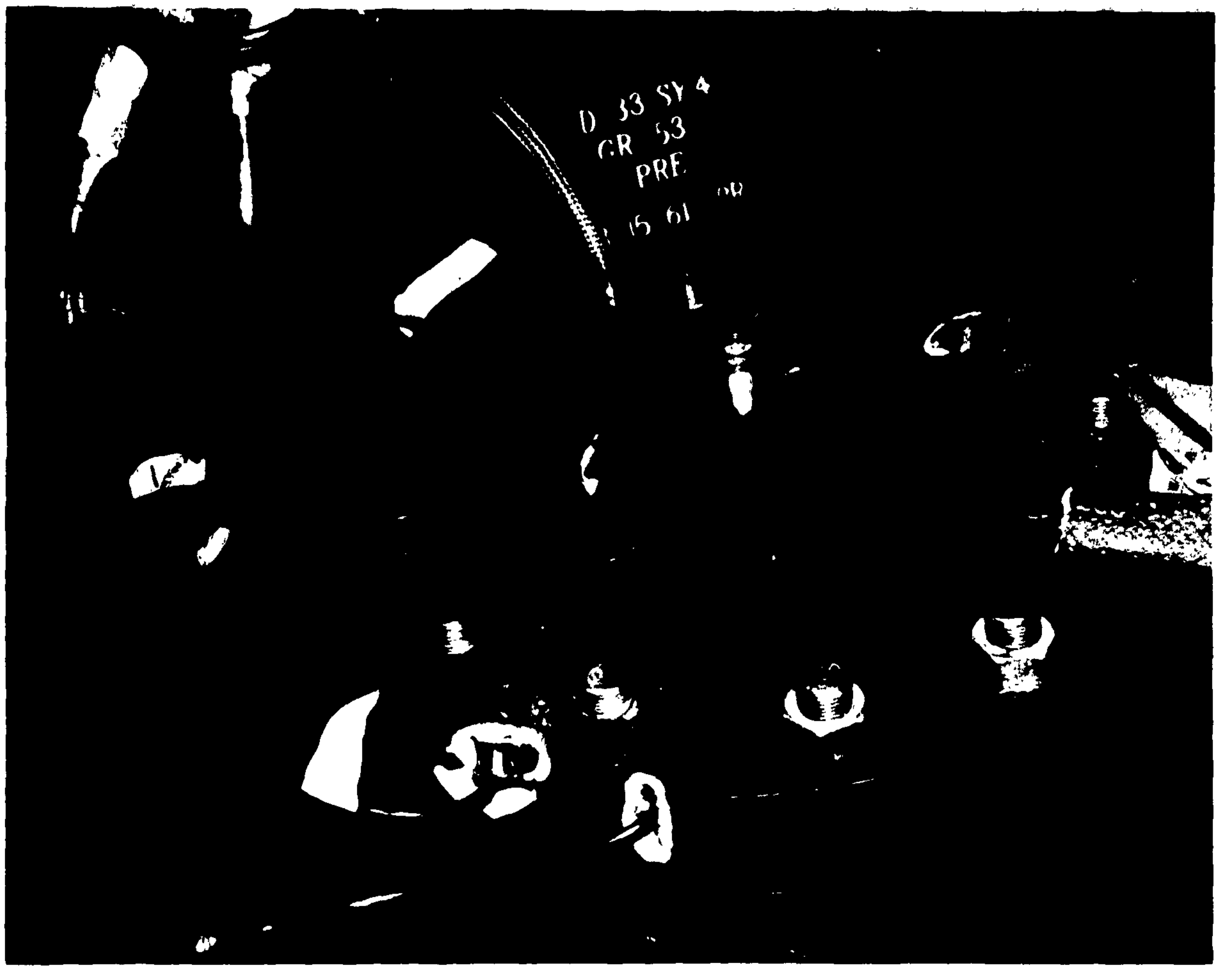

Figure 23: Typical Aft Closure Assembly Before Firing

a. 1.00 - IN. - DIA NOZZLE

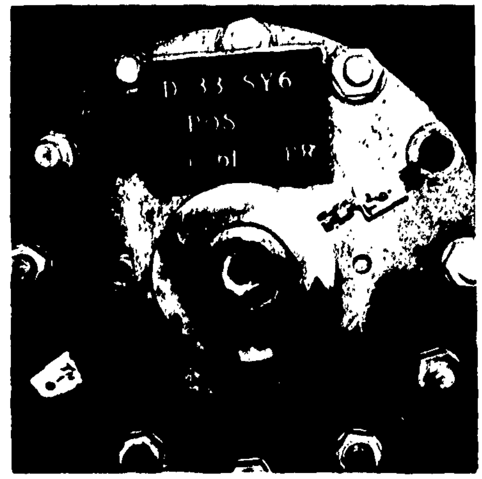

b. 0.80 - IN. - DIA NOZZLE

c. 0.60 - IN. - DIA NOZZLE

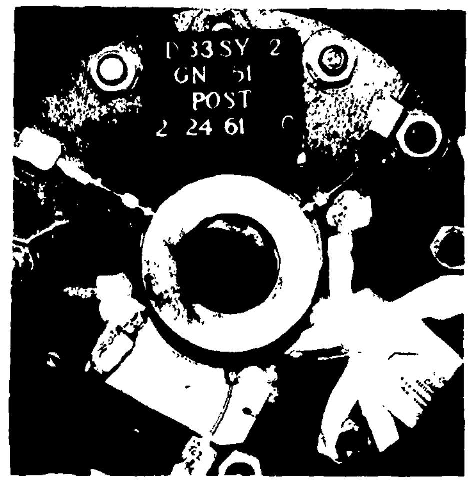

d. 0.45 - IN. - DIA NOZZLE

e. 0.30 - IN. - DIA NOZZLE

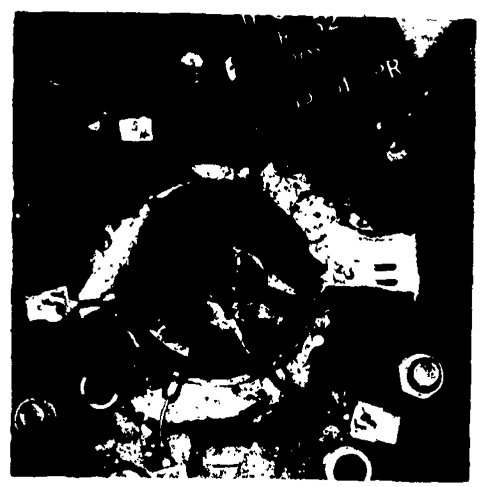

f. 0.15 - IN. - DIA NOZZLE

Figure 24: Postfiring Photographs of Nozzle Exits

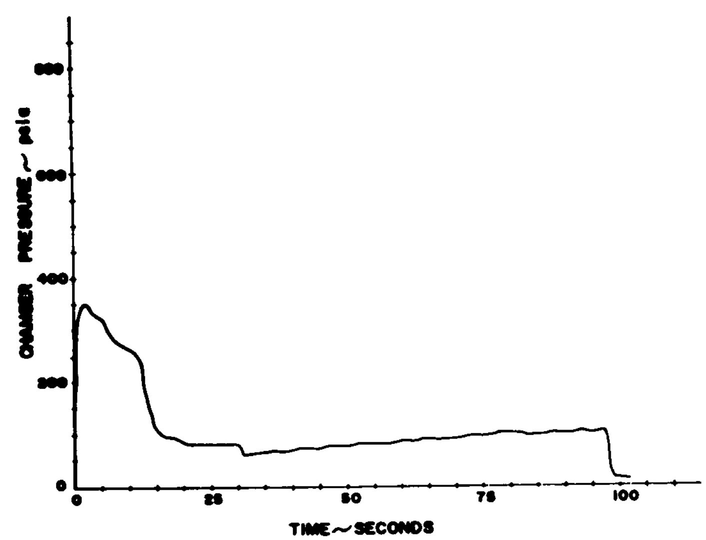

Figure 25: Pressure-vs-Time Curve for Test No. 5

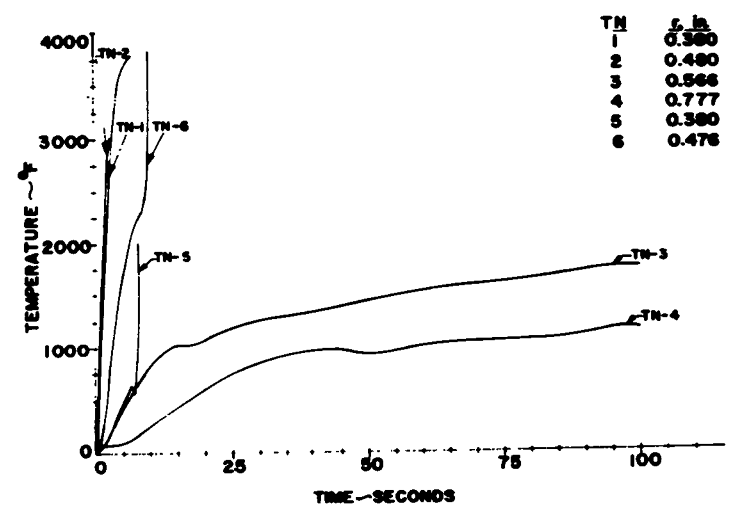

Figure 26: Temperature-vs-Time Curves for Test No. 5

TEST NO. 5

Tungsten Throat Thickness:	0.15 in.
Insulation Thickness:	0.155 in.
Throat Diameter Before Firing:	0.700 in.

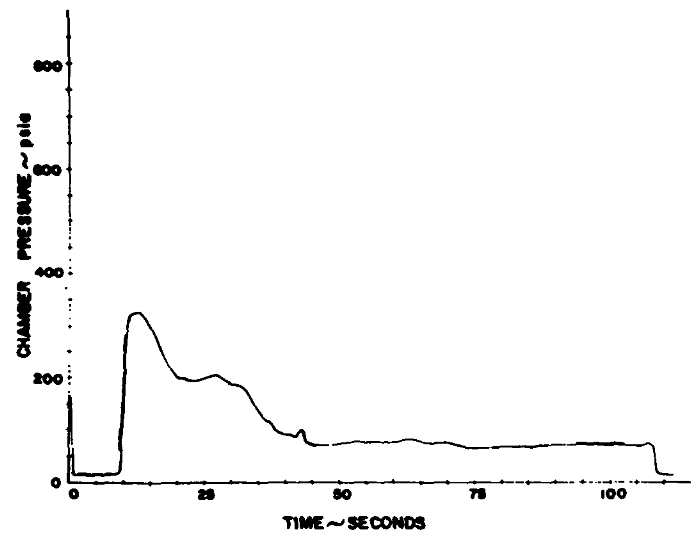

Figure 27: Pressure-vs-Time Curve for Test No. 4

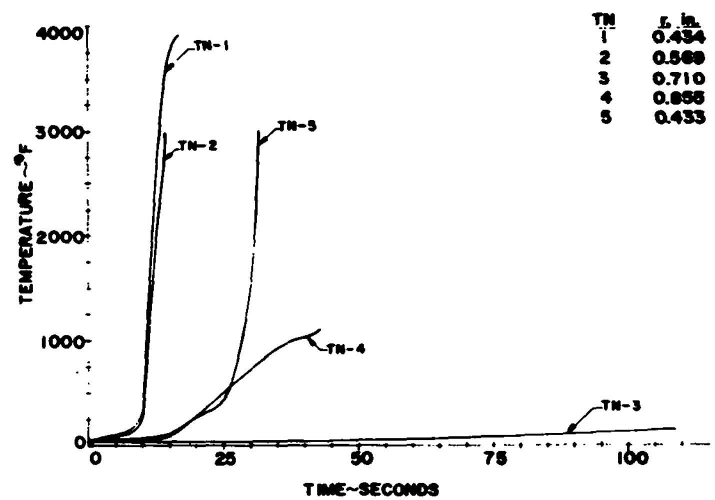

Figure 28: Temperature-vs-Time Curves for Test No. 4

TEST NO. 4

Tungsten Throat Thickness:	0.30 in.
Insulation Thickness:	0.155 in.
Throat Diameter Before Firing:	0.700 in.

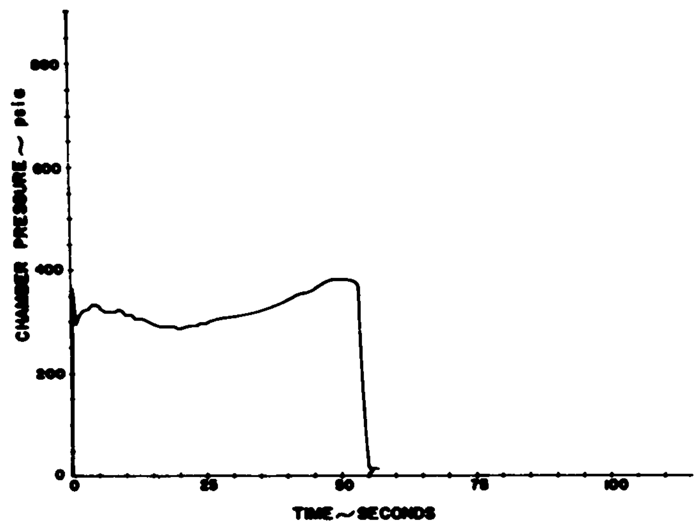

Figure 29: Pressure-vs-Time Curve for Test No. 2

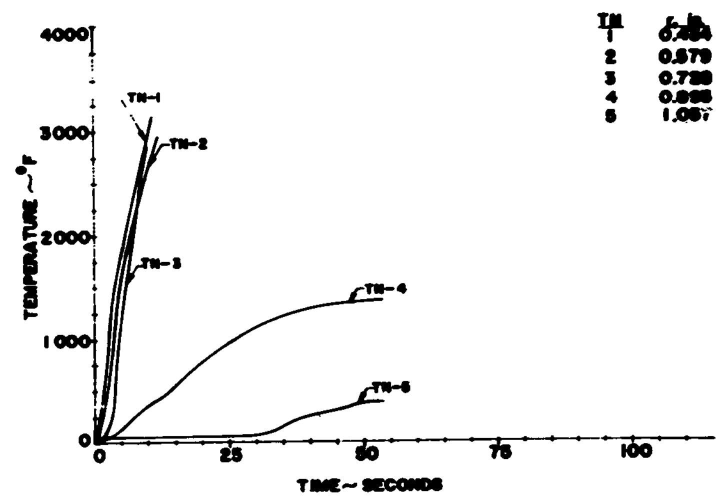

Figure 30: Temperature-vs-Time Curves for Test No. 2

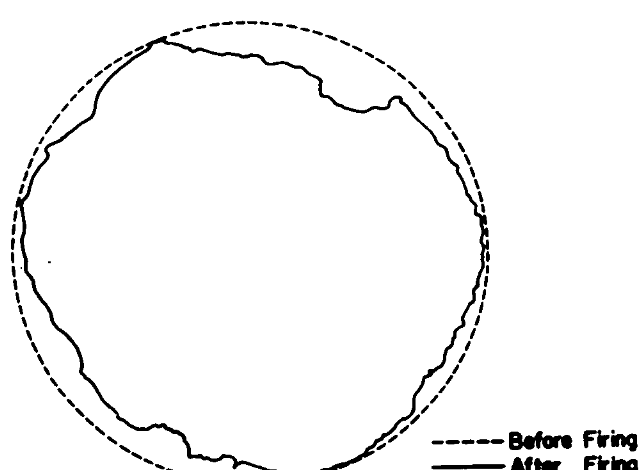

Figure 31: Shadowgraph of Test No. 2 Nozzle Insert

TEST NO. 2

Tungsten Throat Thickness:	0.45 in.
Insulation Thickness:	0.183 in.
Throat Diameter	
Before Firing:	0.700 in.
After Firing:	0.630 in.
Throat Area	
Before Firing:	0.3848 sq. in.
After Firing:	0.3118 sq. in.
Change of Throat Area:	-18.97%

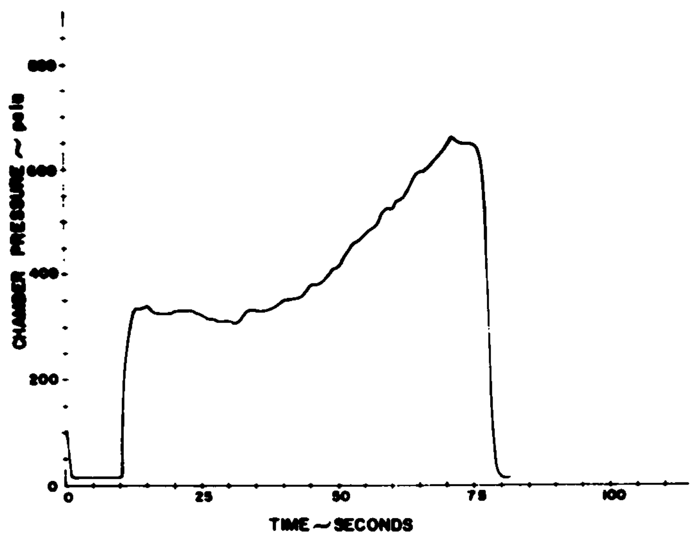

Figure 32: Pressure-vs-Time Curve for Test No. 3

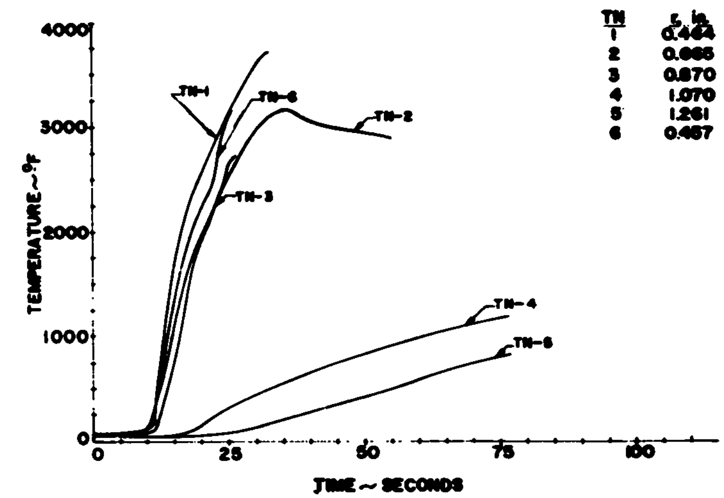

Figure 33: Temperature-vs-Time Curves for Test No. 3

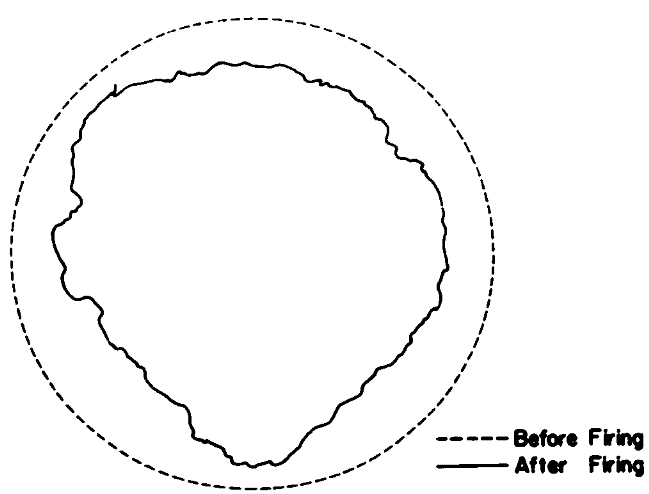

Figure 34: Shadowgraph of Test No. 3 Nozzle Insert

TEST NO. 3

Tungsten Throat Thickness:	**0.60 in.**
Insulation Thickness:	**0.238 in.**
Throat Diameter	
Before Firing:	**0.696 in.**
After Firing:	**0.542 in.**
Throat Area	
Before Firing:	**0.3805 sq. in.**
After Firing:	**0.2305 sq. in.**
Change of Throat Area:	**-39.4%**

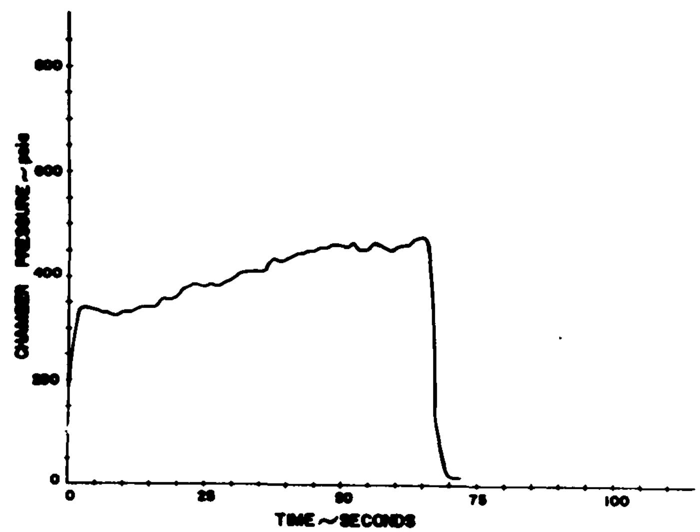

Figure 35: Pressure-vs-Time Curve for Test No. 6

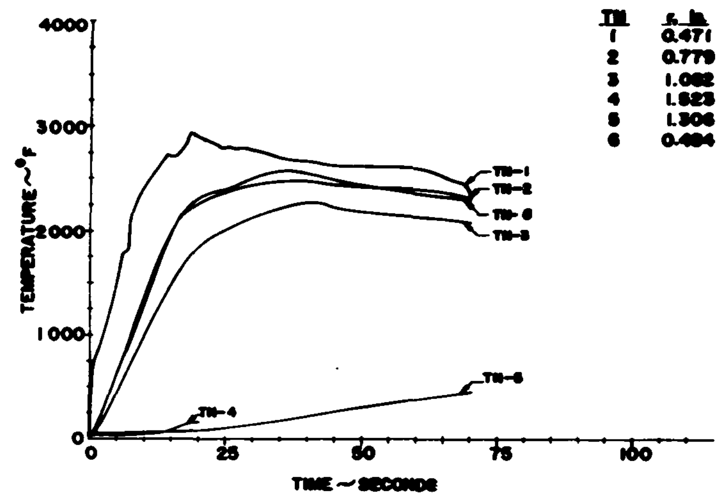

Figure 36: Temperature-vs-Time Curves for Test No. 6

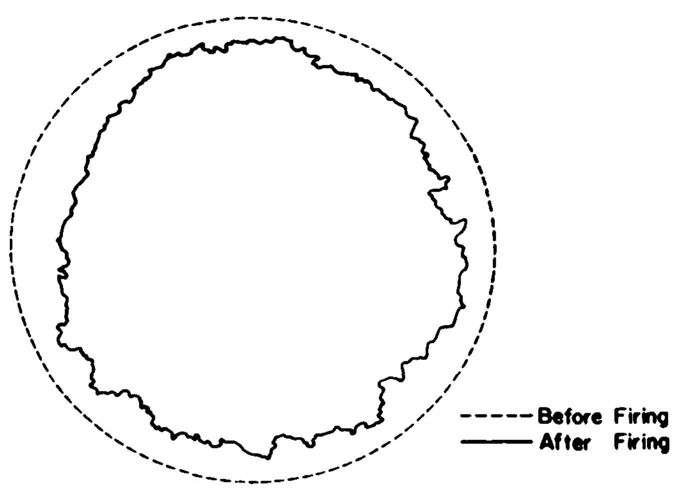

Figure 37: Shadowgraph of Test No. 6 Nozzle Insert

TEST NO. 6

Tungsten Throat Thickness:	0.80 in.
Insulation Thickness:	0.303 in.
Throat Diameter	
Before Firing:	0.705 in.
After Firing:	0.593 in.
Throat Area	
Before Firing:	0.3904 sq. in.
After Firing:	0.2764 sq. in.
Change of Throat Area:	-35.9%

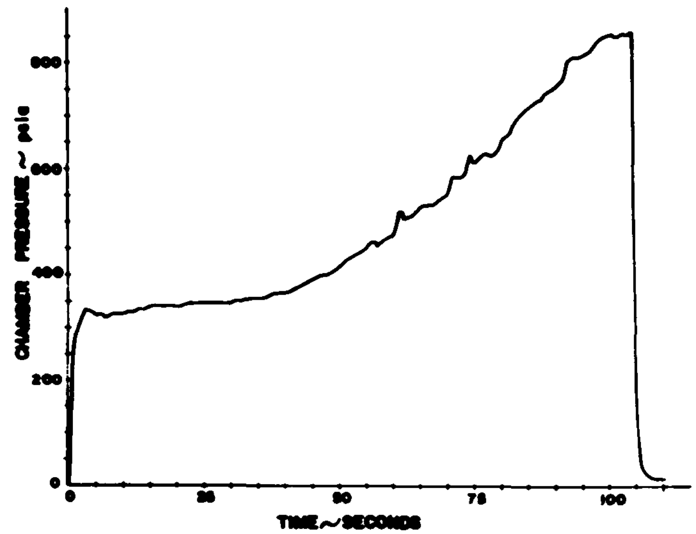

Figure 38: Pressure-vs-Time Curve for Test No. 1

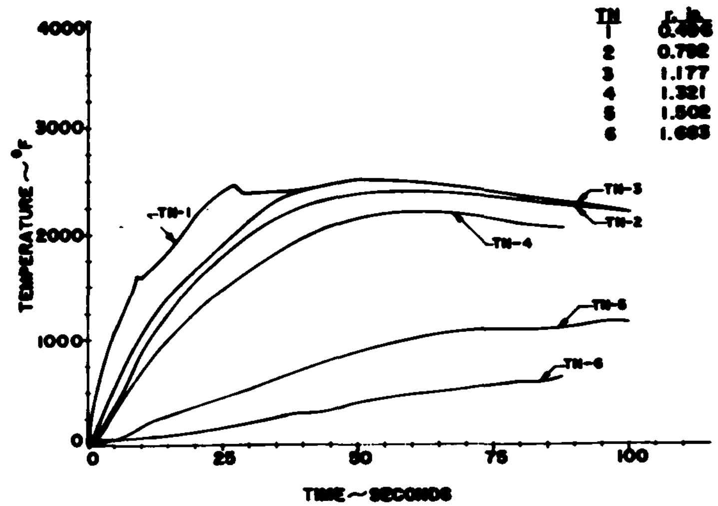

Figure 39: Temperature-vs-Time Curves for Test No. 1

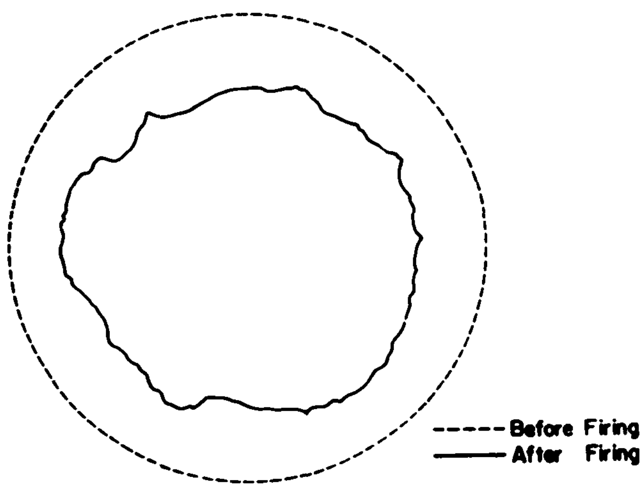

Figure 40: Shadowgraph of Test No. 1 Nozzle Insert

TEST NO. 1

Tungsten Throat Thickness:	1.00 in.
Insulation Thickness:	0.355 in.
Throat Diameter	
Before Firing:	0.698 in.
After Firing:	0.489 in.
Throat Area	
Before Firing:	0.3827 sq. in.
After Firing:	0.1875 sq. in.
Change of Throat Area:	-51.0%.

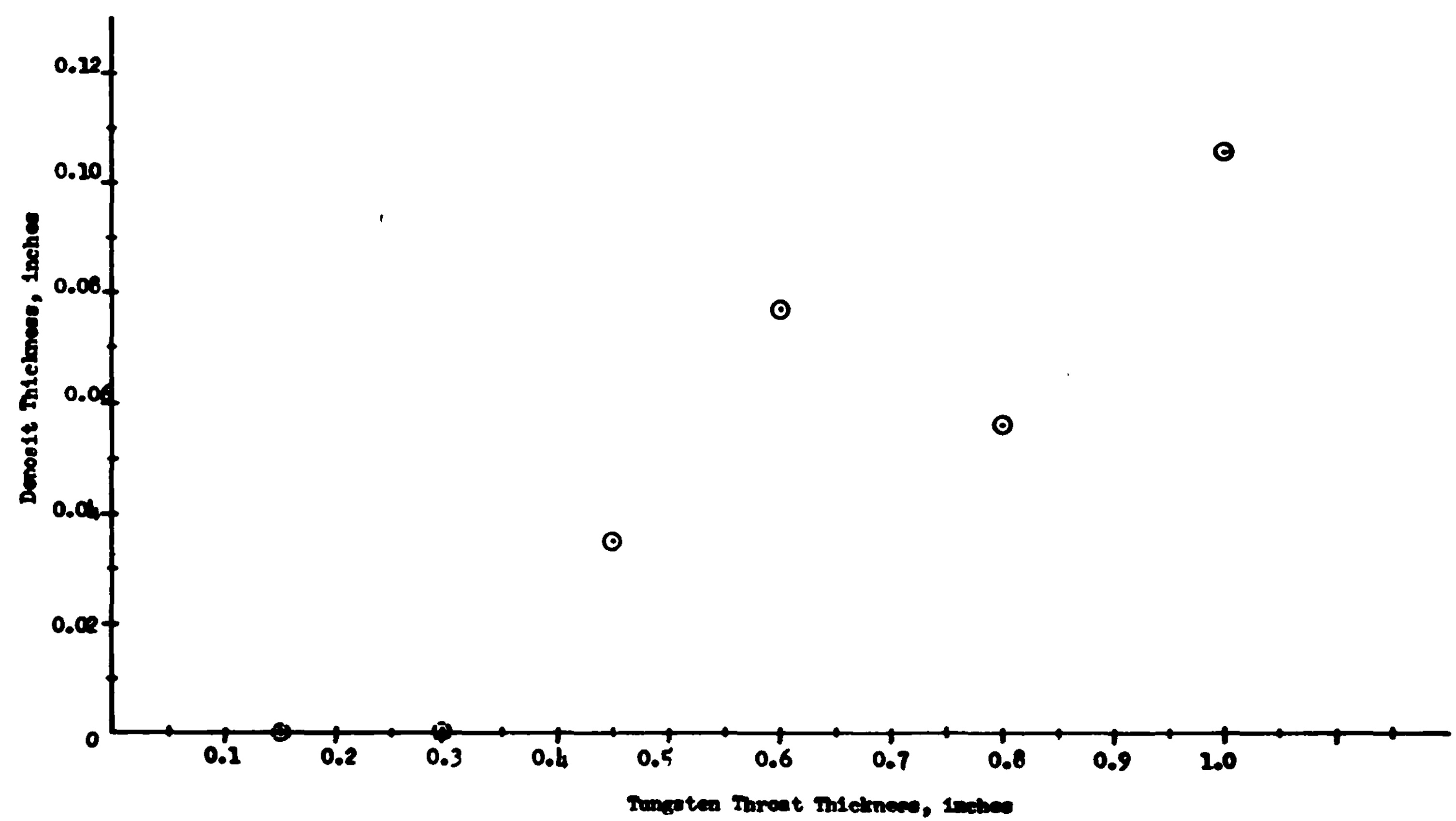

Figure 41: Aluminum Oxide Deposit Thickness as a Function of Tungsten Throat Thickness

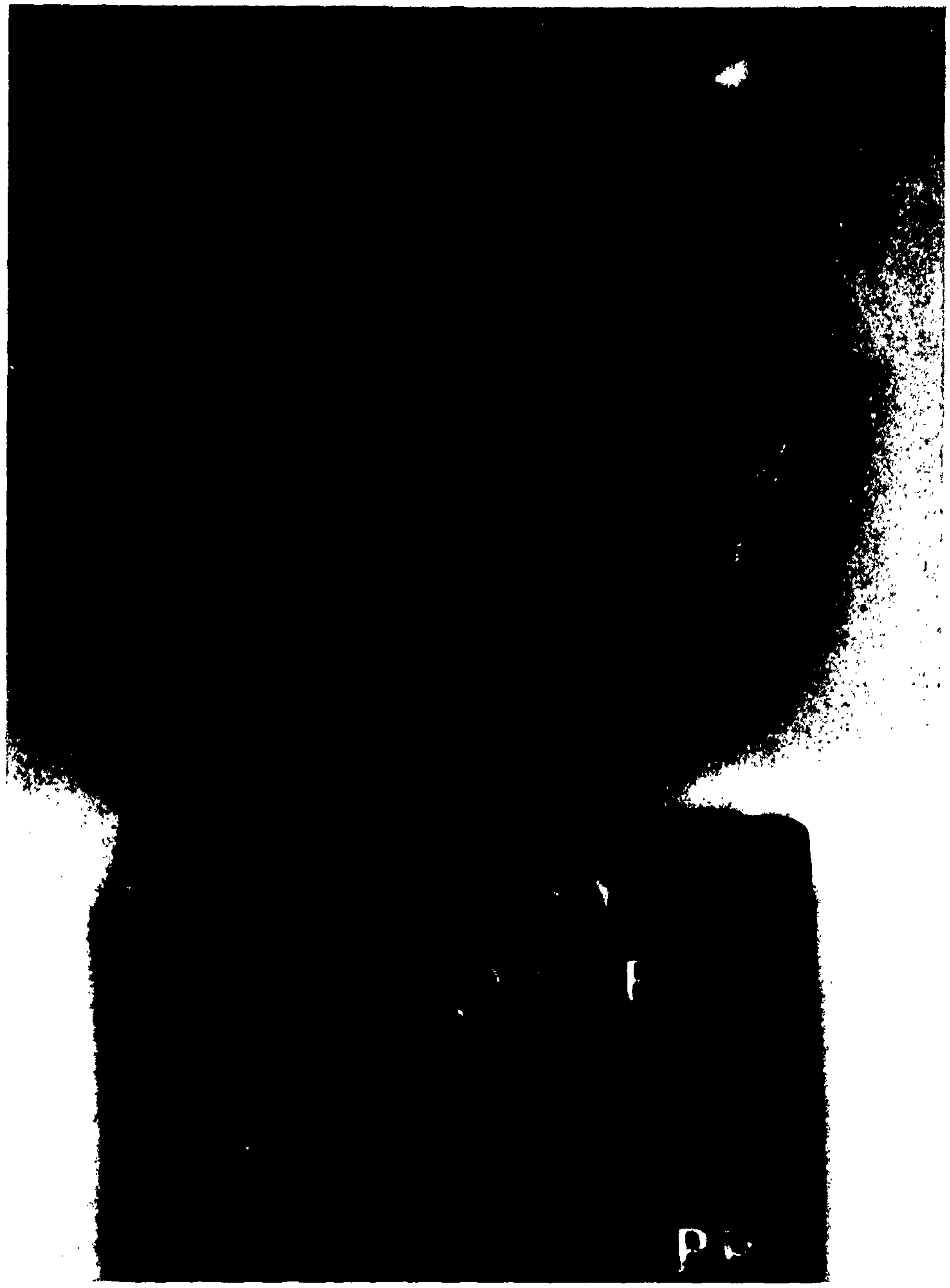

Figure 42: Entrance Section of Test No. 2 Nozzle Insert After Firing

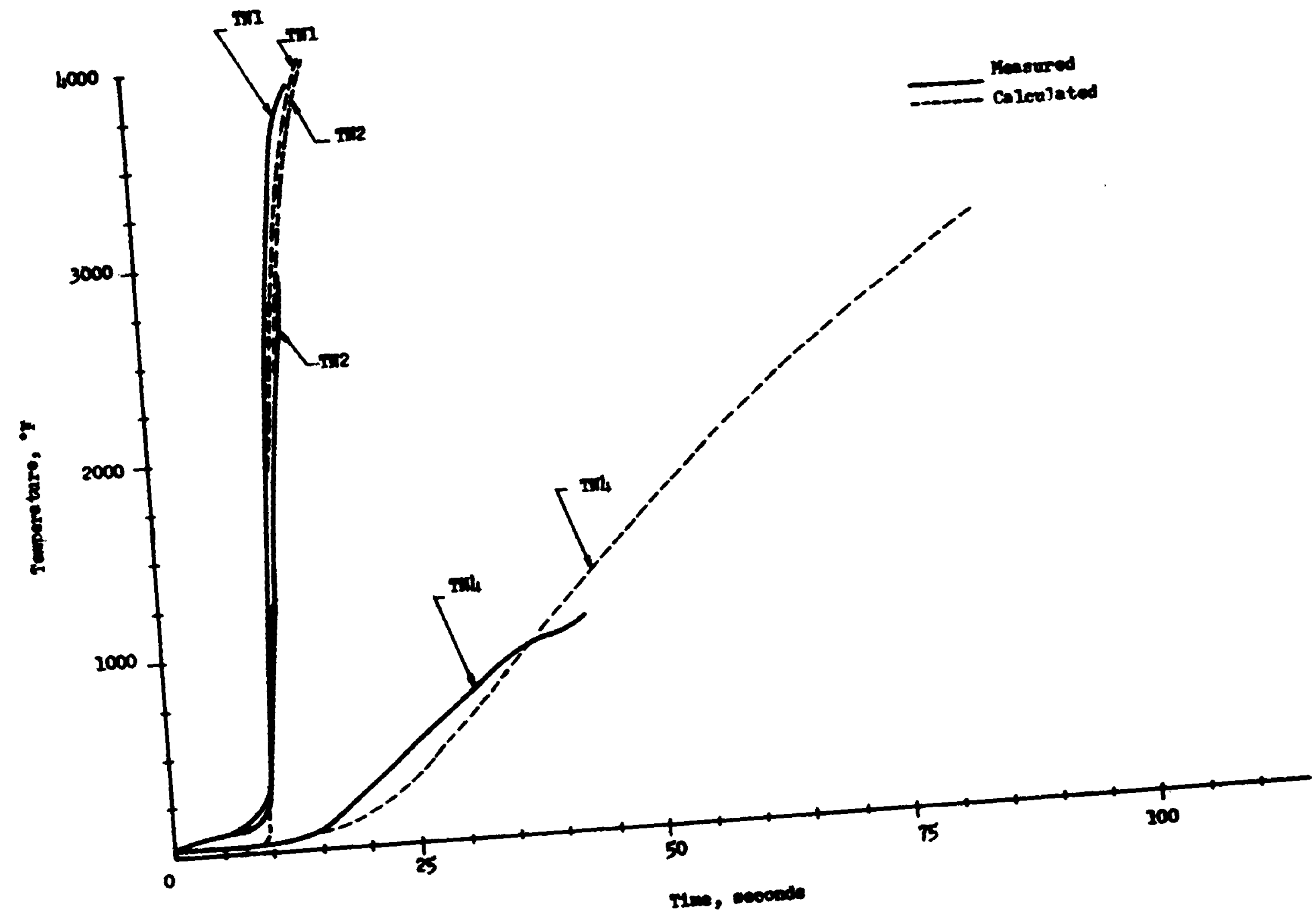

Figure 43: Comparison of Test No. 4 Data with Calculated Temperature Histories

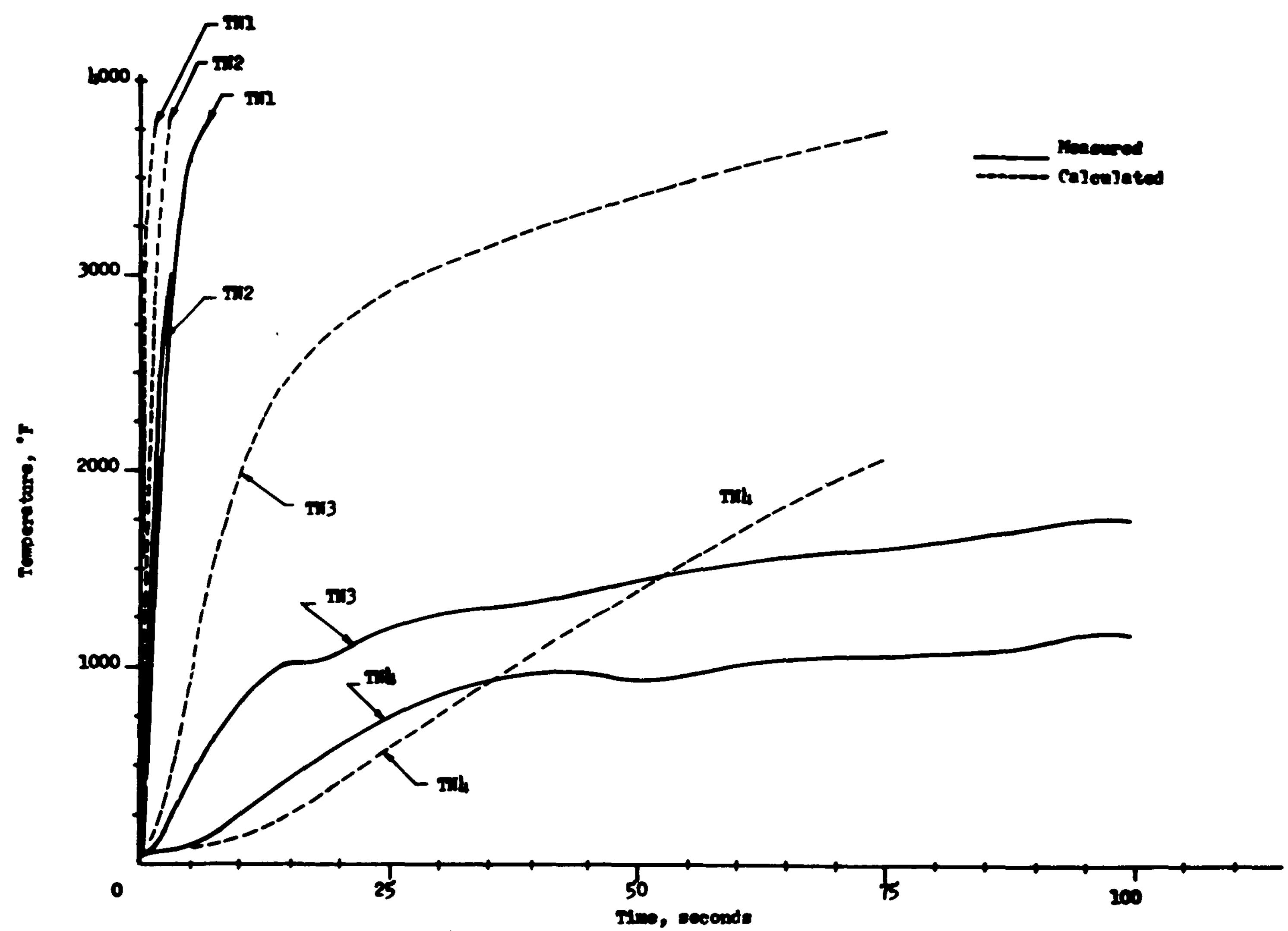

Figure 44: Comparison of Test No. 5 Data with Calculated Temperature Histories

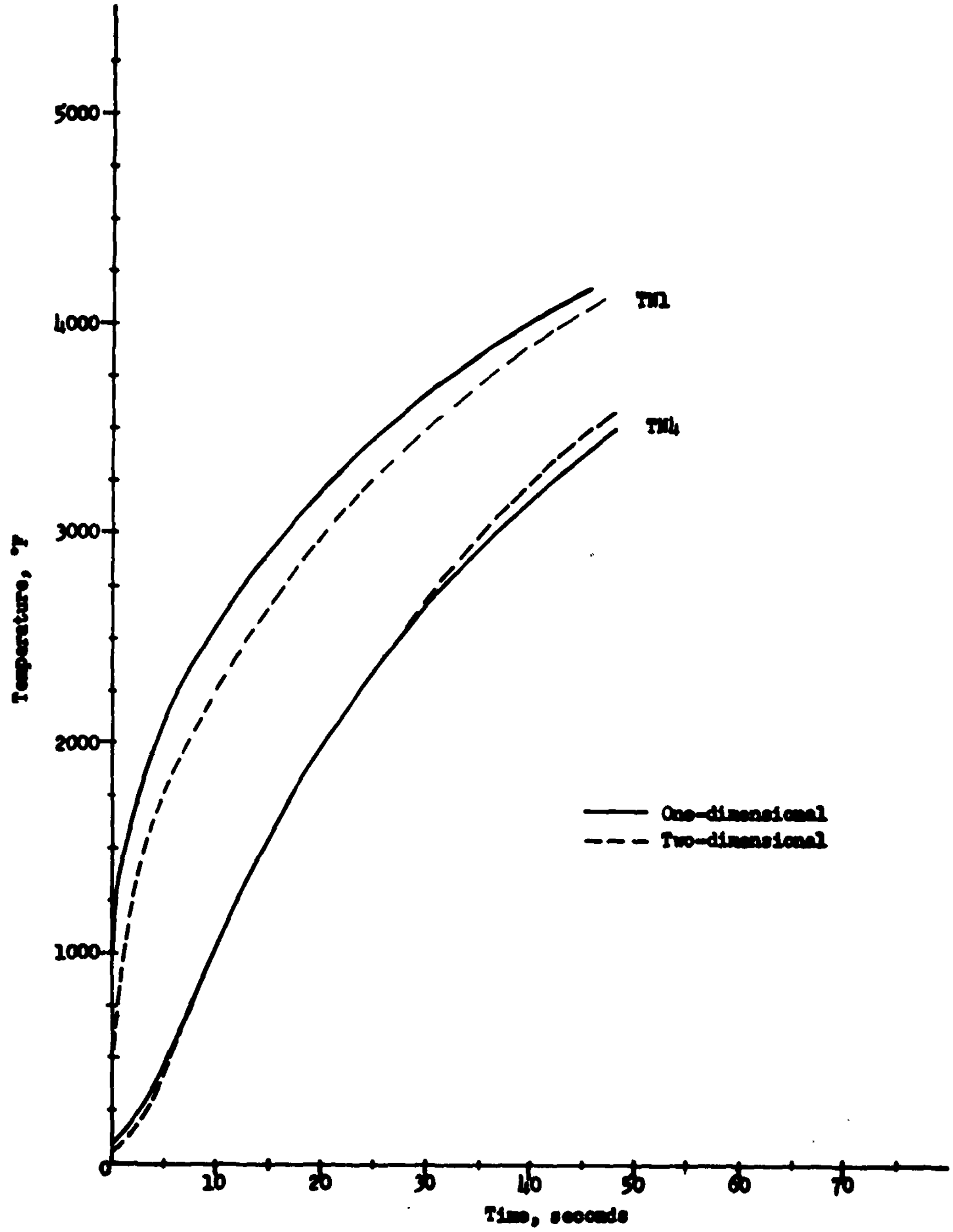

Figure 45: Comparison of Temperatures Based on One- and Two-Dimensional Heat Transfer Calculations for Test Nozzle No. 1

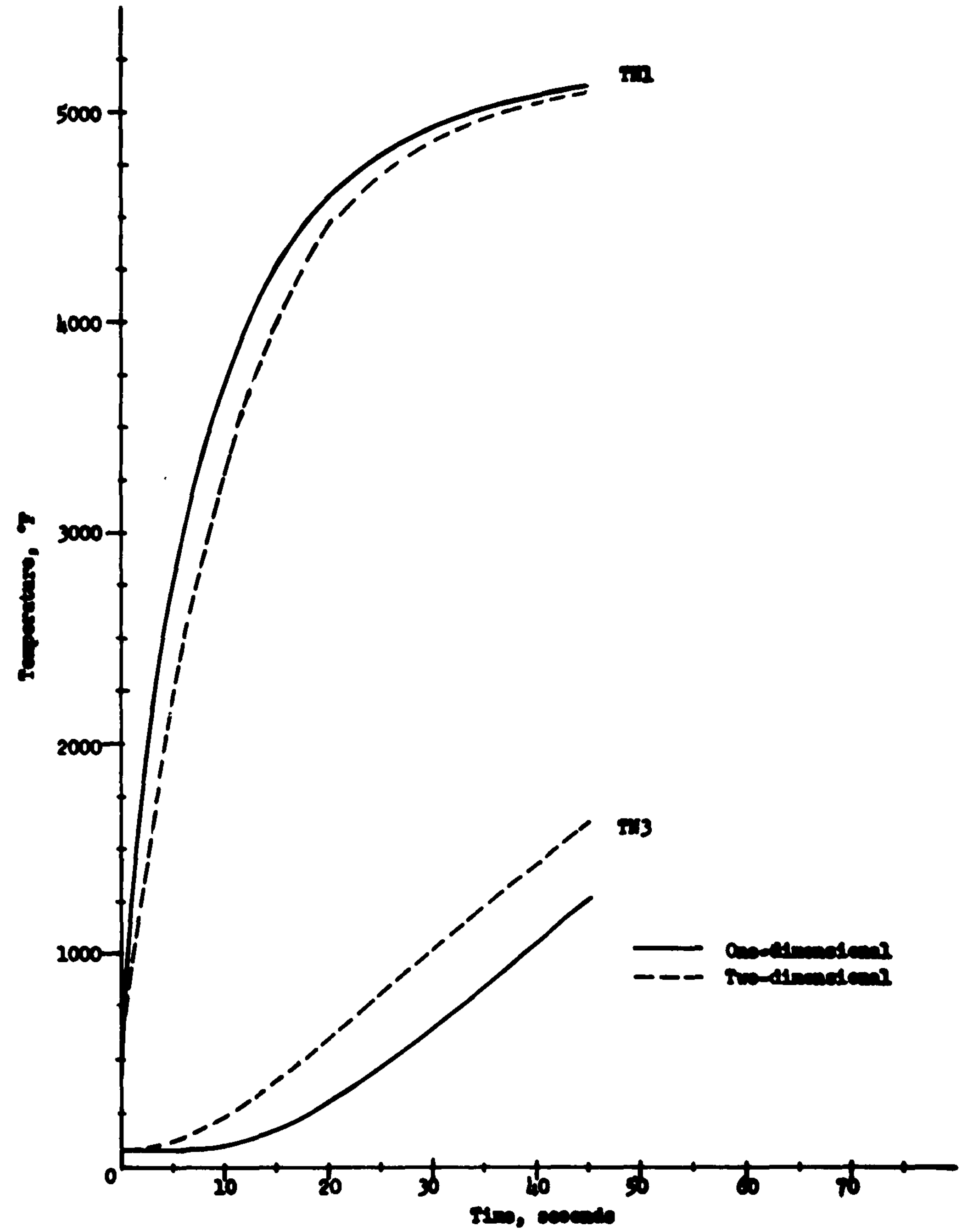

Figure 46: Comparison of Temperatures Based on One- and Two-Dimensional Heat Transfer Calculations for Test Nozzle No. 2

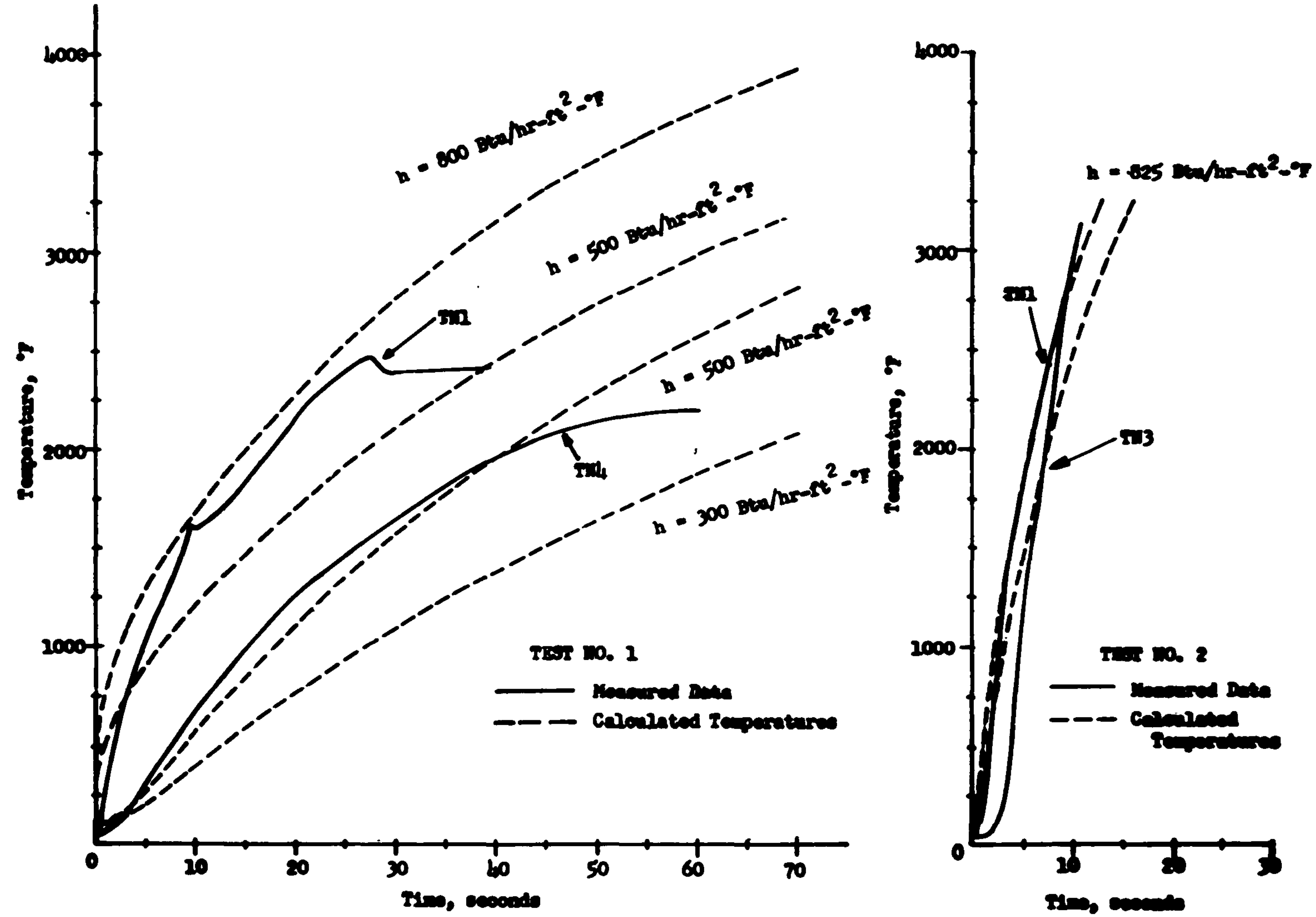

Figure 47: Comparison of Test Data with Calculated Temperature Histories for Various Heat Transfer Coefficients

VII. APPENDIX I

CALCULATION OF HEAT TRANSFER COEFFICIENTS

The equation used to calculate nozzle heat transfer coefficients was based on the equation for turbulent flow in a pipe (Reference 1):

$$\frac{hD}{k} = 0.023 \left(\frac{DG}{\mu}\right)^{0.8} \left(\frac{C_p\mu}{k}\right)^{0.4} \tag{1}$$

Although flow in straight pipes differs considerably from nozzle flow, because of the more fully developed boundary layer in pipe flow, Equation (1) adequately describes the nozzle heat transfer coefficient (References 2, 3).

Considering that

$$G = \frac{4W}{\pi D^2} \tag{2}$$

and

$$W = c_w A_t P_c \tag{3}$$

Equation (1) reduces to

$$h = 0.023 \frac{(c_w P_c)^{0.8} D_T^{1.6}}{D^{1.8}} \cdot \frac{C_p^{0.4} k^{0.6}}{\mu^{0.4}}$$

In aluminized polyurethane propellants, c_w usually varies between 22.7 and 24 lbm/lbf-hr. In addition, the transport properties of 10 polymethane propellants with combustion temperatures between 4600 and 5500°F were examined, and the product $\frac{C_p^{0.4} k^{0.6}}{\mu^{0.4}}$ was found, for all of the propellants, to be within 5% of the average value (Reference 4). This product was also found to decrease, as shown in Figure 1, in the supersonic portion of the

nozzle. For propellants with higher combustion temperatures, this product of the transport properties will probably be slightly higher, but the difference will not have any significant effect on any but the most precise heat transfer calculations.

Equation (4) then reduces to

$$h = 24.7 \frac{P_c^{0.8} d_t^{1.6}}{d^{1.8}} \cdot \frac{C_p^{0.4} k^{0.6}}{\mu^{0.4}} \tag{5}$$

This equation may be used to calculate heat transfer coefficients along the nozzle wall. For calculation of throat heat transfer coefficients, Equation (5) may be further reduced to

$$h = 8.95 \frac{P_c^{0.8}}{d_t^{0.8}} \tag{6}$$

The heat transfer coefficient at the throat is then expressed as a function only of chamber pressure and throat diameter, as is shown in Figure 2.

NOMENCLATURE

A_t	Throat area, in.
C_p	Specific heat, Btu/lb-°F
c_w	Mass flow coefficient, lbm/lbf-hr
D	Diameter, ft
D_T	Throat diameter, ft
d	Diameter, in.
d_t	Throat diameter, in.
G	Mass flow rate, lb/ft^2-hr
h	Heat transfer coefficient, $\frac{Btu}{hr\text{-}ft^2\text{-}°F}$
k	Thermal conductivity, $\frac{Btu}{ht\text{-}ft\text{-}°F}$
P_c	Chamber pressure, psi
W	Weight flow, lbm/hr
μ	Viscosity lbm/ft-hr

REFERENCES

1. W. H. McAdams, Heat Transmission, 3rd Edition, McGraw-Hill Book Co., 1951, p. 319.

2. S. S. Grover, Analysis of Nozzle Heat Transfer Coefficient, Aerojet-General Corporation, Technical Memorandum 113 SRP, 30 April 1959 (Aerojet-General internal publication).

3. S. E. Colucci, "Experimental Determination of Solid Rocket Nozzle Heat Transfer Coefficient," Proceedings of the Fifth AFBMD-STL Aerospace Symposium, Vol. II, Academic Press, New York, 1960.

4. M. H. Landau, Aerojet-General Corporation, Memorandum 5510:0265M, dated 5 November 1958 (Aerojet-General internal publication).

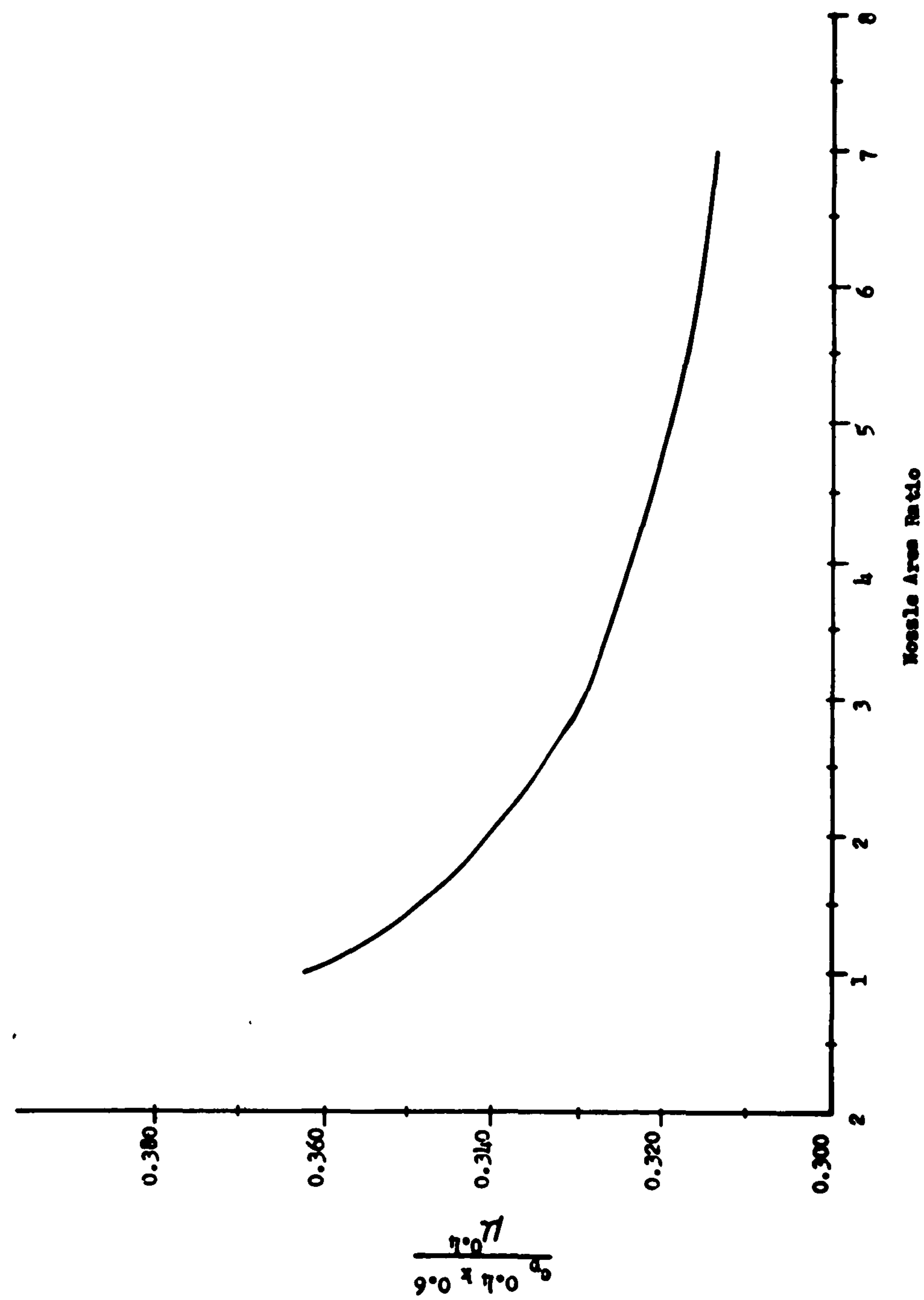

Figure 1: Average Values of $\frac{c_p^{0.4} k^{0.6}}{\mu^{0.4}}$ for Ten Polyurethane Propellants

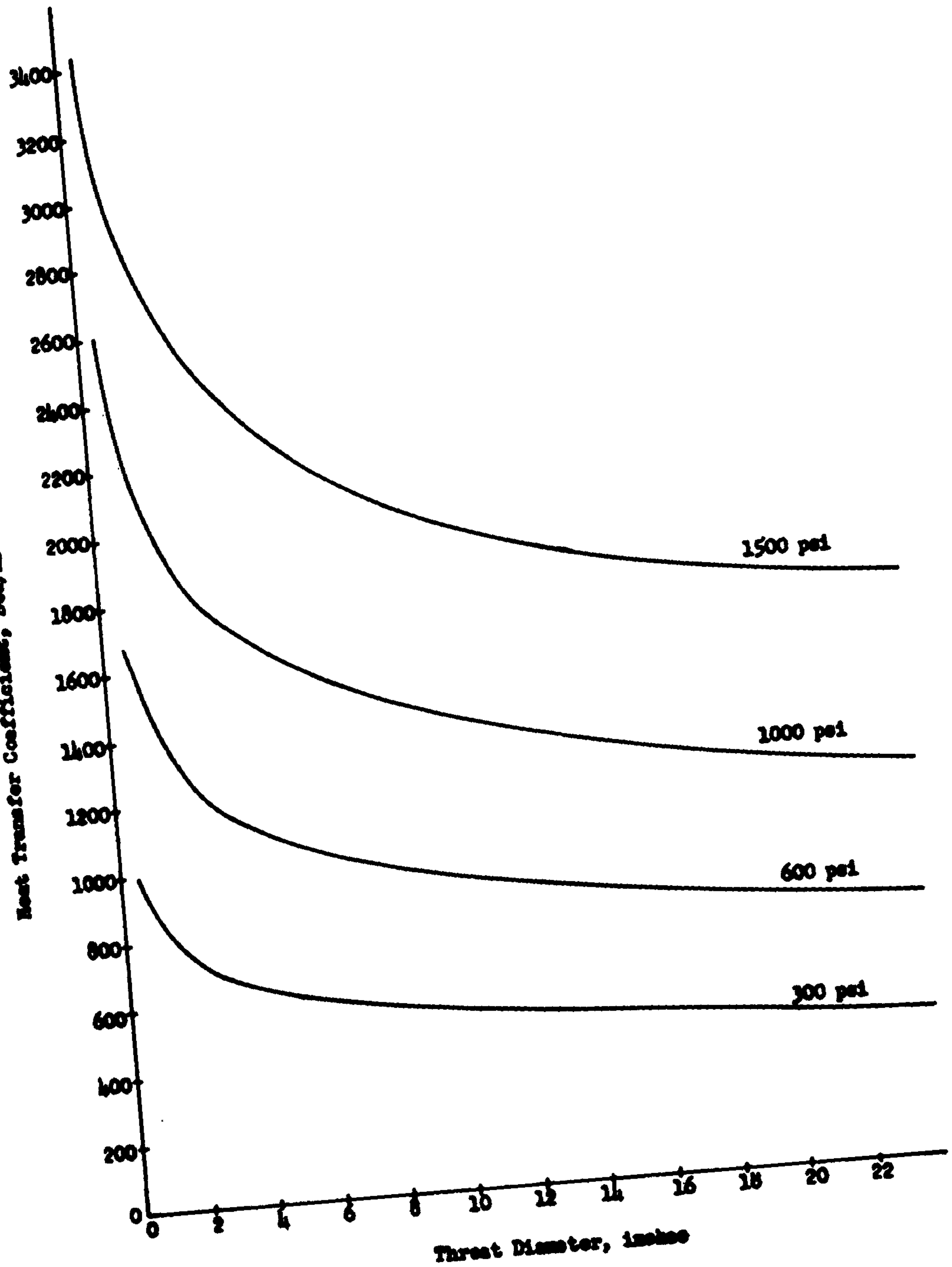

Figure 2: Throat Heat Transfer Coefficient as a Function of Chamber Pressure and Throat Diameter

VIII. APPENDIX II

TABULATION OF IBM OUTPUTS

All the computer runs that resulted in temperature histories of nozzle material systems are tabulated in the following pages. The cases are grouped by the variables which were changed for each run. A pressure change is reflected by a change in heat transfer coefficient. Where one set of temperatures is listed for a case, the time chosen is nearly always the time (usually to the nearest second) at which the maximum allowable flame barrier, heat-sink, or insulator temperature was reached, or, with very long durations, the time the computer was stopped. In some cases, two durations are shown. The other duration represents the time when the maximum allowable flame barrier temperature was reached, even though the limiting insulator temperature was exceeded. For some four-material systems, weights were not calculated because it was decided not to represent these systems on a weight basis.

Appendix II

WADD THERMAL OPTIMIZATION OF NOZZLE MATERIAL SYSTEMS-C.M.GRACEY DEPT 4710

NOMENCLATURE

DIA	-DIAMETER,IN.
HTC	-HEAT TRANSFER COEFFICIENT,BTU/HR.SQ.FT.F.
TG	-GAS TEMPERATURE,F.
T1	-SURFACE TEMPERATURE,F.
T2	-INTERFACE TEMPERATURE BETWEEN MAT-1 AND MAT-2,F.
T3	-INTERFACE TEMPERATURE BETWEEN MAT-2 AND MAT-3,F.
T4	-INTERFACE TEMPERATURE BETWEEN MAT-3 AND MAT-4,F.
T5	-INTERFACE TEMPERATURE BETWEEN MAT-4 AND MAT-5,F.
DUR	-DURATION,SEC.
WT	-WEIGHT PER AXIAL DISTANCE,LB./IN.
P	-MATERIAL DENSITY,LB./CU.FT.
K	-MATERIAL THERMAL CONDUCTIVITY,BTU/HR.FT.F
C	-MATERIAL SPECIFIC HEAT,BTU/LB.F
TM	MATERIAL MAXIMUM ALLOWABLE TEMPERATURE
MAT-1	-THICKNESS OF MATERIAL NO.1,IN.
MAT-2	-THICKNESS OF MATERIAL NO.2,IN.
MAT-3	-THICKNESS OF MATERIAL NO.3,IN.
MAT-4	-THICKNESS OF MATERIAL NO.4,IN.
MAT-5	-THICKNESS OF MATERIAL NO.5,IN.

MATERIAL THERMOPHYSICAL PROPERTIES (UNLESS OTHERWISE SPECIFIED)

MATERIAL	K	C	P	TM
ASBESTOS	.258	.388	108.	3000
ATJ GRAPHITE	51.6	.387	107.9	6600
BERYLLIUM OXIDE	25.	.420	172.	4500
BORON CARBIDE	40.	.500	156.	4400
PYRO GRAPHITE	.176	.480	140.	6600
PYRO GRAPHITE	194.	.480	140.	6600
TANTALUM CARBIDE	6.7	.054	899.	7000
TITANIUM CARBIDE	4.5	.250	306.	5600
TUNGSTEN	60.	.0353	1170.	6100
4130 STEEL	23.7	.107	489.6	700
ZIRCONIUM OXIDE	.584	.200	266.	4600

CASE	DIA	HTC	TG	MAT-1	MAT-2	MAT-3	MAT-4	T1	T2	T3	T4	DUR	WT
TUNGSTEN - ASBESTOS - 4130 STEEL													
6-1A	4.000	1700	7000	1.165	0.275	0.250		5354	2977	80		16	14.74
6-2A	4.000	1700	7000	3.000	0.280	0.250		6076	3116	511		100	47.64
6-3A	4.000	1700	7000	3.000	0.200	0.250		6051	3013	284		96	47.44
6-4A	4.000	1700	7000	1.165	0.200	0.250		5356	2981	82		16	14.61
6-1B	4.000	1700	7000	3.350	0.250	0.250		6109	3010	376		120	55.46
6-1C	4.000	1700	7000	3.350	0.200	0.250		6109	3020	1271		120	55.33
6-1D	4.000	1700	7000	1.650	0.110	0.250		5645	2986	1039		30	21.72
6-1E	4.000	1700	7000	2.250	0.150	0.250		5978	2955	1270		62	32.18
6-1F	4.000	1700	7000	4.500	0.200	0.250		6095	2289	951		160	84.92
6-1G	4.000	1700	7000	2.910	0.200	0.250		6031	3004	962		90	45.50
6-1H	4.000	1700	7000	4.150	0.200	0.250		6099	2484	1191		150	75.32
6-1J	4.000	650	7000	3.350	0.200	0.250		5262	3014	1651		165	55.57
6-2J	4.000	650	7000	5.500	0.292	0.250		5510	3000	1850		416	115.5
6-3J	4.000	650	7000	2.000	0.100	0.250		4860	2993	543		66	27.56
6-4J	4.000	650	7000	1.000	0.100	0.250		4320	3057	199		22	12.19
6-5J	4.000	650	7000	2.500	0.150	0.250		5050	3019	474		98	36.96
6-1X	4.000	1120	7000	3.000	0.200	0.250		5705	2998	328		108	47.44

6-2X	4.000	1120	7000	2.000	0.200	0.250	5401	2986	142	50	27.77
6-3X	4.000	1120	7000	1.000	0.150	0.250	4776	2986	91	15	12.27
6-4X	4.000	1120	7000	4.000	0.200	0.250	5883	2993	606	190	71.36
6-5X	4.000	1120	7000	4.500	0.225	0.250	5951	3002	660	242	85.00
6-6X	4.000	1120	7000	5.000	0.250	0.250	6004	3001	706	300	99.70
6-7X	4.000	1120	7000	5.500	0.250	0.250	5931	2526	576	300	115.6
6-8X	4.000	1120	7000	6.000	0.250	0.250	5878	2118	469	300	132.2
6-1K	4.000	2400	7000	3.750	0.200	0.250	6101	1616	292	70	66.98
6-2K	4.000	2400	7000	3.250	0.200	0.250	6099	1822	348	64	53.02
6-3K	4.000	2400	7000	3.000	0.169	0.250	6096	2061	542	60	47.36
6-4K	4.000	2400	7000	1.750	0.150	0.250	5982	2986	1455	30	23.42
6-5K	4.000	2400	7000	1.000	0.100	0.250	5591	3061	111	11	12.19
6-6K	4.000	2400	7000	4.000	0.200	0.250	6102	1228	110	72	71.36
6-1L	12.00	1700	7000	3.000	0.200	0.250	6107	2638	563	68	100.6
6-2L	12.00	1700	7000	2.750	0.200	0.250	6094	2833	553	62	91.02
6-3L	12.00	1700	7000	2.500	0.160	0.250	6080	3047	912	56	81.56
6-4L	12.00	1700	7000	3.500	0.200	0.250	6103	2130	482	75	120.5
6-5L	12.00	1700	7000	4.000	0.200	0.250	6104	1675	388	80	141.5
6-6L	12.00	1700	7000	1.800	0.117	0.250	5821	2973	891	30	56.78
6-1M	24.00	1700	7000	2.616	0.125	0.250	6108	2888	1284	54	155.4
6-2M	24.00	1700	7000	2.500	0.140	0.250	6106	3011	1076	52	168.3
6-3M	24.00	1700	7000	3.000	0.125	0.250	6114	2483	1136	60	179.8
6-4M	24.00	1700	7000	3.500	0.125	0.250	6113	1965	897	65	212.5
6-5M	24.00	1700	7000	2.000	0.180	0.250	5923	2934	334	34	118.0
6-1N	4.000	1700	8000	1.620	0.110	0.250	6100	2477	531	21	21.24
6-2N	4.000	1700	8000	1.580	0.100	0.250	6070	2470	626	20	20.58
6-3N	4.000	1700	8000	1.250	0.080	0.250	6020	3045	2015	16	15.60
6-4N	4.000	1700	8000	3.000	0.090	0.250	6091	611	213	26	47.17
6-1P	4.000	1700	6500	6.000	0.236	0.250	5890	3000	2250	419	132.1
6-2P	4.000	1700	6500	3.000	0.170	0.250	5668	3008	1490	104	47.36
6-3P	4.000	1700	6500	2.150	0.106	0.250	5490	3016	1797	54	30.25
6-1O	1.000	2250	7000	1.500	0.150	0.250	5512	3032	158	34	8.09
6-2O	1.000	2250	7000	2.000	0.150	0.250	5668	3010	290	61	14.15
6-3O	1.000	2250	7000	2.500	0.150	0.250	5774	2996	471	97	20.25
6-4O	1.000	2250	7000	3.000	0.150	0.250	5858	3006	696	144	27.42
6-1Q	4.000	1700	7500	1.683	0.150	0.250	5998	3003	131	29	22.32
6-2Q	4.000	1700	7500	2.420	0.200	0.250	6094	2339	110	45	35.51
6-3Q	4.000	1700	7500	3.040	0.200	0.250	6099	1680	106	53	48.32
6-4Q	4.000	1700	7500	4.060	0.200	0.250	6102	850	91	59	72.93
6-5Q	4.000	1700	7500	1.720	0.120	0.250	6011	2984	184	30	22.87
6-6Q	4.000	1700	7500	2.250	0.155	0.250	6104	2577	594	43	32.19
6-1R	12.00	1360	7000	3.150	0.170	0.250	6059	3013	1264	90	106.3
6-2R	12.00	1360	7000	2.500	0.100	0.250	5904	3005	462	59	81.33
6-3R	12.00	1360	7000	1.500	0.100	0.250	5474	3019	199	24	46.81
6-4R	12.00	1360	7000	5.000	0.100	0.250	6102	1791	519	137	186.2
6-5R	12.00	1360	7000	3.250	0.190	0.250	6077	2991	294	95	110.4
6-6R	12.00	1360	7000	3.500	0.150	0.250	6104	2898	486	106	116.2
6-7R	12.00	1360	7000	4.000	0.150	0.250	6100	2500	425	118	136.9
6-1S	24.00	1180	7000	3.600	0.200	0.250	6086	2991	1109	110	219.7
6-2S	24.00	1180	7000	3.000	0.150	0.250	5966	3017	357	80	180.0
6-3S	24.00	1180	7000	2.500	0.150	0.250	5813	2979	249	57	148.4
6-4S	24.00	1180	7000	2.000	0.100	0.250	5623	2988	310	39	117.5
6-5S	24.00	1180	7000	1.250	0.100	0.250	5168	2991	154	18	73.66
6-1U	8.000	1480	7000	3.250	0.280	0.250	6095	2984	80	99	82.00
6-2U	8.000	1480	7000	2.000	0.100	0.250	5766	2995	319	40	45.85

6-3U	8.000	1480	7000	1.500	0.075	0.250	5523	2992	291	24	33.01
6-4U	8.000	1480	7000	2.750	0.150	0.250	5991	2988	321	72	66.41
6-5U	8.000	1480	7000	4.000	0.150	0.250	6099	2437	427	121	102.6
6-6U	8.000	1480	7000	3.500	0.200	0.250	6098	2807	290	107	86.21
6-1W	18.00	1240	7000	3.350	0.200	0.250	6067	3020	286	99	158.8
6-2W	18.00	1240	7000	2.000	0.150	0.250	5658	2996	170	39	90.76
6-3W	18.00	1240	7000	1.500	0.150	0.250	5387	2993	113	24	62.84
6-4W	18.00	1240	7000	4.000	0.150	0.250	6100	2650	463	121	187.9
6-5W	18.00	1240	7000	3.750	0.150	0.250	6101	2842	479	115	174.2
6-6W	18.00	1240	7000	3.500	0.280	0.250	6085	2983	80	106	167.2
6-7W	18.00	1240	7000	2.750	0.100	0.250	5923	2996	529	69	127.2
6-1Z	4.733	1218	7000	3.000	0.150	0.250	5816	2998	469	101	52.18
6-5Z	4.733	1218	7000	3.300	0.120	0.250	5883	3007	749	123	59.29
6-12Z	4.733	1218	7000	3.200	0.120	0.250	5865	3012	712	116	54.26
6-13Z	4.733	1218	7000	3.220	0.130	0.250	5867	3008	653	117	54.76
6-2Z	6.700	615	7000	2.000	0.120	0.250	4892	3023	402	61	39.76
6-6Z	6.700	615	7000	2.750	0.200	0.250	5153	2992	314	103	58.62
6-11Z	6.700	615	7000	2.800	0.150	0.250	5174	2997	506	107	59.81
6-14Z	6.700	615	7000	2.875	0.150	0.250	5195	2994	528	112	58.93
6-3Z	9.610	304	7000	1.000	0.100	0.250	3742	2980	314	34	25.48
6-7Z	9.610	304	7000	2.000	0.200	0.250	4240	3008	281	88	52.79
6-10Z	9.610	304	7000	2.500	0.150	0.250	4419	2996	604	123	68.21
6-15Z	9.610	304	7000	2.600	0.140	0.250	4455	2997	698	131	67.96
6-4Z	11.88	205	7000	0.750	0.100	0.250	3446	3009	330	34	23.49
6-8Z	11.88	205	7000	1.500	0.200	0.250	3763	3007	258	78	66.76
6-9Z	11.88	205	7000	2.000	0.150	0.250	3949	3009	593	115	63.18
6-16Z	11.88	204	7000	2.070	0.150	0.250	3968	3008	621	121	61.90
TUNGSTEN-ASBESTOS-TITANIUM											
6-2Y	4.000	1700	7000	3.600	0.090	0.250	6099	2779	1037	129	59.89
TUNGSTEN-ASBESTOS-TUNGSTEN											
6-3Y	4.000	1700	7000	3.000	0.075	0.250	6058	3006	1163	98	50.35
TUNGSTEN-ATJ GRAPHITE-TUNGSTEN											
6-4Y	4.000	1700	7000	1.000	2.000	0.250	6101	4448	2822	109	19.09
TUNGSTEN-ASBESTOS-4130 STEEL											
10-A	4.000	1700	8000	0.940	0.162	0.250	6116	3868	83	13	11.50
10-B	4.000	1700	7000	2.222	0.158	0.250	6109	3814	403	72	31.68
11-A	4.000	1700	8000	0.500	0.112	0.250	6160	4970	89	6.75	6.26
11-B	4.000	1700	7000	1.125	0.114	0.250	6115	4806	346	30	13.90
13-A	4.000	1700	8000	0.820	0.115	0.250	5560	3090	86	8	10.14
21-A	4.000	2350	8000	1.035	0.067	0.250	6100	2681	138	9	12.60
21-B	4.000	2350	8000	0.632	0.049	0.250	5541	2771	122	4	7.53
22-A	4.000	650	6500	1.522	0.146	0.250	4441	3020	234	46	19.77
22-B	4.000	650	6500	3.500	0.100	0.250	5013	2980	1348	200	58.60
22-C	4.000	650	6500	0.420	0.053	0.250	3771	3187	220	8	6.42
23-C	4.000	650	6000	6.808	0.353	0.250	4332	924	125	250	161.9
23-A	24.00	1670	8000	1.289	0.501	0.250	6138	2918	80	14	78.20
23-B	4.000	2390	8000	1.015	0.065	0.250	6118	2737	139	8.75	12.33
TUNGSTEN-ASBESTOS(K=0.060,C=0.116)-4130 STEEL											
1-A	4.000	1700	7000	3.350	0.194	0.250	6094	3001	170	103	55.31
2-A	4.000	1700	7000	1.650	0.048	0.250	6085	2999	665	114	21.60
TUNGSTEN-ASBESTOS(C=0.116)-4130 STEEL											
3-A	4.000	1700	7000	3.350	0.402	0.250	6094	2996	207	115	55.87
TUNGSTEN-ASBESTOS(K=1.500,C=0.116)-4130 STEEL											
4-A	4.000	1700	7000	3.350	0.972	0.250	6114	2989	361	123	57.47
4-B	4.000	1700	7000	1.650	0.486	0.250	5664	2988	254	31	22.47
4-C	4.000	1700	7000	2.250	0.698	0.250	5887	3001	263	56	33.43

4-D	4.000	1700	7000	2.910	0.842	0.250	6042	2994	318	88	47.15
TUNGSTEN-ASBESTOS(K=1.500)-4130 STEEL											
5-A	4.000	1700	7000	3.350	0.530	0.250	6140	2993	592	135	56.22
5-B	4.000	1700	7000	1.650	0.275	0.250	5684	2933	370	33	22.06
5-C	4.000	1700	7000	2.250	0.395	0.250	5918	2995	398	61	32.72
5-D	4.000	1700	7000	2.910	0.475	0.250	6066	2982	494	101	46.18
TUNGSTEN (K = 10.0)-ASBESTOS-4130 STEEL											
20-B	4.000	1700	7000	0.437	0.067	0.250	6109	2636	141	9	5.36
20-E	4.000	1700	7000	1.165	0.200	0.250	6105	1623	80	11	14.61
17-F	4.000	1700	7000	2.250	0.150	0.250	6108	80	80	10	32.18
17-M	4.000	1700	7000	2.250	0.150	0.250	6104	80	80	20	32.18
TUNGSTEN(K=20.)-ASBESTOS-4130 STEEL											
20-M	4.000	1700	7000	1.165	0.100	0.250	6102	2046	147	25	14.43
17-H	4.000	1700	7000	2.250	0.150	0.250	6097	2819	81	28	32.18
TUNGSTEN(K=25.)-ASBESTOS-4130 STEEL											
20-L	4.000	1700	7000	1.165	0.100	0.250	6093	2787	82	28	14.43
TUNGSTEN (K = 30.0)-ASBESTOS-4130 STEEL											
20-A	4.000	1700	7000	1.471	0.118	0.250	6103	2729	222	37	18.94
20-F	4.000	1700	7000	1.165	0.200	0.250	5998	2983	90	26	14.61
17-D	4.000	1700	7000	2.250	0.150	0.250	6104	1536	132	51	32.18
TUNGSTEN(K=50.)-ASBESTOS-4130 STEEL											
20-D	4.000	1700	7000	1.165	0.200	0.250	5542	2986	83	18	14.61
17-E	4.000	1700	7000	2.250	0.150	0.250	6020	2988	278	62	32.18
TUNGSTEN(K=80.)-ASBESTOS-4130 STEEL											
20-K	4.000	1700	7000	1.165	0.100	0.250	5095	3065	132	14	14.43
17-J	4.000	1700	7000	2.250	0.150	0.250	5610	2986	197	44	32.18
17-J	4.000	1700	7000	2.250	0.150	0.250	6094	4301	489	73	32.18
TUNGSTEN(K=20.,C=0.0653)-ASBESTOS-4130 STEEL											
17-A	4.000	1700	7000	2.250	0.150	0.250	6100	302	84	52	32.18
20-J	4.000	1700	7000	1.165	0.150	0.250	6102	2093	146	46	14.52
TUNGSTEN(K=30.0,C=0.0653)-ASBESTOS-4130 STEEL											
20-G	4.000	1700	7000	1.165	0.200	0.250	5989	2993	128	47	14.61
21-C	4.000	1700	7000	2.250	0.150	0.250	6103	1562	212	94	68.87
TUNGSTEN(K=50.,C=0.0653)-ASBESTOS-4130 STEEL											
17-B	4.000	1700	7000	2.250	0.150	0.250	6013	2994	509	113	32.18
20-H	4.000	1700	7000	1.165	0.150	0.250	5542	3019	147	33	14.64
TUNGSTEN(K=80.0,C=0.0653)-ASBESTOS-4130 STEEL											
17-G	4.000	1700	7000	2.250	0.150	0.250	5603	2988	364	80	32.18
20-N	4.000	1700	7000	1.165	0.150	0.250	5063	3025	120	25	14.52
TUNGSTEN(K=110.0,C=0.0653)-ASBESTOS-4130 STEEL											
17-N	4.000	1700	7000	2.250	0.150	0.250	5295	3012	304	66	32.18
17-M	4.000	1700	7000	2.250	0.150	0.250	6104	4863	1140	132	32.18
C=0.0653											
17-K	4.000	1700	7000	2.250	0.150	0.250	5296	2993	164	36	32.18
17-K	4.000	1700	7000	2.250	0.150	0.250	6095	4823	578	72	32.18
TUNGSTEN(K=150.0,C=0.0653)-ASBESTOS-4130 STEEL											
17-O	4.000	1700	7000	2.250	0.150	0.250	4960	2986	256	55	32.18
17-O	4.000	1700	7000	2.250	0.150	0.250	6104	5199	1229	128	32.18
17-L	4.000	1700	7000	2.250	0.150	0.250	4962	2972	141	[illegible]	32.18
17-L	4.000	1700	7000	2.250	0.150	0.250	6095	5168	654	70	32.18
TUNGSTEN-ZRO-4130 STEEL (MERM MOTOR DESIGN DATA)											
7-1A	0.700	1310	6187	1.200	0.450	0.250	5319	4600	624	105	6.57
7-2A	0.700	1310	6187	0.060	0.300	0.250	4862	4743	80	4	0.63
7-3A	0.700	1310	6187	1.000	0.345	0.250	5274	4595	828	74	4.93
7-3B	0.700	1310	6187	1.000	0.355	0.250	5280	4606	800	74	4.96
7-4A	0.700	1310	6187	0.800	0.375	0.250	5219	4591	508	49	3.77
7-4B	0.700	1310	6187	0.800	0.289	0.250	5205	4572	765	48	3.61
7-5A	0.700	1310	6187	0.600	0.316	0.250	5162	4612	236	30	2.62

7-5B	0.700	1310	6187	0.600	0.226	0.250	5169	4625	809	30	2.47
7-6A	0.700	1310	6187	0.450	0.290	0.250	5050	4555	131	18	1.81
7-6B	0.700	1310	6187	0.450	0.175	0.250	5057	4568	796	18	1.74
7-7A	0.700	1310	6187	0.300	0.300	0.250	4983	4596	89	10	1.28
7-7B	0.700	1310	6187	0.300	0.131	0.250	4993	4610	816	10	1.13
7-8A	0.700	1310	6187	0.150	0.110	0.250	4836	4588	300	6	0.66
7-8B	0.700	1310	6187	0.150	0.082	0.250	4847	4602	844	4	0.63
7-4C	0.700	1310	5600	0.800	0.303	0.115	5002	4596	637	70	3.26
7-5C	0.700	1310	5600	0.600	0.238	0.115	4955	4593	345	42	2.16
7-6C	0.700	1310	5600	0.450	0.183	0.115	4906	4587	310	26	1.47
7-7C	0.700	1310	5600	0.300	0.155	0.115	4840	4583	311	14	0.92
7-8C	0.700	1310	5600	0.150	0.155	0.230	4795	4637	101	6	0.67
ATJ GRAPHITE-ZRO-4130 STEEL											
27-A	4.000	2390	8000	0.565	0.087	0.250	6640	4314	249	8	1.96
TITANIUM CARBIDE - ASBESTOS - 4130 STEEL											
24-A	4.000	650	6000	1.417	0.386	0.250	5509	1081	102	200	6.56
24-B	4.000	650	6000	0.998	0.250	0.250	5558	2395	347	200	4.20
8-A	4.000	1700	7000	0.140	0.040	0.250	5655	1938	94	3	1.38
TITANIUM CARBIDE-ASBESTOS(K=1.500,C=0.116)-4130 STEEL											
7-A	4.000	1700	7000	0.140	0.177	0.250	5648	1849	116	3	1.56
TITANIUM CARBIDE-ASBESTOS(C=0.116)-4130 STEEL											
14-A	4.000	1700	7000	0.140	0.097	0.250	5632	1012	132	3	1.66
TITANIUM CARBIDE-ASBESTOS(K=1.500)-4130 STEEL											
15-A	4.000	1700	7000	0.140	0.074	0.250	5666	2072	91	3	1.63
TITANIUM CARBIDE (K = 15.0)-ASBESTOS-4130 STEEL											
14-B	4.000	1700	7000	0.465	0.100	0.250	5656	1968	365	11	2.45
15-B	4.000	1700	7000	0.675	0.092	0.250	6105	2755	175	27	3.16
15-C	4.000	1700	7000	0.650	0.050	0.250	6093	2792	446	26	2.99
TITANIUM CARBIDE (K = 20.0)-ASBESTOS-4130 STEEL											
24-C	4.000	1700	7000	0.927	0.129	0.250	6100	2784	196	39	4.11
24-E	4.000	1700	7000	0.900	0.075	0.250	6096	2832	400	38	3.87
TITANIUM CARBIDE (K = 30.0)-ASBESTOS-4130 STEEL											
14-C	4.000	1700	7000	1.471	0.158	0.250	6101	2813	258	69	6.37
14-D	4.000	1700	7000	1.450	0.120	0.250	6106	2884	398	69	6.21
TITANIUM CARBIDE (K = 50.0)-ASBESTOS-4130 STEEL											
24-D	4.000	1700	7000	2.727	0.213	0.250	6100	2898	422	159	12.86
24-F	4.000	1700	7000	2.700	0.200	0.250	6102	2922	463	157	12.68
TANTALUM CARBIDE-ASBESTOS-4130 STEEL											
25-A	4.000	2390	8000	0.226	0.043	0.250	7052	2950	144	4	2.67
25-B	4.000	650	6000	0.464	0.096	0.250	5125	3014	279	30	5.98
25-C	4.000	650	7000	0.236	0.056	0.250	5222	3064	182	8.25	1.63
25-J	4.000	650	6000	0.800	0.150	0.250	5402	2998	386	80	7.81
TANTALUM CARBIDE (K = 20.0)-ASBESTOS-4130 STEEL											
25-D	4.000	1700	7000	0.927	0.101	0.250	6105	2761	186	25	10.49
TANTALUM CARBIDE (K = 35.0)-ASBESTOS-4130 STEEL											
25-F	4.000	1700	7000	1.764	0.188	0.250	6103	2821	264	56	18.72
25-H	4.000	1700	7000	1.650	0.100	0.250	6109	3004	418	53	17.11
TANTALUM CARBIDE (K = 50.0)-ASBESTOS-4130 STEEL											
25-E	4.000	1700	7000	2.730	0.168	0.250	6090	2832	362	100	34.93
TANTALUM CARBIDE (K = 70.0)-ASBESTOS-4130 STEEL											
25-G	4.000	1700	7000	4.210	0.201	0.250	6102	2970	600	195	59.89
ATJ GRAPHITE-ASBESTOS-4130 STEEL											
26-A	4.000	2390	8000	1.154	0.082	0.250	6712	2746	133	16	2.73

26-B	4.000	1700	7000	0.770	0.067	0.250		5178	3064	155		9	2.11
26-C	4.000	650	6000	5.477	0.326	0.250		4504	1359	178		250	14.69
26-D	4.000	650	6000	2.000	0.100	0.250		4533	3008	742		89	4.39
26-E	4.000	1700	7000	2.000	0.200	0.250		5924	3008	137		49	4.60
26-F	4.000	2390	8000	1.000	0.050	0.250		6432	3138	250		11	2.45
26-G	4.000	2390	8000	2.000	0.100	0.250		6695	1815	135		25	4.39
TUNGSTEN - ATJ GRAPHITE - ASBESTOS - 4130 STEEL													
18-A	4.000	1700	7000	0.250	0.500	0.100	0.250	5016	4013	2957	95	8	4.18
18-A	4.000	1700	7000	0.250	0.500	0.100	0.250	6099	5638	5094	267	18	4.18
18-B	4.000	1700	7000	0.250	1.000	0.100	0.250	5542	4762	3032	173	20	
18-B	4.000	1700	7000	0.250	1.000	0.100	0.250	6092	5606	4461	443	34	
18-C	4.000	1700	7000	0.250	1.500	0.100	0.250	5803	5151	2995	301	37	
18-C	4.000	1700	7000	0.250	1.500	0.100	0.250	6105	5617	3952	594	53	
16-L	4.000	1700	7000	0.250	2.000	0.050	0.250	5998	5447	3012	1014	63	6.86
16-W	4.000	1700	7000	0.250	2.500	0.100	0.250	6101	5605	3000	697	91	8.10
16-U	4.000	1700	7000	0.250	2.750	0.100	0.250	6105	5611	2813	706	101	8.69
16-M	4.000	1700	7000	0.250	3.000	0.050	0.250	6049	5524	2321	1023	100	9.19
16-V	4.000	1700	7000	0.250	3.500	0.100	0.250	6102	5606	2236	648	126	10.64
18-D	4.000	1700	7000	0.250	4.500	0.100	0.250	6099	5600	1576	502	151	13.58
18-E	4.000	1700	7000	0.250	6.000	0.100	0.250	6101	5602	850	366	171	18.72
16-G	4.000	1700	7000	0.500	1.000	0.100	0.250	5686	4392	3100	298	28	7.76
16-H	4.000	1700	7000	0.500	2.000	0.100	0.250	6037	5038	3019	582	74	9.81
16-T	4.000	1700	7000	0.500	2.400	0.100	0.250	6105	5179	2958	729	98	10.74
16-J	4.000	1700	7000	0.500	2.500	0.050	0.250	6104	5174	2824	1314	103	10.87
16-K	4.000	1700	7000	0.500	3.000	0.050	0.250	6104	5170	2445	1222	121	12.13
16-X	4.000	1700	7000	0.500	3.500	0.100	0.250	6104	5169	2136	652	136	13.63
16-Q	4.000	1700	7000	0.750	1.500	0.100	0.250	5949	4452	3030	473	59	11.80
16-I	4.000	1700	7000	0.750	2.000	0.100	0.250	6071	4723	3005	675	88	12.92
16-Z	4.000	1700	7000	0.750	2.500	0.100	0.250	6100	4780	2715	791	111	14.15
16-Y	4.000	1700	7000	0.750	3.000	0.100	0.250	6101	4776	2353	698	129	15.47
16-O	4.000	1700	7000	0.750	3.500	0.100	0.250	6103	4774	2022	642	145	16.89
18-F	4.000	1700	7000	1.000	0.500	0.100	0.250	5601	3391	3005	216	26	13.07
18-F	4.000	1700	7000	1.000	0.500	0.100	0.250	6096	4643	4351	547	43	13.07
16-F	4.000	1700	7000	1.000	1.000	0.100	0.250	5850	3869	3041	375	46	14.05
18-P	4.000	1700	7000	1.000	1.000	0.100	0.250	5830	4058	2981	359	45	
18-P	4.000	1700	7000	1.000	1.000	0.100	0.250	6106	4558	3873	682	63	
16-N	4.000	1700	7000	1.000	1.500	0.100	0.250	5993	4191	2994	554	71	15.12
16-E	4.000	1700	7000	1.000	2.000	0.100	0.250	6110	4481	3008	781	104	16.30
16-D	4.000	1700	7000	1.000	2.200	0.100	0.250	6110	4473	2853	780	112	16.80
16-C	4.000	1700	7000	1.000	2.350	0.100	0.250	6102	4435	2700	752	116	17.18
16-P	4.000	1700	7000	1.000	2.500	0.100	0.250	6103	4442	2595	748	122	17.57
16-R	4.000	1700	7000	1.000	3.000	0.100	0.250	6102	4426	2237	698	139	18.94
18-R	4.000	1700	7000	1.000	3.000	0.100	0.250	6102	4428	2239	698	139	
18-G	4.000	1700	7000	1.000	4.500	0.100	0.250	6100	4402	1338	465	175	
18-H	4.000	1700	7000	1.000	6.000	0.100	0.250	6100	4396	743	256	189	29.22
18-J	4.000	1700	7000	2.500	0.500	0.100	0.250	6059	3139	2999	746	98	
16-B	4.000	1700	7000	2.500	0.850	0.180	0.250	6108	3221	2959	423	120	39.11
18-K	4.000	1700	7000	2.500	1.500	0.100	0.250	6102	3035	2461	808	145	
16-L	4.000	1700	7000	2.500	2.500	0.100	0.250	6099	2895	1834	646	177	
18-M	4.000	1700	7000	2.500	3.500	0.100	0.250	6101	2836	1321	503	200	
18-M	4.000	1700	7000	2.500	4.500	0.100	0.250	6100	2794	342	211		
16-A	4.000	1700	7000	3.000	0.500	0.220	0.250	6109	2985	2880	302	121	48.79
TUNGSTEN(K=25.0)-ATJ GRAPHITE-ASBESTOS-4130 STEEL													
18-S	4.000	1700	7000	1.000	0.500	0.100	0.250	6090	4622	4012	468	42	
18-S	4.000	1700	7000	1.000	0.500	0.100	0.250	5740	3736	2986	230	29	
18-T	4.000	1700	7000	1.000	1.000	0.100	0.250	6082	4484	3019	438	57	
18-U	4.000	1700	7000	1.000	1.500	0.100	0.250	6097	4469	2192	366	70	

18-V	4.000	1700	7000	1.000	2.000	0.100	0.250	6099	4443	1236	95	78	
18-W	4.000	1700	7000	1.000	2.500	0.100	0.250	6102	4446	903	177	80	
18-X	4.000	1700	7000	1.000	3.500	0.100	0.250	6098	4432	307	99	80	
18-Y	4.000	1700	7000	1.000	4.500	0.100	0.250	6098	4431	131	83	80	
TUNGSTEN - BEO - ASBESTOS - 4130 STEEL													
19-H	4.000	1700	7000	0.750	0.750	0.100	0.250	5944	4463	2972	369	48	10.84
19-G	4.000	1700	7000	1.000	0.750	0.100	0.250	6000	4238	3009	462	60	14.10
19-J	4.000	1700	7000	1.000	0.800	0.100	0.250	6030	4313	3020	502	65	14.28
19-K	4.000	1700	7000	1.000	0.850	0.100	0.250	6048	4354	2987	523	69	14.42
19-F	4.000	1700	7000	1.000	1.000	0.100	0.250	6101	4481	2447	591	82	14.86
19-E	4.000	1700	7000	1.000	1.500	0.100	0.250	6101	4441	2083	469	102	16.43
19-D	4.000	1700	7000	1.000	2.000	0.100	0.250	6105	4435	1328	323	114	18.16
19-C	4.000	1700	7000	1.000	2.350	0.100	0.250	6101	4420	911	228	116	19.46
19-B	4.000	1700	7000	3.000	0.350	0.200	0.250	6104	2944	2786	362	129	48.76
19-A	4.000	1700	7000	3.350	0.250	0.220	0.250	6101	2768	2681	316	136	56.37
TUNGSTEN-BEO(K=15.)-ASBESTOS-4130 STEEL													
19-L	4.000	1700	7000	1.000	1.000	0.100	0.250	6102	4476	1885	306	70	14.86
TUNGSTEN - BORON CARBIDE - ASBESTOS - 4130 STEEL													
28-E	4.000	1700	7000	0.250	1.500	0.100	0.250	5229	4401	726	87	24	6.73
28-D	4.000	1700	7000	0.250	2.500	0.100	0.250	5363	4454	145	85	26	9.63
28-B	4.000	1700	7000	0.750	2.000	0.010	0.250	5542	3357	2997	2626	88	14.03
28-C	4.000	1700	7000	0.750	2.500	0.100	0.250	5570	3426	3007	949	114	15.90
28-J	4.000	1700	7000	0.750	3.000	0.100	0.250	6102	4765	1624	601	190	17.70
28-K	4.000	1700	7000	0.750	3.500	0.100	0.250	6097	4750	1211	450	200	19.66
28-N	4.000	1700	7000	1.000	1.000	0.100	0.250	5970	4115	3021	60	77	14 66
28-H	4.000	1700	7000	1.000	1.250	0.100	0.250	6048	4308	3001	757	101	15.37
28-A	4.000	1700	7000	1.000	2.000	0.100	0.250	6080	4363	2326	767	150	
28-G	4.000	1700	7000	1.000	2.500	0.100	0.250	6103	4416	1967	727	182	19.43
28-L	4.000	1700	7000	1.000	3.000	0.100	0.250	6101	4403	1537	587	200	21.30
28-M	4.000	1700	7000	1.000	3.500	0.100	0.250	6082	4366	1075	397	200	23.32
TUNGSTEN - PYRO GRAPHITE - PYRO GRAPHITE - 4130 STEEL													
30-A	4.000	1700	7000	1.000	2.000	0.200	0.250	5772	3510	2996	170	108	15.82
30-A	4.000	1700	7000	1.000	2.000	0.200	0.250	6025	4227	3810	322	150	15.82
30-E	4.000	1700	7000	1.000	1.000	0.200	0.250	6099	4504	4318	177	87	14.76
30-J	4.000	1700	7000	0.850	2.500	0.200	0.250	6099	4628	4118	510	200	17.07
30-B	4.000	1700	7000	0.750	2.000	0.200	0.250	5634	3644	3011	138	88	14.15
30-B	4.000	1700	7000	0.750	2.000	0.200	0.250	6100	4730	4254	366	150	14.15
30-F	4.000	1700	7000	0.750	1.000	0.200	0.250	6098	4828	4615	158	75	11.44
30-C	4.000	1700	7000	0.500	2.000	0.200	0.250	6106	5185	4706	355	136	10.96
30-G	4.000	1700	7000	0.500	1.000	0.200	0.250	6101	5200	4955	97	63	8.38
30-D	4.000	1700	7000	0.250	2.000	0.200	0.250	6108	5618	5075	311	115	8.05
30-H	4.000	1700	7000	0.250	1.000	0.200	0.250	6095	5607	5317	115	50	5.59
PYRO GRAPHITE - PYRO GRAPHITE - 4130 STEEL													
31-A	4.000	1700	7000	2.000	0.150	0.250		4419	2687	90		31	5.27
31-A	4.000	1700	7000	2.000	0.150	0.250		6625	6342	1165		150	5.27
31-B	4.000	1700	7000	2.500	0.150	0.250		5582	4415	329		88	6.61
31-B	4.000	1700	7000	2.500	0.150	0.250		6700	6420	1951		236	6.61
31-C	4.000	1700	7000	1.500	0.100	0.250		6704	6517	1689		113	3.94
31-D	4.000	1700	7000	0.500	0.100	0.250		6697	4493	343		28	1.92
PYRO GRAPHITE - BORON CARBIDE - ASBESTOS - 4130 STEEL													
32-A	4.000	1700	7000	1.000	1.000	0.100	0.250	5304	4406	2827	382	54	5.30
32-B	4.000	1700	7000	1.000	2.000	0.100	0.250	5268	4301	995	164	64	8.33

CASE	DIA	MAT-1	MAT-2	MAT-3	MAT-4	MAT-5	T1	T2	T3	T4	T5	DUR	WT
TUNGSTEN-PYRO GRAPHITE-ASBESTOS-4130 STEEL													
33-A	4.000	1700	7000	1.000	0.500	0.100	0.250	5533	3109	2986	259	30	13.26
33-B	4.000	1700	7000	1.000	1.000	0.100	0.250	5652	3272	3004	448	52	14.46
33-C	4.000	1700	7000	1.000	1.500	0.100	0.250	5721	3397	2995	652	78	15.78
33-D	4.000	1700	7000	1.000	2.000	0.100	0.250	5776	3518	2997	871	109	17.23
33-E	4.000	1700	7000	1.000	2.500	0.100	0.250	5821	3627	3001	1094	145	18.81
33-F	4.000	1700	7000	1.000	3.000	0.100	0.250	5860	3724	3006	1311	186	20.15
33-G	4.000	1700	7000	0.500	0.500	0.100	0.250	5071	3268	3026	145	15	7.06
33-H	4.000	1700	7000	0.500	1.000	0.100	0.250	5227	3457	3002	260	29	8.11
33-J	4.000	1700	7000	0.500	1.500	0.100	0.250	5363	3655	3006	412	47	9.31
33-K	4.000	1700	7000	0.500	2.000	0.100	0.250	5434	3821	3005	586	69	10.63
33-L	4.000	1700	7000	0.500	2.500	0.100	0.250	5507	3960	3002	772	95	12.08
33-M	4.000	1700	7000	0.500	3.000	0.100	0.250	5567	4077	2996	964	125	13.66

TUNGSTEN-ATJ GRAPHITE-BORON CARBIDE-ASBESTOS-4130 STEEL (HTC=1700,TG=7000)												
34-A	4.000	0.750	1.000	1.000	0.100	0.250	6099	4775	3656	2763	811	122
34-C	4.000	0.500	1.000	1.000	0.100	0.250	6101	5169	3696	2928	810	112
34-B	4.000	0.250	1.000	1.00C	0.100	0.250	6080	5572	3876	2998	746	98

Aeronautical Systems Division, Wright-Patterson Air Force Base, Ohio. Rpt. No. WADC-TR-59-602 Pt. II. INVESTIGATION OF MATERIALS CAPABILITIES OF MATERIAL SYSTEMS IN SOLID ROCKET MOTORS Part II. ANALYSIS OF HEAT TRANSFER FACTORS. Interim Rpt, February 1962, 94p incl. illus., tables.
Unclassified report

Temperature histories of various nozzle materials systems were analyzed parametrically, and a series of hot-flow tests were conducted in support of the analytical study. Results of the analyses showed the interrelationship of material combinations in relation

(over)

1. Analyses and test program
2. Material nozzle systems
3. Thermophysical properties effects
4. Duration

I. AFSC Project 7350 Task 73500
II. Contract No. AF 33 (616)-7365
III. Aerojet-General Corp.
IV. E. M. Sadownick
V. Aval. fr. OTS:
VI. In ASTIA collection

to duration. Results of the test program showed (1) effects of flame barrier and insulation thickness on duration capability, (2) the proximity of actual to calculated temperature distributions, and (3) the effect of aluminum oxide deposition on materials system capability

Aeronautical Systems Division, Wright-Patterson Air Force Base, Ohio. Rpt. No. WADC-TR-59-602 Pt. II. INVESTIGATION OF MATERIALS CAPABILITIES OF MATERIAL SYSTEMS IN SOLID ROCKET MOTORS Part II. ANALYSIS OF HEAT TRANSFER FACTORS. Interim Rpt, February 1962, 94p incl. illus., tables.
Unclassified report

Temperature histories of various nozzle materials systems were analyzed parametrically, and a series of hot-flow tests were conducted in support of the analytical study. Results of the analyses showed the interrelationship of material combinations in relation

(over)

1. Analyses and test program
2. Material nozzle systems
3. Thermophysical properties effects
4. Duration

I. AFSC Project 7350 Task 73500
II. Contract No. AF 33 (616)-7365
III. Aerojet-General Corp.
IV. E. M. Sadownick
V. Aval. fr. OTS:
VI. In ASTIA collection

to duration. Results of the test program showed (1) effects of flame barrier and insulation thickness on duration capability, (2) the proximity of actual to calculated temperature distributions, and (3) the effect of aluminum oxide deposition on materials system capability